

SEDIMENTARY STRUCTURES and their relation to bedforms and flow conditions

Jan H. van den Berg and S. Djin Nio

© 2010 EAGE Publications bv

All rights reserved. This publication or part hereof may not be reproduced or transmitted in any form or by any means, electronic or mechanical, including photocopy, recording, or any information storage and retrieval system, without the prior written permission of the publisher.

ISBN 978-90-73781-76-4

EAGE Publications bv
PO Box 59
3990 DB HOUTEN
The Netherlands

Contents

1. Introduction	1
2. Fundamentals of Flowing Water and Sediment Transport	8
3. Bed Forms and Sedimentary Structures Formed by Unidirectional Flow	19
4. Influence of Wave Action on Bed Forms and Sedimentary Structures	49
5. Influence of Tides on Sedimentary Structures	64
6. Soft-Sediment Deformation Structures	81
7. Eolian Sedimentary Structures	88
8. References	102
9. Color Plates	112
Index	140

1 Introduction

Sedimentary structures that show up in outcrops and cores tell us about physical, biological and sometimes also chemical conditions at the time they were formed. Varying hydraulic or aerodynamic conditions result in *assemblages* of structures that often bear diagnostic features of sedimentary environments. Therefore an understanding of the origin of sedimentary structures and their assemblages is a prerequisite for sedimentologists and petroleum geologists involved in core description and interpretation. The main objective of this book is to bring together the present basic knowledge on the relation between sedimentary structures, bedforms and hydraulic conditions. The book is part of post-graduate Short Courses in Advanced Sedimentology and Stratigraphy for the petroleum industry offered by ENRES International. In these courses much attention is given to the recognition of sedimentary environments from diagnostic features of sedimentary structures and assemblages of structures. For this purpose practicals are given using a selection of lacquer peels and cores representing typical fluvial to estuarine, coastal and eolian environments. This material including its interpretation is published as a regularly updated stand-alone document that can be obtained from ENRES.

One of the pioneering publications on this subject was a series of SEPM symposium papers published in 1965 (Middleton, 1965b). A more comprehensive publication on sediment movement by fluid flow and the resulting sedimentary structures was followed in 1972 (Blatt, Middleton and Murray, 1972). After that many excellent publications and textbooks were published (e.g. Allen, 1984, 1985; Bridge and Demicco, 2008; Collinson and Thompson, 1989; Harms *et al.*, 1982; Hsü, 1989; Leeder, 1999; Reineck and Singh, 1980). These publications are partly covering a much wider scope as presented in this book, but are at some points not going into the desired details and are partly outdated.

We have no intention to offer a new comprehensive textbook. The main goal of this book is to introduce the terminology and fundamental concepts that are necessary for the description and interpretation of the hydraulic background of sedimentary structures in siliciclastic deposits. Another objective of this book is to put this topic within the newly developed framework of modern stratigraphy (e.g. sequence stratigraphy and climate stratigraphy). Also some important new insights from recent research at the University of Utrecht and unique data of sedimentary structures from outcrops up to 15m below mean sea level have been added. A specially-designed Core Simulation software has been developed in cooperation with Statoil which will be used during the course and the practicals.

Short description of the book

Sedimentary deposits almost always contain sedimentary structures. These structures may be of physical, chemical or biological origin. Another reasonable way of classifying them is on the basis of

time of development relative to time of deposition (*primary* sedimentary structures and *secondary* sedimentary structures). This results in a twofold classification (Figure 1.1): Physical primary sedimentary structures are the most widespread and are the most useful in the interpretation of flow conditions during sedimentation. Understanding the relationship between these flow conditions and primary physical sedimentary structures is essential in the process-related interpretation of *depositional facies* (i.e. process sedimentology). This book will focus on these primary physical sedimentary structures and their relation to flow conditions.

	PHYSICAL	CHEMICAL	BIOLOGICAL
PRIMARY	Stratification Sole marks	Stratification	Bioturbation (tracks, trails)
SECONDARY	Deformation Intrusion Desiccation	Nodules Concretions Deformations Stylolites	Bioturbation (burrows)

Figure 1.1. Classification of sedimentary structures.

When the flow of water (or air) over a bed of non-cohesive sediment is strong enough to move the particles of the bed material the bed becomes moulded into a bed configuration made up of many individual topographic elements termed *bedforms*. Bedforms migrate and by doing so produce *stratification*, some of which may be preserved in the geological record. Because bedforms and their dynamics are governed by fluid processes, they and their stratification, provide an unequalled basis for making palaeo-hydraulic or -aerodynamic interpretations of ancient depositional environments.

Each depositional facies or environment is characterized by its flow conditions, sediment- and morphodynamics (i.e. *sediment dynamics*) and, as a result, characteristic sedimentary structures and assemblages of structures are produced. The ideal situation would be that one or a combination of a few features would be diagnostic for a certain depositional environment. Unfortunately, this is never so. ***A single sedimentary structure is rarely diagnostic for a certain process, let alone for a complex environment.*** There are always combinations of many characteristics that lead to the most likely solutions. More than one solution, as certainty about the exact nature of the palaeo-environment is seldom reached. Knowledge of the physical background of the preserved structures is a prerequisite to understanding the mutual relations of structures found in cores that guide us to these solutions and help us to keep our imagination of the palaeo-environment within realistic borders.

The book starts with an overview on the most important fundamental aspects of flowing water and

sediment transport. It is a theoretical discussion and is necessary to understand and to interpret its products, i.e. bedforms and the related internal sedimentary structures. The reader may start with the chapter on bedforms and their related internal sedimentary structures ([chapter 3](#)), and consult the theoretical discussion in [chapter 2](#) if necessary. The subsequent chapters are dealing with specific bedforms and their internal structures from some important sedimentary depositional environments (e.g. fluvial, tidal, wave dominated and eolian depositional facies). A chapter on soft sediment deformation has also been included in this book.

Some words on the classification, nomenclature, the stratigraphic hierarchy of stratal patterns and their related geological time dimensions

Layers of sedimentary rock are characterised by *beds or strata*. Both terms are being used approximately synonymous and are used to distinguish layers above and below separated by a surface showing a discontinuity in rock type, internal structure or texture (see [Blatt et al., 1980](#)). Strata are commonly used in stratigraphy and are generally referring to all types and thicknesses of layers. Beds are commonly defined as layers greater than 1 cm in thickness, while *laminae* are layers less than 1 cm in thickness (see [Chapter 2](#)). [Campbell \(1967\)](#) identified laminae, *laminasets*, beds and *bedsets* as components of a sediment body. These components can be grouped into *stratal unit* and are the basic building blocks of sedimentary depositional facies and the stratigraphic record (see [Van Wagoner et al., 1990](#)). A bed or bedset may be composed of different types of primary sedimentary structures, and the interpretation of the vertical and lateral succession of these structures may give information on the sediment dynamics of the depositional facies. Specific association of sedimentary structures defines the sedimentary depositional facies (see [Figure 1.2](#)). Subsequently, a series of vertical stacking of facies which pass gradually into each other defines a specific sedimentary *facies sequences* and/or *facies associations* (e.g. a coarsening upward of a deltaic sequence, etc.; see e.g. [Reading, 1996](#), [Walker and James, 1992](#)). A stacking of different facies sequences and/or facies associations produces the stratigraphic record which for example in sequence stratigraphy may represent a stratigraphic sequence.

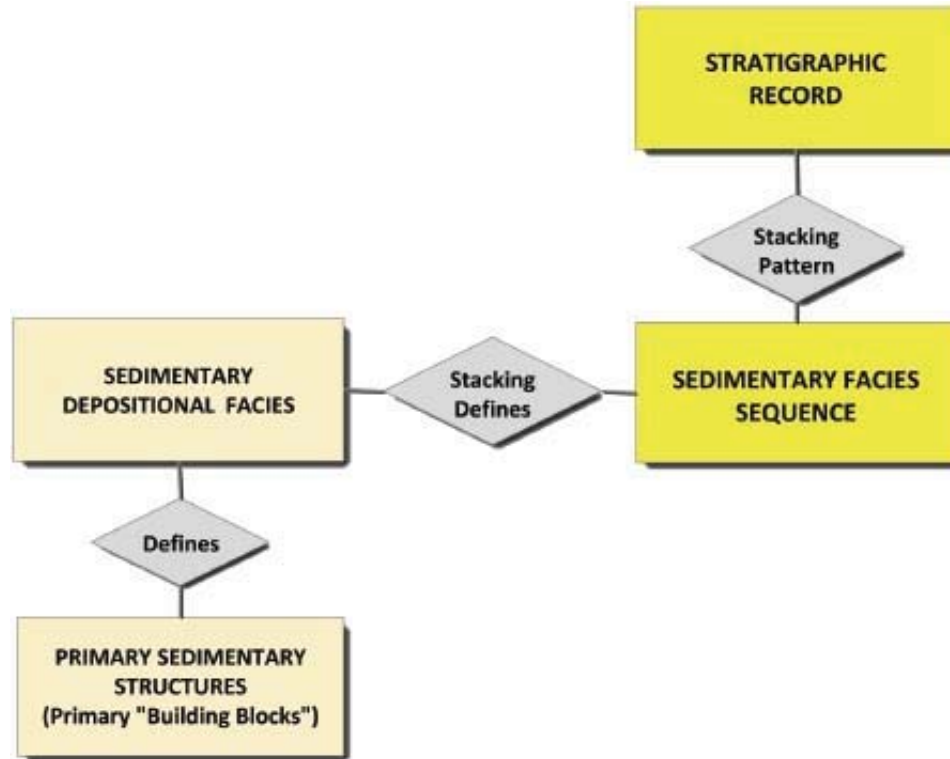


Figure 1.2. Hierarchy of the major components of sedimentology and stratigraphy.

It is obvious that a good understanding of the hierarchical relationship of the stratal units and patterns, and their geological time dimensions is essential for a proper sedimentological and stratigraphic interpretation.

This book will not go in detail of these aspects; more detailed discussion on those is presented in other ENRES' courses on Advanced Sedimentology and Stratigraphy. However, to put this book in a proper context within the whole spectrum of sedimentology and stratigraphy, some important aspects on the observation scale and the hierarchical order of the different units are briefly discussed here:

- Observation scales
- Stratigraphic time dimensions

Observation scales

Observation scales can be very different, ranging from seismic to wireline logs in wells to outcrops and to cores. Wireline logs represent the continuous recording of geophysical parameters along a borehole and usually represent data over an extended vertical section covering whole or several stratigraphic intervals. Borehole data only show a one-dimensional (1D) picture, while seismic data show an extended 2D or sometimes a 3D picture. Both approaches provide geophysical data that must be converted to sedimentary and information on geology needs an interpretation. For this purpose, outcrop analogues and cores are used for calibration. However, the different observation scales are a constraint in the interpretation and calibration. [Figure 1.4](#) shows an example of the different observation scales. Wireline log data from a borehole show, as mentioned earlier an extended vertical

section where a stratigraphic subdivision can be made. The borehole example is from the Permian Rotliegend, showing the standard set of wireline logs (i.e. gamma, sonic, and density logs), the electrofacies analysis and the Integrated Prediction Error Filter Analysis (INPEFA) log transform. The electrofacies analysis shows a succession of sands (orange-yellowish colours) and silts-shale (greenish-blue colours) and represents a stacking of fluvial channels and floodbasin fines. The INPEFA log transform represents climate change events (at the turning points) and the climate development trends. A general sequence stratigraphic and climate stratigraphic subdivision has been made based on the definitions made by *Catuneanu et al. (2009)* and *Nio et al. (2005)*.

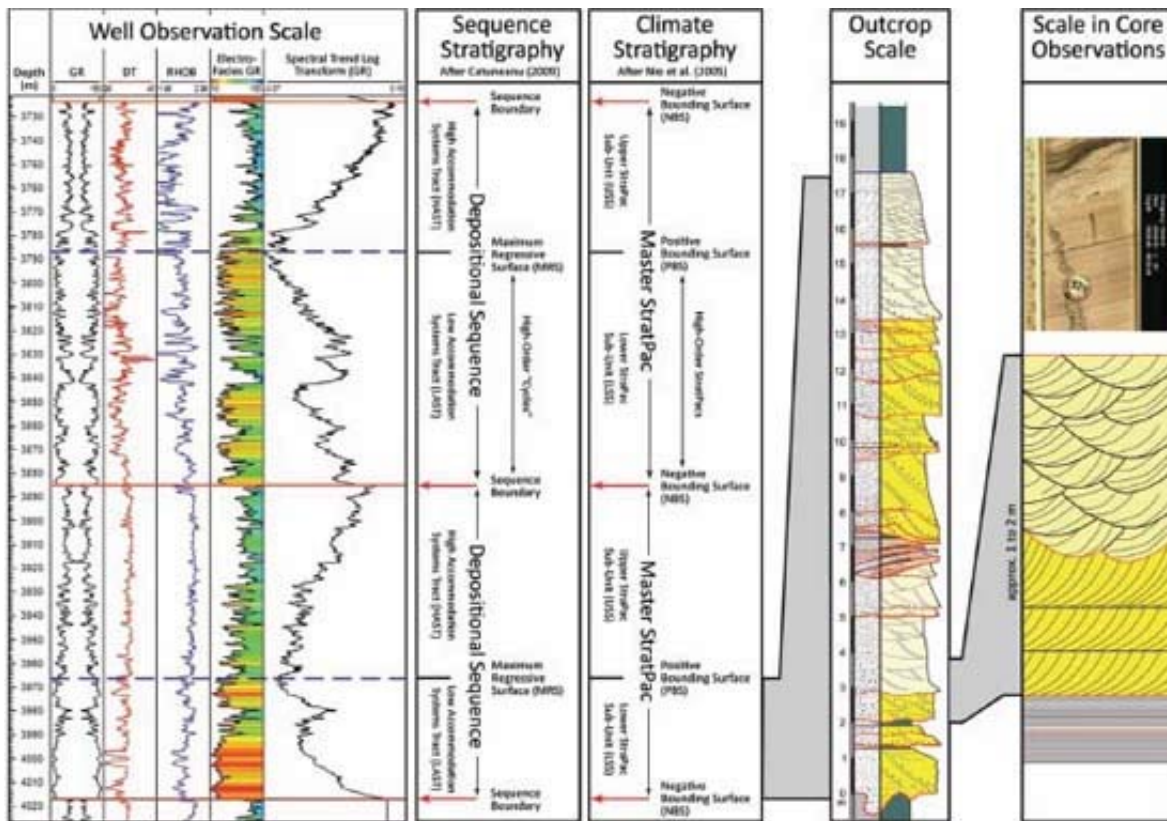


Figure 1.3. Example of observation scales from borehole to outcrop and core. See text for explanation.

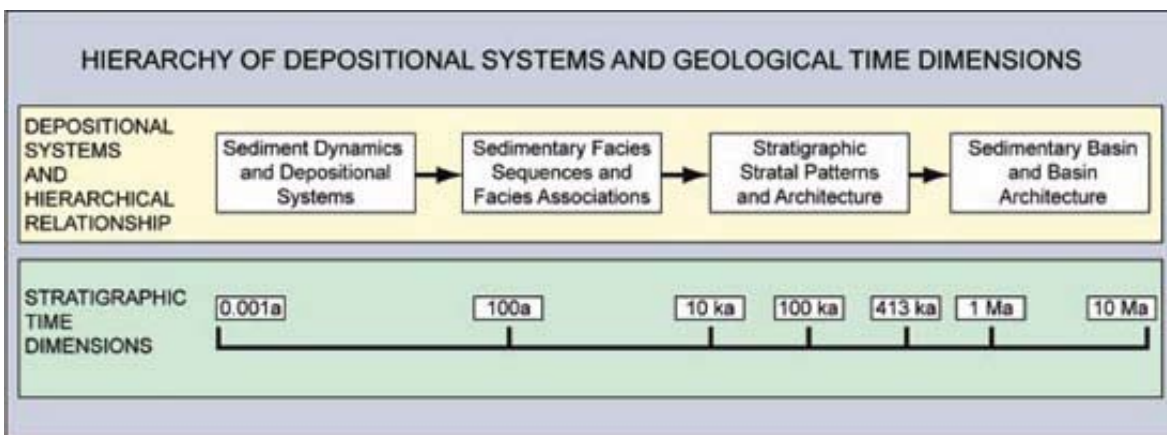


Figure 1.4. Hierarchy of geological dimensions and their relationship to the spectrum of geological time (here shown on a logarithmic scale).

As for a comparison, an example of a sedimentological log measured from an outcrop analogue is shown. Outcrop examples generally show a more extensive 2D view as compared to the 1D view of borehole data. Depending on the outcrop exposure conditions, outcrop exposures rarely show the same vertical stratigraphic extent as in boreholes (see also [Plate 7](#))

Observation scales in cores are even more limited as they generally show a one-dimensional view. In addition, the vertical extent represents only a small part or several smaller parts of the total borehole section. Analysis and diagnostic interpretation of sedimentary structures in cores require a conversion of one dimensional observation to 2D- or even 3D geometric properties of specific sedimentary structures, its relation to sediment dynamics and its position in the surrounding sedimentary structures.

Stratal Units	Definitions SED - Sedimentology SQS - Sequence Stratigraphy CMS - Climate Stratigraphy	Depositional Dynamics / Conditions	Tool Resolution			
			Seismic	Wireline Log	Core	Outcrop
Sequence (SQS)	(SQS) - A relatively conformable succession of genetically related strata bounded by unconformities or their correlative conformities		Seismic	Wireline Log	Core	Outcrop
Stratigraphic Package or StratPac (CMS)	(CMS) - A relatively conformable succession of genetically (climate) related strata corresponding to a full climate minimum-maximum cycle, bounded by a major climate minimum event and their correlative surfaces					
Systems Tract (SQS)	(SQS) - A linkage of contemporaneous depositional systems, forming the subdivision of a sequence					
StratPac Sub-Unit (CMS)	(CMS) - A succession of genetically (climate) related depositional systems forming a distinct stacking pattern and bounded by major climate change events and their correlative surfaces					
Parasequence Set (SQS)	A succession of genetically related parasequences forming a distinct stacking pattern and commonly bounded by major marine flooding surfaces and their correlative surfaces					
Parasequence (SQS)	(SQS) - A relative conformable succession of genetically related beds or bedsets bounded by marine flooding surfaces and their correlative surfaces					
Sedimentary Facies Sequence (SED)	(SED) - A series of facies which pass gradually from one into the other and is bounded by a sharp or erosive junction or non-deposition surface					
Bedset	A relative conformable succession of genetically related beds bounded by surfaces (called bedset surfaces) of erosion, non-deposition or their correlative conformities					
Bed	A relative conformable succession of genetically related lamina sets or co-sets bounded by surfaces of erosion or non-deposition					
Co-Sets of Cross-Lamination or Cross-Bedded Sets	A relative conformable succession of genetically related cross-laminated or cross-bedded sets bounded by surfaces of erosion or non-deposition					
Lamina Set or Cross-Laminated Set	A relative conformable succession of genetically related laminae bounded by surfaces (lamina sets or surfaces) of erosion or non-deposition					
Lamina	The smallest megascopic unit					

Figure 1.5. Hierarchy of stratal units as used in sedimentology, sequence stratigraphy and climate stratigraphy, indicating the approximate association of each level with different aspects of the depositional dynamics and conditions. Also showing the possibilities for resolving each type of unit depending on the source of data (seismic, log, core or outcrop).

Stratigraphic time dimensions

Having defined a hierarchy of stratal units, it is important to understand the relationship of the different levels in the hierarchy with geological time. [Figure 1.4](#) shows the time frame (on a logarithmic scale) for the various levels in the sedimentation system, from the depositional environment up to the scale of a basin. [Figure 1.5](#) gives an overview of depositional dynamics and conditions with which each level is generally associated.

Sediment dynamics and the development of depositional facies are part of the domain of the sedimentologists. Processes in this domain are within the short time-scale (minutes to hundreds of years) in the geological time spectrum (see [Figure 1.4](#)). This part of the time-spectrum can be observed directly and comparisons between ancient preserved sediments and sediment dynamic processes that are observable at the present-day, either in the field or can be simulated in the laboratory.

Processes at all longer time-scales (10ka to 1Ma), are the domain of the stratigrapher and are not amenable to direct observation. However, there is a close relationship between the stratigraphic and sedimentological domains. *Sequence stratigraphy*, for instance deals with the sedimentary facies response to base-level changes. *Climate stratigraphy* deals with the sedimentary facies response to climate change mainly within the Milankovitch Band.

Acknowledgements

This book is an update and extension of lecture notes supporting the regular Sedimentology Master Course intended for students of Physical Geography at Utrecht University, The Netherlands, which the first author wrote together with Richard Boersma and André van Gelder. Allard Martinius from Statoil provided most of the core images Their contribution is gratefully acknowledged.

We also thank the following publishers for granting permission to reproduce figures for which they hold copyright: Allen & Unwin, Crows Nest, New South Wales, Australia: [Figure 4.12, 7.5](#); Academic Press, Oval Street, London, UK: [Figure 4.2, 4.5](#); The Geological Society of America, Boulder, Colorado: [Figure 3.18](#); Harper and Collins, New York, USA: [Figure 6.1, 6.2](#); SEPM, Tulsa, Oklahoma, USA: [Figure 3.19, 3.28, 3.29, 4.6, 4.10,4.14, 4.16, 5.1, 7.12](#). Springer-Verlag, Heidelberg, Germany: [Figure 3.9, 5.17](#); Blackwell, Oxford, UK: [Figure 3.10, 3.12, 3.15, 3.24, 4.3, 4.7, 4.15, 7.8, 7.9](#).

2 Fundamentals of Flowing Water and Sediment Transport

Introduction

In this chapter we will examine properties and parameters of unidirectional flows, *flow resistance* exerted by the bed and sediment transport that are crucial for an understanding of the bedform configurations in which sedimentary structures are formed. *Unidirectional* flows are induced by tidal waves or driven by gravity in rivers or density underflows. They are characterized by a mean flow direction that remains constant for many hours, in contrast to *oscillatory wave-induced* flows that on a time scale of the order of seconds reverse in direction.

Parameters, definitions and fundamental properties of flowing water

Important physical properties of flowing water include its *density* and *viscosity*. Flow has a direction and velocity, which in combination forms a flow or *current vector*. This vector has a direction with the components *x*, *y* and *z*, which may change in space and/or time. In the case of unidirectional flow in a channel, important flow characteristics are the *water depth*, the *wet channel cross-section* and the *water discharge*. At the bottom, the flow is retarded due to the rough surface of particles (*skin resistance*) and the *turbulence* created at the lee-side of bed forms (*form roughness*). This flow resistance results in a *bed shear stress*, which in combination with density, can be converted to a parameter with the dimension of *flow velocity*: the *shear velocity*. The turbulence intensity and energetic- dynamic condition of the flow can be characterized by a *Reynolds Number*, a *Froude Number* and a *stream power* parameter (Table 2.1). These flow parameters are important, as they have an intimate relation with bed forms and channel pattern.

Parameter	unity	symbol
Density	kgm ⁻³	ρ
molecular viscosity	kgm ⁻¹	μ
kinematic viscosity	m ² s ⁻¹	$\nu = \mu/\rho$ (10 ⁻⁶ at 20 °C)
water depth	m	<i>H</i>
wet channel cross-section	m ²	<i>a</i>
depth-averaged current velocity	ms ⁻¹	<i>u, U</i>
channel water discharge	m ³ s ⁻¹	$Q=Ua$
Pressure	Nm ⁻²	<i>p</i>

bed shear stress	Nm^{-2} (Pa)	τ_0
shear velocity	ms^{-1}	$u_* = \sqrt{\tau_0/\rho}$
Reynolds Number	-	$Re = Uh/\nu$
Froude Number	-	$Fr = U/\sqrt{gh}$
Stream power	Wm^{-2}	ω

Table 2.1. Flow parameters.

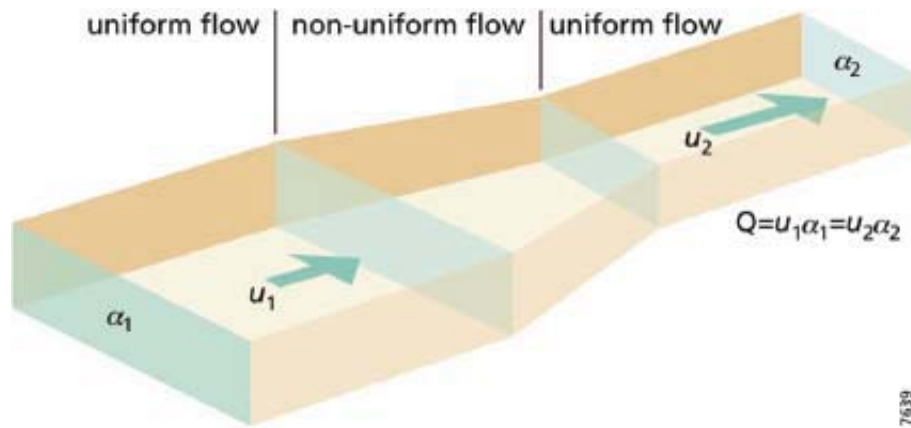


Figure 2.1. Definition of uniform and non-uniform flow (modified after Bridge, 1996).

Consider a flow in a straight channel with varying α ; but a constant Q (Figure 2.1). Assuming that the fluid is incompressible (constant density), an expression for the conservation of mass (and volume) is:

$$Q = U_1 \alpha_1 \rho_1 = U_2 \alpha_2 \rho_2, \quad (\text{m}^3 \text{s}^{-1}) \quad (2.1)$$

which is the simplest form of what is called the equation of continuity. If the depth-averaged flow velocity, U , does not change in the direction of the flow it is called *uniform*. If U changes in the downstream direction, which in this case in fact means that the value of α ; changes, the flow shows a *convective acceleration* and is *non-uniform*. If no change of U occurs in time, the flow is *steady*, if there is a change in time it is *unsteady*. Thus, in the case of no change of flow velocity in time and space, the flow is steady and uniform, a condition named *permanent*.

A flow may be *laminar* or *turbulent*, which appears to be a function of a Reynolds Number, Re as defined in Table 2.1. The transition is found at values of $500 < Re < 2000$. Except for a very thin near-bed layer - the *viscous sublayer*, δ - the flow in natural channels is always turbulent. The thickness of δ depends on viscosity and shear stress, $\delta = (11,6\nu)/u_*$. At low velocity the sublayer forms a very thin blanket over a sand-bed (normally less than one mm). The laminar flow follows weak spiral motions that are oriented parallel to the flow direction (Figure 2.2). These vortices give rise to a streaky structure in the near-boundary flow that varies in character in time and space. The viscous sublayer is very important because bed particles immersed within it are protected from the largest turbulent

motions above and grains moving within it are concentrated in lanes beneath the low-speed streaks. As the thickness of the sublayer reduces with increasing flow strength, grains protrude through it, starting with the largest particles. When the thickness of the sublayer is more than the median grain size of the bed material at the surface, the bed is called *hydraulic rough*. If not, it is *hydraulic smooth*.

In case of the non-uniform steady flow illustrated in [Figure 2.1](#), the cross-sectional area decreases downstream, thus the average velocity must increase in that direction (*conservation of mass*) and the average hydrographic pressure must therefore decrease. The latter follows from the general law of conservation of energy: when friction losses of the fluid (to heat) can be neglected – which is generally the case over a short distance in the flow direction – this means that the sum of potential and kinetic energy of the mass, m , of flowing water is constant (*conservation of energy*), thus: kinetic energy + potential energy = $0.5mU^2 + mgh = \text{constant}$ or, written as the one-dimensional *Bernoulli equation*:

$$H = \frac{U^2}{2g} + h + \Delta z \quad (\text{m}) \quad (2.2)$$

with g = acceleration due to gravity and H = energy height. In case of an *ideal* (frictionless) fluid H is a constant. All terms in [equation \(2.2\)](#) have the dimension (m) and therefore can visualized in a plot of height versus distance. [Figure 2.3](#) shows a case of a flow over a sill (or bed form). As the flow increases in velocity over the sill, $h_2 + \Delta z$ must become smaller than h_1 , resulting in a somewhat lower water level above the sill. However, a second possibility would be that the flow reduces in velocity above the sill, with a marked increase in water level. The first case, as presented in [figure 2.3](#), represents *tranquil* or *subcritical* flow conditions. The second possibility, in which the water surface is in phase with the bed, occurs at *shooting* or *supercritical* flow conditions ([Fig. 3.6](#)). A Froude number, Fr , defines the presence of these two conditions:

$$Fr = \frac{U}{\sqrt{gh}} \quad (-) \quad (2.3)$$

The flow is tranquil at values Fr below unity and is supercritical above this value. If there is a spatial transition between these two types of flow, it is manifested by an abrupt step in the water surface, called a *hydraulic jump*. Above a bed form in a supercritical flow, the flow velocity is reduced. Therefore, in this area sediment tends to deposit. Bed forms in supercritical flows therefore have the tendency to grow in height, until some critical point is reached where the surface wave breaks. The resulting turbulence then disintegrates the bed form. Thus, bed forms in supercritical conditions are highly unstable. In subcritical conditions the opposite is true, as the flow accelerates over bed forms, impeding sedimentation and their further growth.

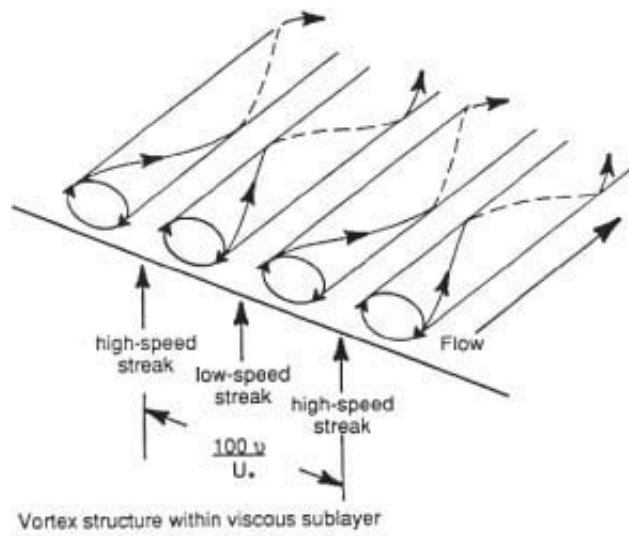
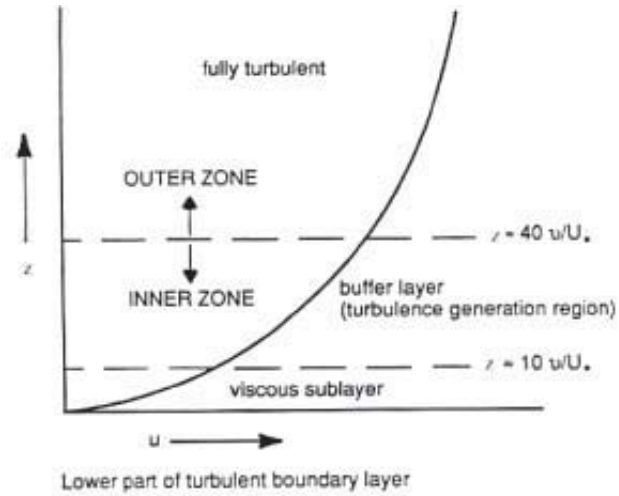


Figure 2.2. Main features of the lower part of the turbulent boundary layer (Bridge, 1996).

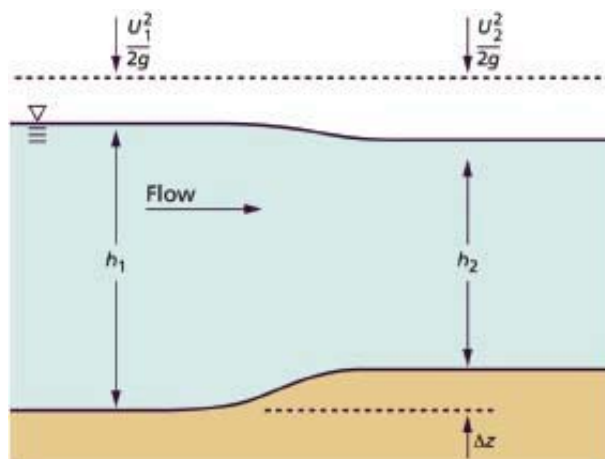


Figure 2.3. Tranquil flow over a sill.

Vertical flow structure

When flow is steady and uniform, the *gravity force* exerted on the flow equalizes the *resistance force* at the bed:

$$\tau_0 = \rho g h S \quad (\text{Nm}^{-2}) \quad (2.4)$$

with S = water level gradient (-). The shear stress is maximal at the bed τ_0 , and decreases to zero at the water surface. The resistance at the bed produces turbulence. Near the bed the turbulence is intense and whirls are small. The turbulence intensity decreases with distance to the bed. The intense small-scale turbulence vanishes and only relatively large eddies reach the water surface. Up to an elevation of $0.2h$ from the bed, the increase of characteristic eddy length is proportional to the bed distance. Based on this relation and the assumption that the shear stress in this water layer does not change with height above the bed, it can be deduced that flow velocity increases with distance to the bed according to a logarithmic curve:

$$u_z = \frac{u_*}{\kappa} \ln \frac{z}{z_0} \quad (\text{ms}^{-1}) \quad (2.5)$$

with u_z = current velocity at distance z to the bed κ is the von Kármán constant (typically the value 0.41 is used) and z_0 = height above the bed where the current velocity is virtually zero, according to a best fit logarithmic curve (Fig. 2.4A). Since the vertical flow profile above the *turbulent logarithmic layer* (*buffer layer*, see Figure 2.2) does not deviate very much from that lower layer, the logarithmic curve is generally assumed to be valid for the whole water column (Figure 2.4 A). In permanent flow conditions the depth-averaged flow velocity occurs at $z = h/e \simeq 0.36h$. It should be realized, however, that this only applies for steady and uniform conditions, which in reality are generally not met. Vertical diffusion of turbulence is more intense near the bed. Therefore, the vertical flow structure here reacts rapidly to unsteady and non-uniform conditions and shows less deviation from the logarithmic shape than flow at larger distance from the bed.

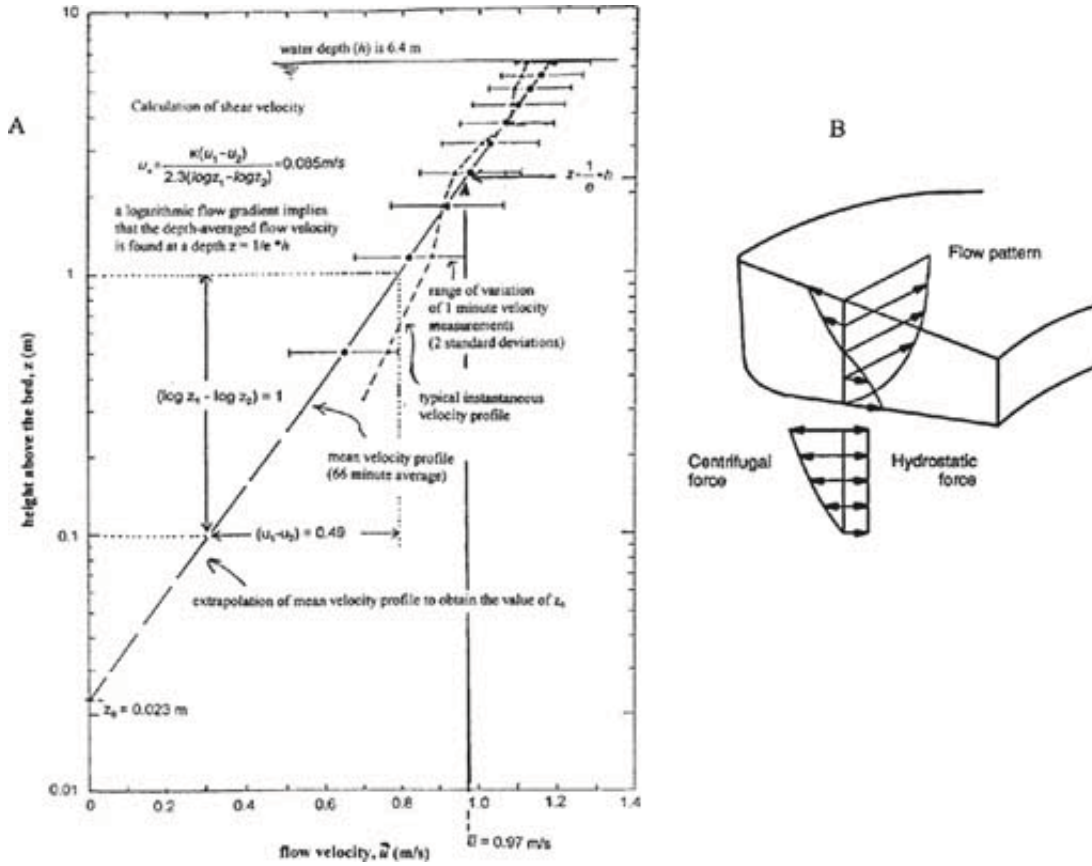


Figure 2.4. Vertical flow gradients.

A: Example of measured vertical flow gradient, based on a sampling period of 66 minutes (modified after Middleton, 1977);

B: vertical variation in centrifugal and hydrostatic forces and resulting cross-channel flow in a river bend (Bridge, 1996). The value of z_0 is a measure of the hydraulic resistance exerted by the bed.

With increasing hydraulic roughness, the value of z_0 increases.

In bends of river or tidal channels, a centrifugal force is exerted on the fluid. This force is counteracted and balanced by a hydrostatic force produced by the elevated water level at the outer bank of the channel bend (Figure 2.4 B). The centrifugal force, F_c , in a channel bend with a radius of curvature r is:

$$F_c = mU^2 / r \quad (\text{N}) \quad (2.6)$$

The magnitude of the centrifugal force near the water surface is larger than the hydrostatic force. Near the bed the opposite is true. As a result, in river bends a *helical* flow pattern develops (Figures 2.4B and 2.5). Also, flow in bends tends to become concentrated near the outer bank. Both factors contribute to the typical asymmetry of channel cross-section in river bends, which due to hysteresis, reaches its maximum development in the downstream part of the bend.

Bed roughness

The flow velocity in an alluvial channel is strongly related to the frictional resistance exerted by the bottom of the river and the vegetation that grows in the river. The first roughness predictor was proposed in 1768 by Antoine de Chézy. Equation 2.4 and 2.5 imply:

$$U = C\sqrt{hS} \quad (\text{ms}^{-1}) \quad (2.7)$$

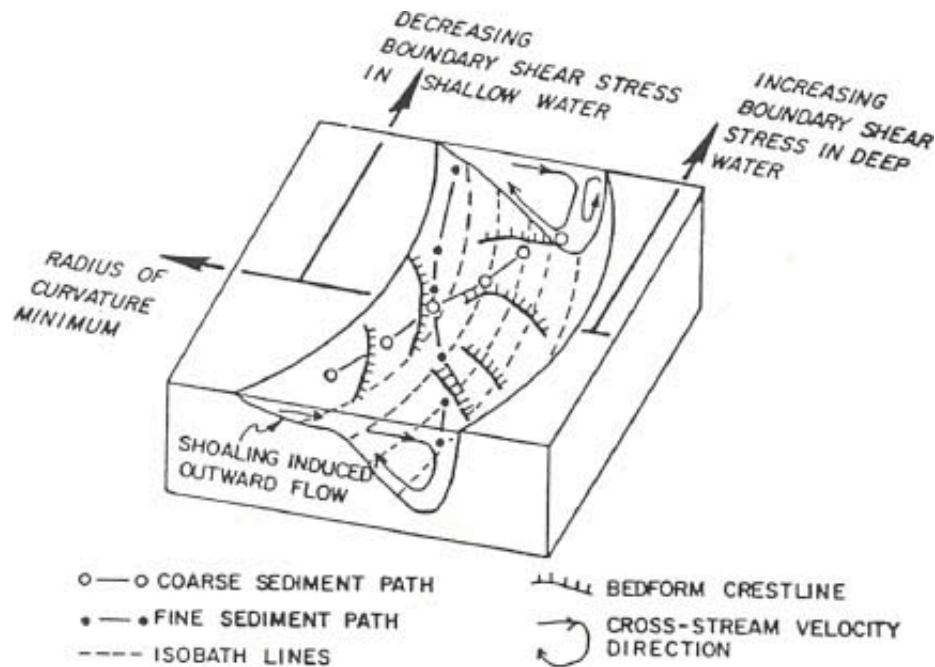


Figure 2.5. Flow and channel bed in a simple channel bend.

in which C = Chézy roughness coefficient ($\text{m}^{1/2}\text{s}^{-1}$). In case the flow is not retarded by vegetation or man-made structures, such as groynes, the value of C largely depends on the hydraulic roughness of the grains on the bed surface and bed forms. These roughness elements can be expressed in *equivalent (Nikuradse) roughness lengths*, k . Chézy's C is converted to Nikuradse's k by using the White-Colebrook formula:

$$C = 18 \log \frac{12h}{k' + k''} \quad (\text{m}^{1/2}\text{s}^{-1}) \quad (2.8)$$

in which k' = roughness length due to grains (*skin friction*) and k'' = roughness length due to bed forms such as ripples and dunes (*form roughness*; van Rijn, 1993). Skin friction is mainly caused by the larger grains because they protrude above the average bed level. Therefore, flow resistance by grains is a function of the larger grain sizes in the river bed. In the case of a sand bed, the skin friction is reasonably well approximated by $k' = 3D_{90}$; in gravel-bed rivers $k' = D_{90} = 90$ percentile of the non-cohesive bed material. Form roughness is dictated by the frequency, shape and magnitude of the turbulent wakes behind bed forms (see also chapter 3). As a rule of the thumb, the form roughness of ripples equalizes the bed form height, whereas in the case of dunes, the value of k'' is about half the dune height. As mentioned earlier, roughness can also be estimated from the vertical flow gradient. In case of a permanent flow over a plane bed $k = 33 z_0$ (see also Figure 2.4).

Transport of cohesionless sand and gravel in steady, unidirectional flows

Consider a river flow over a sandy, cohesionless plane bed. If the (lift) force, F_D , produced by the fluid shear on the bed for a short time interval exceeds the gravity force, F_G , sand will be transported. Since $F_D \propto \tau_0 D^2$, and $F_G \propto (\rho_s - \rho)gD^3$, the initiation of particle motion should depend on a critical value of:

$$\frac{F_D}{F_G} = \frac{\tau_0}{(\rho_s - \rho)gD} = \frac{\rho u_*^2}{(\rho_s - \rho)gD} = \theta \quad (2.9)$$

where ρ_s = sediment density, D = particle diameter and θ = *mobility (Shields)* parameter. In case of well-sorted bed material, the mobility of all particles at the bed surface may be represented by the median grain size, D_{50} . Combining equation (2.9) with (2.7) then results in the following expression:

$$\theta = \frac{U^2}{C^2 \Delta D_{50}} \quad (-) \quad (2.10)$$

in which $\Delta = (\rho_s - \rho)/\rho$. In the *Shields diagram*, which is a plot of θ and the Grain Reynolds Number, $Re_* = u_* D/\nu$, (Figure 2.6) a curve known as the *Shields criterion* represents the initiation of general motion of particles along the bed in a well-sorted, cohesionless grain mixture. So this criterion, θ_{cr} , does not indicate the absolute beginning of any motion of particles – which in fact is about a three times smaller value of θ_{cr} – but represents the condition at which grain collisions start to become a significant factor in the process of bed material transport. The original curve for θ_{cr} was derived from experiments with coarse sand and gravel. Later on, it was adapted and extended to smaller grain sizes by Miller *et al.* (1977). The Shields curve ends in fine silts. In finer sediments (clay), cohesion plays an important role in the entrainment (erodibility) of the sediment. In fact, many natural deposits coarser than fine silt are not without cohesion, as they contain appreciable amounts of clay. Cohesive mud particles are held together mainly by electro-chemical forces. The magnitude of these forces depends on mineralogy, (e.g., exchangeable cations), the size, shape and spacing of the clay aggregates and the ionic properties of the pore water. Resistance properties also depend on the state and history of consolidation. For example, there may be a flocculated structure, a pelleted structure due to desiccation, bioturbation, or ejected pseudofaeces, produced by filter feeding bivalve mollusks or a fissility, due to release of former compaction.

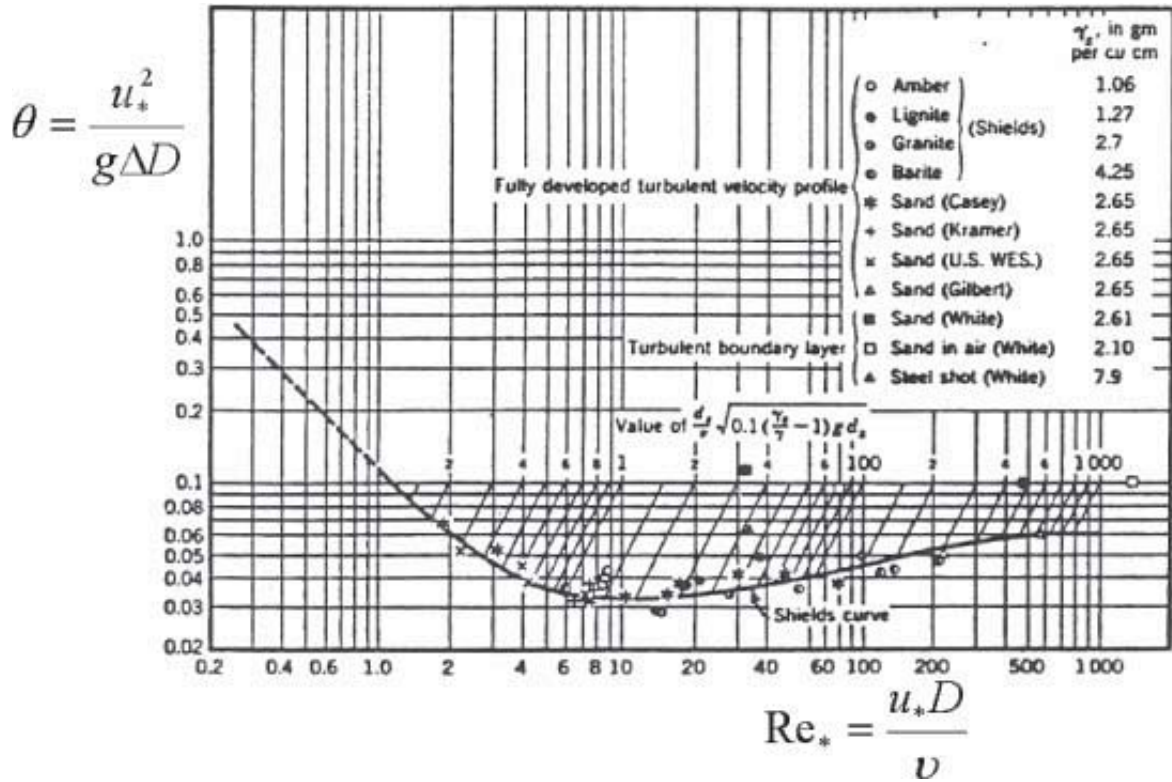


Figure 2.6A. The initiation of general particle motion along the bed (Shields criterion) in the case of well sorted bed material according to Shields (1936).

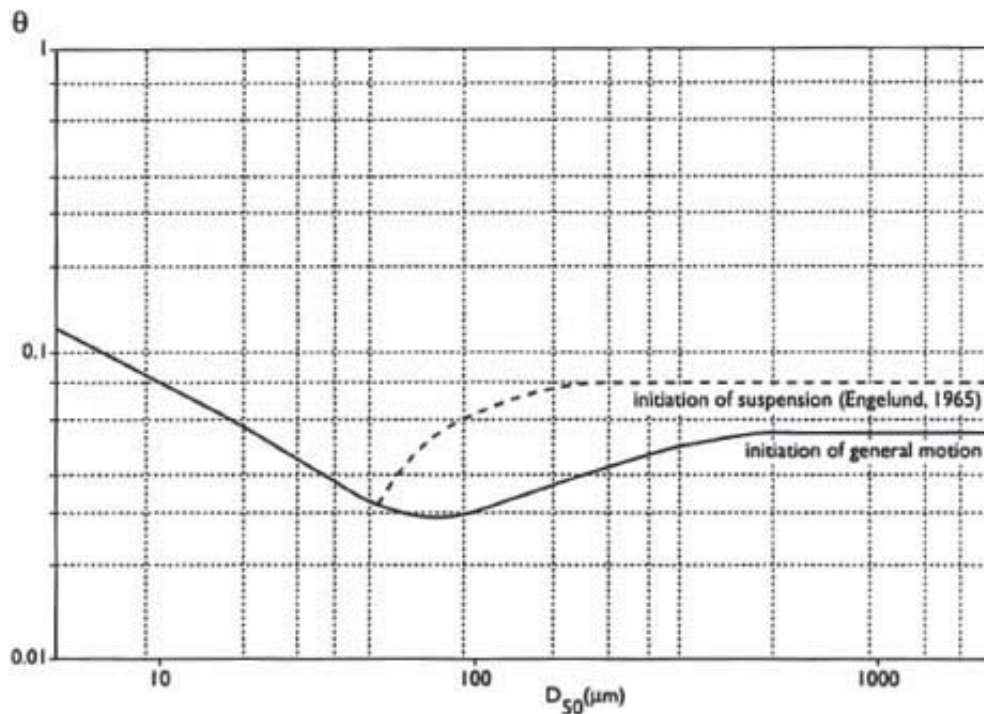


Figure 2.6B. The modified Shields criterion and the initiation of general motion in the suspension mode in a

mobility-grain size plot at a water temperature of 20 °C. As viscosity is not incorporated a changing water temperature will shift the curves somewhat along the x-axis.

In a river, three types of sediment transport occur, *bed-load transport*, *suspended bed-material transport*, and *wash load*. Bed-load transport is defined as the transport along the bed, by *sliding*, *rolling* and *saltation*. As a particle is lifted from the bed by turbulent lift forces or the impact of another grain, almost immediately turbulent movements of the water govern its trajectory. Therefore, pure saltations are restricted to a layer of a thickness of only a few particle diameters. All bed material transport above this relatively thin saltation layer is defined as suspended bed material load. The concentration of suspended bed material diminishes with increasing distance to the bed and is a function of turbulent diffusion and the particle fall velocity. The latter two factors are represented in the mobility parameter θ . Therefore, this parameter is found in many predictors of suspended bed material transport. The magnitude of both the suspended bed material transport and of the bed-load transport is predictable using parameters of the local hydraulic boundary conditions. In fine sands and coarse silts or high-energy conditions, suspended bed material transport is (much) larger than bed-load transport. The concentration and transport of wash load is independent of local hydraulic conditions and hardly changes with water depth. Wash load consists of fine silt and clay that does not interact with the bed material. It originates from hill slope and riverbank erosion and is simply washed through the channel. In the alluvial environment it may only deposit in abandoned channels and on the floodplain.

Selective transport on a plane bed and its effect on sediment sorting during deposition

Selective transport of bed material occurs if the criterion of *equal mobility* is not met. This means that the proportions of bed material transport rates of the various grain size fractions and their fractional representation in the bed material are not the same. In many gravel bed rivers, the criterion of equal mobility is never met, not even at extreme floods, and selective transport always occurs. In the case of a sand-gravel mixture as a bed material, the coarser particles tend to protrude from the bed surface, are more *exposed* to the flow and therefore, show higher mobility as compared to the situation of well-sorted bed material. Conversely, smaller particles tend to be *hidden* between the larger elements and therefore move less easily. For a very similar reason, the mobility threshold for the initiation of motion in [Figure 2.6](#) increases at grain sizes smaller than about 700 μm . The particles become more embedded in the viscous sublayer, beyond the reach of flow turbulence. In sands, heavy minerals are transported as bed load. They may be concentrated at the bed surface as a result of *hiding* and of selective erosion of the larger, light minerals. Hiding is supported by *kinetic sieving* (also: *kinematic sorting*) in a bed-load transport layer, the small particles fall within the pores of the larger ones, forcing the large particles to migrate to the upper part of the moving bed layer. In situations of a sand bed with a small admixture of gravel, shear sorting brings the gravel to the surface, where it is easily transported by the flow without being deposited. This process is called *gravel overpassing*: for instance, on glaciofluvial outwash plains (sandurs) gravel may overpass sand bars and deposit in channels, giving rise to a marked difference in grain size between bar surface and channel fill deposits (see also [Plate 4](#)). If gravel is the main constituent of the bed, during very high flow energy conditions, hiding may not be effective and sand particles are sucked out the pores between the gravel particles. During such conditions, *open work* gravels may be deposited. In less energetic conditions, pores are filled with sand, resulting in *closed work* gravels. Concentrations of large immobile or hardly moving grains, such as large extraformational clasts, which are left on the eroded bed surface, are commonly referred to as

a *lag deposit*. The term *armouring* refers to the situation in which there are sufficiently large immobile (or intermittently mobile) grains on the bed to protect the potentially mobile grains underneath. It should be realized that such protection is a precondition to equal mobility. This means that a *mobile* bed armour or *pavement* is generally found at all discharge stages in gravel-bed rivers. A pavement may also refer to a static armour layer if the flow strength is insufficient to erode the pavement, even at flood events. As a result of several of the processes mentioned above, an upward coarsening of the sediment in individual bed-load transport layers is produced. In deposited sediments, this is termed *reverse* or *inverse grading* (opposite: *normal grading*).

3 Bed forms and Sedimentary Structures Formed by Unidirectional Flow

Introduction

This chapter will focus on the types of bedforms that develop under unidirectional flows, their prediction from local flow and bed material conditions and the sedimentary structures they produce. But before entering into this matter first some general features of stratification must be introduced.

Stratification

Sediments are almost never completely structureless. Apparent lack of structures is mostly caused by weathering and poor exposure conditions. In seemingly homogeneous sediments structures can often be enhanced by various techniques, such as impregnation, polishing, etching, X-rays and lacquer peels.

One of the most conspicuous properties of any *sedimentary sequence* is the occurrence of *stratification* (Figure 3.1). A *stratum* (plural: *strata*) can be defined as a sedimentary unit of relatively uniform composition, which is separated from sediments above and below by a discontinuity in lithological composition, internal structure or texture. A discontinuity may be sharp or gradual. A single bed is generally built up during a single sedimentary ‘event’. In some cases, however, a bed may be constructed during several depositional events without recognizable discontinuities between each episode. This may happen, for instance, in turbidite sequences (Figure 3.27), where the next current ‘eats up’ part of the preceding one. This leads to the formation of *amalgamated* beds. Layers that are produced by a single event may consist of different structural intervals (divisions) that reflect characteristic stages of the event, such as a waning current or a decreasing wave energy. Stratification on a vertical scale smaller than one centimetre is generally called *lamination*, thicker stratification is named *bedding*. All stratification that is inclined due to primary processes (i.e., not tectonic deformation or tilting) is referred to as *cross-stratification*.

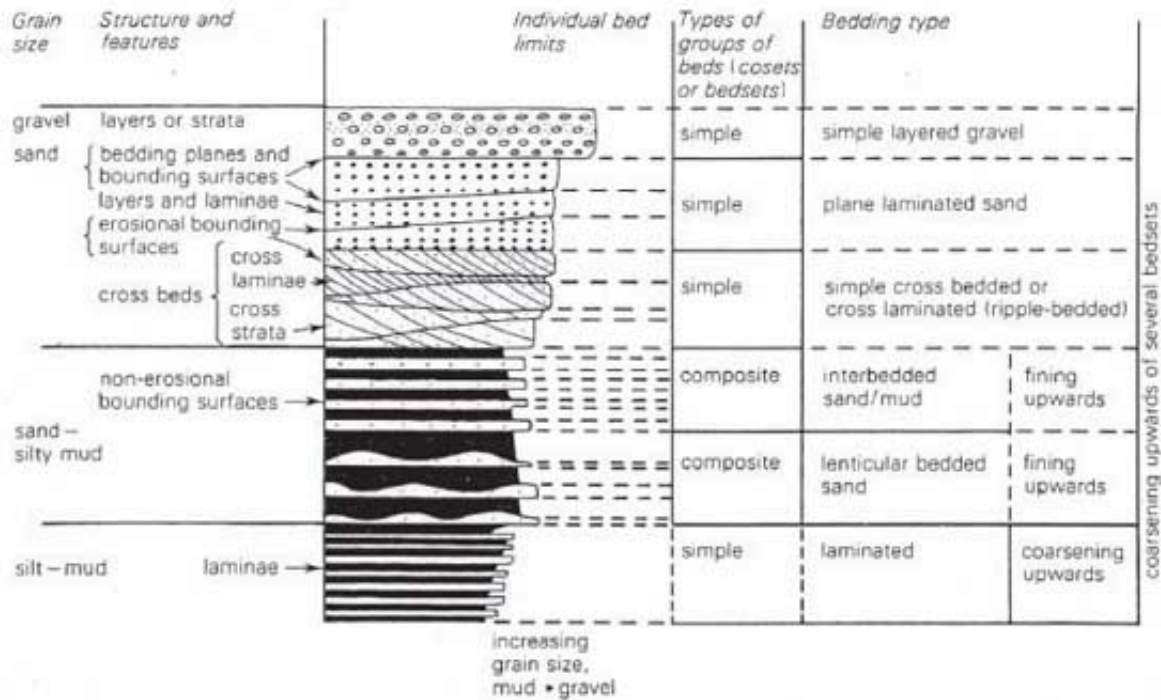


Figure 3.1. Stratification types. Note the effect of heterolithic alternations on stratification terminology. (after McKee and Weir, 1953, Campell, 1967 and Reineck and Singh, 1973, modified by Collinson and Thompson, 1989).

Individual laminae (singular: lamina) are not necessarily connected with discrete sedimentary events. Even under completely steady and uniform flow conditions, lamination may originate as a result of irregularities in the intensity of the flow-turbulence. Lamination may be reflected in (a combination of):

- segregation of different minerals (e.g., micas, heavy minerals),
- segregation of different grain sizes, with or without grading,
- differences in sorting (clay/matrix content) and/or
- differences in organic material content.

In some instances, lamination may be the result of different sedimentary events. If this results in thin, regular alternations of different lithologies, the sediment is termed a *laminite*. In case of an irregular alternation, the sediment is termed a *heterolithic* bed. Laminites that are produced by seasonal fluctuations in organic productivity or the amount of suspended matter are termed *varves*.

Lower boundaries of *sets* of ripple or dune cross-stratification are always erosional (see also Fig. 3.18). Often relatively coarse grains are collected at this boundary, which enhances its visibility. The shape of the boundary depends on the ripple or dune form. Instead, bars may be underlain by a non-erosional boundary. Erosional structures without a relation to bedforms include sole marks (Figure 3.2). Sole marks are geometrical features produced on a sediment bed by erosion by a strong current (*flute casts*) or by mechanical disruption of the bed by large objects carried by a strong current (*tool marks*). Sole marks are so named because they occur on the under-surfaces of some sandstones, turbidites and other beds and are casts or moulds of depressions that were formed in the underlying, generally soft, clayey sediments. Flutes form through the erosion of muddy sediment surfaces by eddies in the passing

turbulent current and are subsequently infilled with sediment as the flow decelerates. The resulting casts can be recognized by their elongated teardrop shape, with tapered ends pointing downstream. Tool marks (*bounce* or *skip*, *prod*, *groove* and *chevron*) form when objects (mud clasts, plant debris, etc.) being carried by a current leave an impression on the sediment's surface, which is subsequently eroded and elongated by the current. As with flutes, casts eventually form as a result of sediment infilling. Groove casts, one of the more common tool marks, are elongate ridges which form as a result of the infilling of grooves cut by objects (twigs, pebbles, etc.) dragged along by a current and range in width from a few millimetres to several tens of centimetres (Figure 3.2).

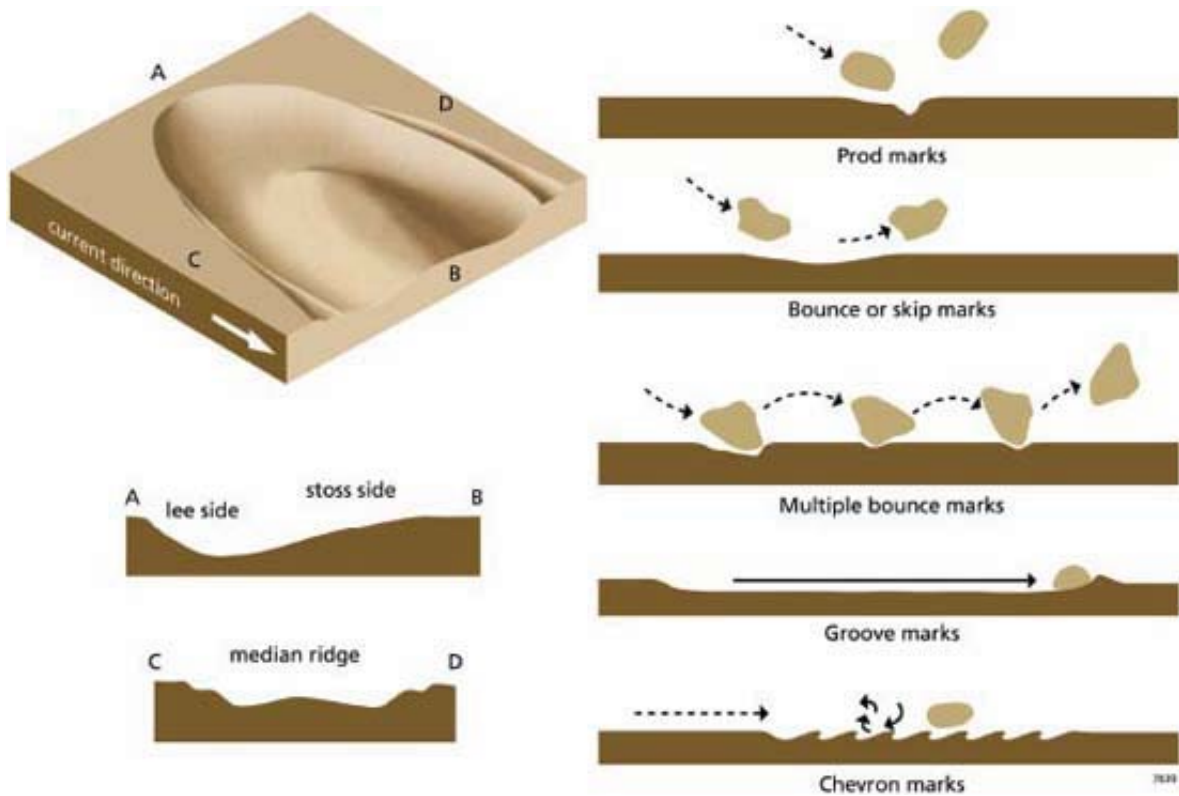


Figure 3.2. Sole marks. Left row: erosive structure produced by turbulence; Right row: structures produced by objects in the flow (tool marks).

It is important to remember that although sedimentary structures provide valuable information about current velocity, flow depth, transport directions and other environmental parameters, it is rarely possible to reconstruct a sedimentary environment on the basis of individual structures alone. They can only give an indication of the processes that were active at a certain time and place during deposition. Identical processes may occur in completely different environments. Oscillatory water movements for instance, may lead to the formation of *wave ripples* in inland pools a few centimetres deep as well as on the continental shelf in water depths of hundreds of metres. A second important point to keep in mind is that bed forms, and especially the larger types, always need time to adapt to changing circumstances (*lag* or *hysteresis* effect). Equilibrium bed forms may not have time to form under tidal flow or in rivers with rapidly changing discharge and in other environments with a variable regime. Finally, it must be stressed that strata deposited by normal (low energy) processes may be completely destroyed by 'catastrophic'/high-energy events before having a chance to become preserved in the sedimentary record. Therefore, low-energy structures generally have a low *preservation potential*. The

sedimentary record thus tends to be biased towards the higher energy processes.

Bed forms and flow regime

Numerous flume experiments as well as observations in the field establish that loose granular material (silt, sand and gravel), when subject to a unidirectional flow, exhibit a variety of bed forms. The type of bed form depends on current velocity near to the bed, flow depth, grain size and time. As current velocity increases and grain size remains constant, the sequence of bed forms in fine to medium sand in deep water flows is: *lower plane bed* with little or no sediment movement, *ripples*, straight crested or 2D *dunes*, 3D dunes (with a curved, discontinuous crest line pattern), *washed out dunes* and *upper plane bed* with abundant sediment movement (Figure 3.3). Aqueous dunes are also termed *megaripples*.

3D dunes and ripples may be *lunate* or *linguoid* forms (Figure 3.4). Lunate ripples and dunes are usually found in relatively deep water ($h/H > 3$); linguoid-shaped ripples and dunes are formed in relatively shallow water. Equilibrium ripples and dunes are asymmetric bed forms, with a steep lee-side face. Ripples and dunes are bed form configurations of the *lower* or *tranquil flow regime*. In tranquil flow (A–D in Figure 3.3), the bed form topography and the water surface are out of phase. If the flow depth decreases and the current velocity remains constant, the bed forms will transform, at a certain flow depth, to configurations of the *rapid* or *upper* flow regime. These are plane beds with abundant sediment movement, *standing waves* and *antidunes*. Though the transition from subcritical to supercritical flow takes place at $Fr = 1$, the bed form transition to upper flow regime plane bed (or upper plane bed; E–H in Figure 3.3) already occurs at lower values of the Froude Number, down to $Fr = 0.75$. Figure 3.5 shows the equilibrium existence of tranquil flow bed forms in unidirectional steady and uniform flow as related to a dimension-less (Bonnefille) particle parameter, D_* , and a mobility parameter, related to skin friction (plane bed), θ' :

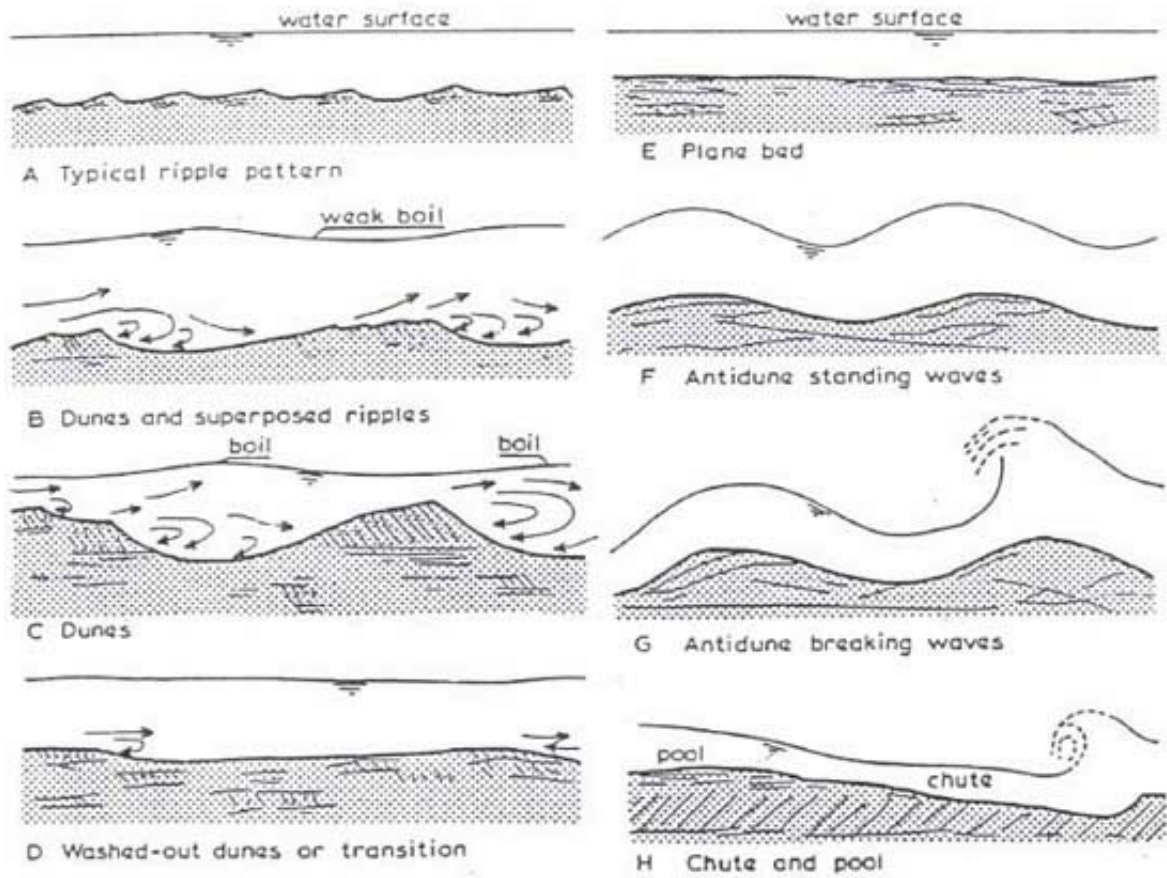


Figure 3.3. Bed forms in shallow, permanent flow. Flow velocity increases from A to H (Simons and Richardson, 1963).

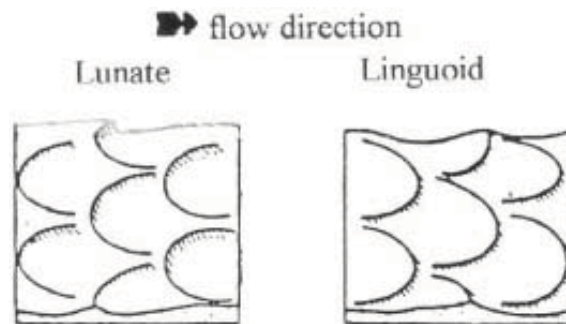


Figure 3.4. Patterns of lunate and linguoid ripples or dunes.

$$D_* = D_{50} \left(\frac{(\rho_s - \rho)g}{\rho v^2} \right)^{\frac{1}{3}} \quad (-) \tag{3.1}$$

and

$$\theta' = \frac{\rho_s U^2}{\left(18 \log \frac{4h}{D_{90}}\right)^2 (\rho_s - \rho) D_{50}} \quad (-) \quad (3.2)$$

Some almost straight lines that crosscut the diagram of [Figure 3.5](#) represent lower boundaries of antidune occurrence for a number of flow depths ($Fr = 0.75$). Ripples can only form in hydraulic smooth bed conditions. The thickness of the viscous sublayer reduces with increasing flow shear. In the case of bed material with a median grain size larger than about $700 \mu\text{m}$ the value of the shear stress required to move the sediment, the thickness of the sublayer is less than the median particle size. Thus, the bed is hydraulically rough and no ripples are formed. Conversely, dunes cannot exist at a median grain size smaller than about $125 \mu\text{m}$, the exact value depending on fluid viscosity. Flume experiments indicate that after a sudden increase of the flow velocity that brings the value of the mobility parameter from the lower plane bed into the area of dune existence, at first straight ripples are formed, which are soon remoulded into 3D ripples. It may then take more than an hour before the bed configuration is transformed to dunes. Therefore in short-lasting flow events, such as in some turbidity currents, time may be too short for the generation of dunes and instead only ripples are formed. Another observation is that 2D ripples is not a stable, equilibrium bed form. Even at very low flow velocities, 2D ripples will ultimately transform into 3D forms. The possibility of such long-term adaptations of the bed are often neglected in studies of equilibrium bed states, and the length of flume experiments therefore often is insufficient. [Carling et al. \(2005\)](#) demonstrated in flume experiments that for near threshold flow of gravel motion, conditions that generally are assumed to result in a plane bed (see [Fig. 3.5](#)) on a time scale of several days produce 2D dunes. These 2D dunes might change in 3D dunes if flow conditions persist for many days. In practice, such prolonged permanent and high flow velocities necessary to move gravel are rarely met in nature. Therefore the notion that 2D dunes and their deposits indicate less energetic conditions in general remains valid. The physical reason for the existence of ripples and dunes has still not satisfactorily been explained. However, it is quite obvious that they are different. If the water depth is not too shallow to obstruct the development of dunes, their height is always more than 10 cm, whereas the maximum height of ripples is about 4 cm. Ripples are often formed on the lower part of the dune's stoss side, where the bed is locally hydraulically smooth. Ripples cannot exist on the highest part of a constructive dune, as this area is hydraulically rough. Thus, if ripples are found on the crestal part of a dune, it means that the dune is degenerating (see also [Figure 3.19](#)).

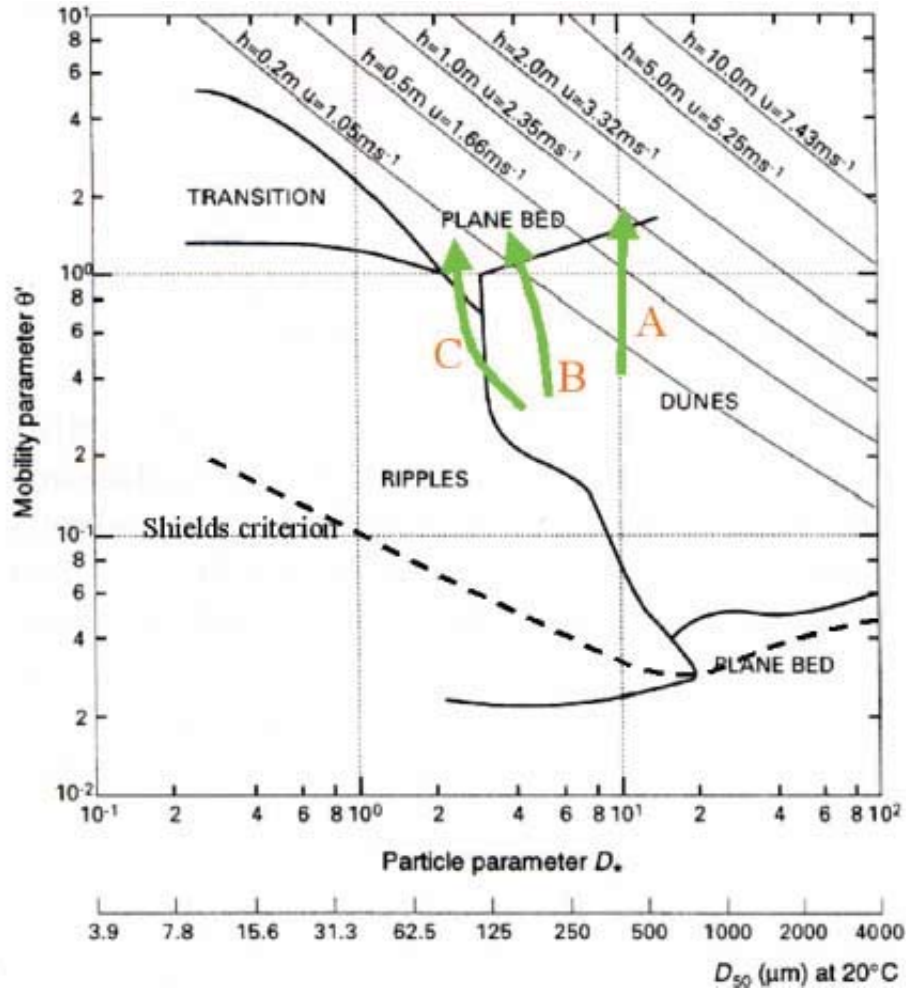


Figure 3.5. Bed form states in unidirectional, steady and uniform water flows in relation to grain mobility and grain size parameters. Almost straight cross-cutting lines represent the lower limit of antidune bed forms ($Fr = 0.75$) for several flow depths. Arrows indicate possible transitions of dunes to upper plane bed in the case of very fine to medium sand and shallow water: A. Froude-forced (in case of shallow water); B. Mobility-forced (in case of deep water) and C. Viscosity-forced. Note that ripples may be formed below the Shields criterion. (modified after Van den Berg and Van Gelder, 1993; 1998).

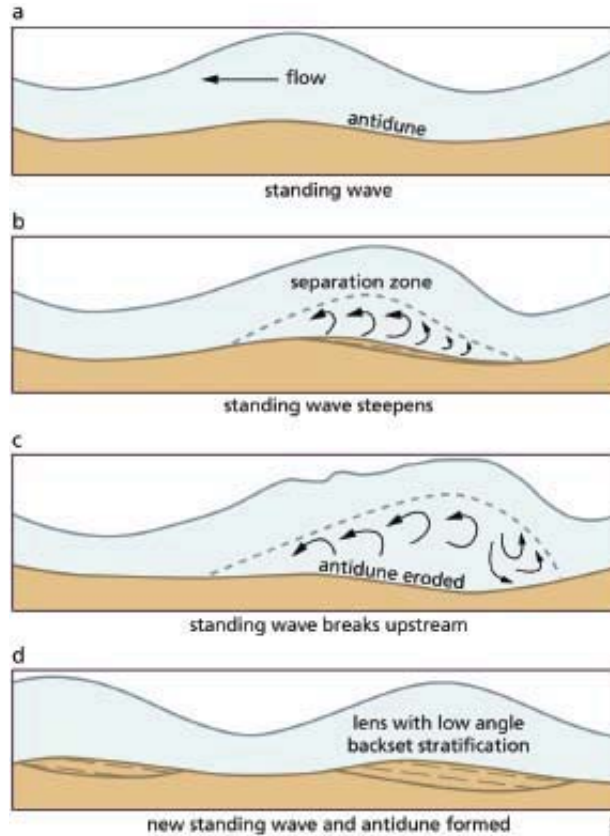


Figure 3.6. The antidune – plane bed cycle (modified after Middleton, 1965a).

In the literature devoted to dune to upper-stage plane bed transition, it is almost always suggested that there is only one transition, whereas bed form stability diagrams, such as that of Southard and Boguchwal (1990), clearly indicate that two transitions are possible, forced by a high Froude number, Fr , or by a high mobility, θ . In fact, there are not two but three possible transitions, which can be defined as (A) Froude-forced, (B) mobility-forced and (C) viscosity-forced (arrows in Figure 3.5). Mobility forced transitions (B) are for instance important in meandering rivers with a fine sand bed, Froude-forced transitions (C) are common in shallow braided rivers and viscosity-forced transitions (A) may occur in rivers with very fine sand and a large seasonal fluctuation in water temperature (Fredsoe, 1981; Julien and Raslan, 1998): with the lowering of the water temperature the viscosity increases, which reduces the value of the particle parameter D_* . In case of fine sand as a bed material, this may result in a change from a hydraulically rough to a hydraulically smooth condition, and thus a shift from dunes to ripples as a stable bed form configuration. As a consequence, the hydraulic resistance becomes much lower and the flow velocity increases, which in turn results in an increase of the mobility parameter, θ , which accounts for a further shift into the stability field of a mobility-forced plane bed. In case of silt with increasing mobility, ripples do not simply transform into an upper plane bed but to an unstable alternation in time and space of ripples, plane bed and erosional scours: processes of rapid erosion related to swift morphological changes of the river bed that are common in conditions of high sediment mobility are limited due to the low permeability of the silt bed. Before particles can be eroded, they must be freed from the framework of their deposits. This means that water must first penetrate into the bed to widen the pores before particles can be lifted and transported. In case of silt, penetration of water into the bed is hindered by the low permeability, resulting in

negative pore pressures that keep the grains together until the pore space dilates by penetrating water. The erosion is limited and scours may develop, which, as erosion shifts to deposition, alternates with ripples and plane bed in time and space (van den Berg and van Gelder, 1993; Van Maren *et al.*, 2008).

As mentioned before, bedforms that form in supercritical conditions are unstable. Upper plane bed generally alternates in time with antidunes in cycles of tens of seconds to several minutes duration: antidunes grow in height while migrating upstream until the water waves on top transform into hydraulic jumps and break. Then turbulence resets the bed to a plane or wavy condition (Figure 3.6). With a further increase of flow energy the hydraulic jumps become permanent and the bed transforms into a series of *chute-and-pools*. Flow is supercritical in the chute and passes through the hydraulic jump into subcritical in the pool. Erosion in the supercritical chute makes this stable bedform configuration move upstream. In case of fine sand, the rapid erosion in the chute is limited by the velocity of pore space dilation – which is proportional to permeability – and as a result, the bedform shape reverses to so-called *cyclic steps*. With increasing flow energy the difference in Froude number between pool and chute increases and related to this, the bedforms grow in length (Cartigny *et al.*, 2009; see Figure 3.7). The transitions of chute-and-pools to cyclic steps is gradual. Antidunes are one order of magnitude smaller and may temporarily appear superimposed on these larger bedforms.

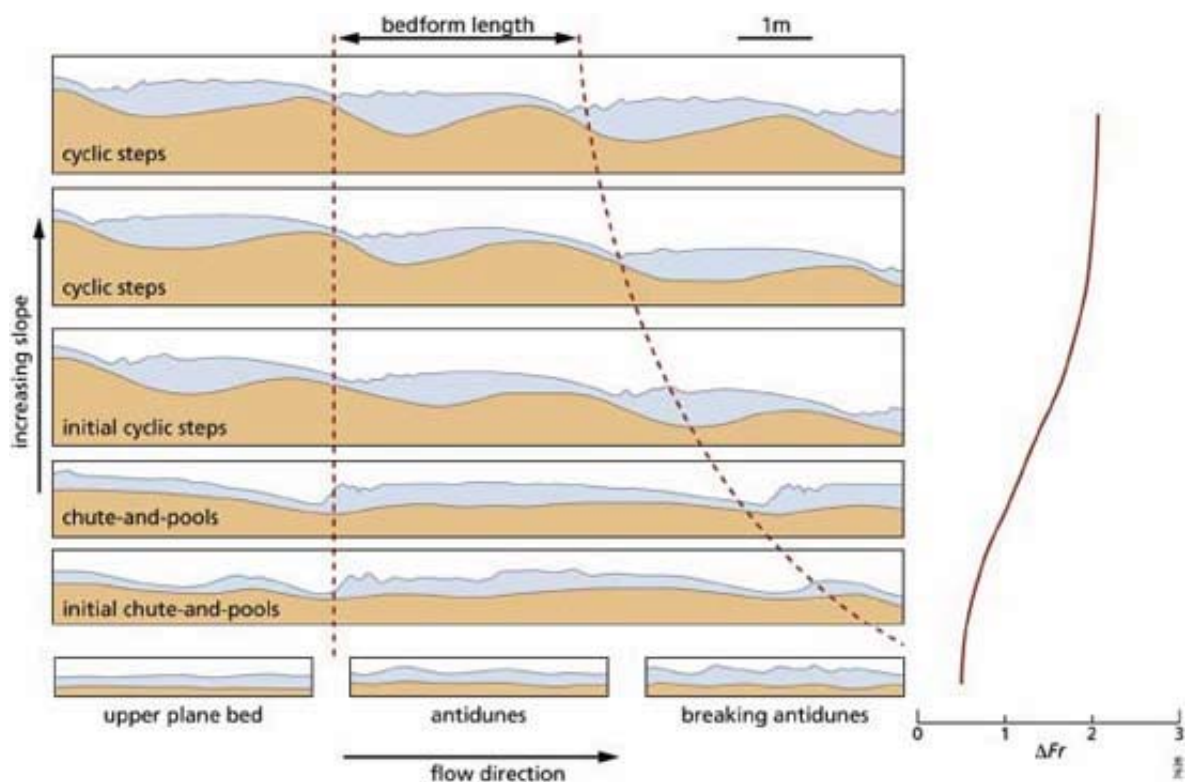


Figure 3.7. Upper flow regime bedforms plotted against the slope. Drawings from video images of the flume experiments with well-sorted medium sand ($D_{50} = 265 \mu\text{m}$; vertical relief is exaggerated by 50%). ΔFr is average spatial difference between maximum and minimum Froude number (modified after Cartigny *et al.* (2009)).

Bed form morphology and the generation of cross-stratification in ripples and dunes

The terminology used for describing the morphology of current ripples and dunes is given in [Figure 3.8](#). The *brink-point* of the ripple or dune is the highest point of the slip face. This does not necessarily coincide with the summit of the bed form. Similarly, the toe point, which forms the base of the slip face, is not necessarily the lowest point of a dune. When the internal structure of a bed form corresponds to the outer form ([Figure 3.9](#)), the structure is said to be *form-concordant*. *Form-discordant* structures usually reflect previous, often opposite, directions of flow. Previous higher or lower stage circumstances may also be seen recorded in form-discordant structures.

Accretion on the lee side occurs intermittently by the avalanching of grains from the brink-point. The bed load accumulates at the top of the slip face until a critical slope is reached, the *static angle of repose* ([Figure 3.10](#)). When this slope is surpassed, a mass of sediment fails along a very flat, spoon-shaped scar. The small sandy debris flow or *grain flow* initiated by the failure continues until the *dynamic angle of repose* is reached of $30\text{--}35^\circ$, a value depending on grain size and shape. Well-rounded, calcareous grains generally show lower angles of repose, but irregularly shaped, angular fragments of calcareous material may reach the same inclination as quartz sand. An avalanche may erode the upper, relatively coarse part of the previous one, which contributes to a fining upwards of the deposit. Another factor that accounts for this is the larger momentum of the large particles on top of the grain flow, which tend to bring them further downslope.

The ultimate shape of the dune lee side profile depends on the balance between bed load avalanching and deposition from suspension. In the early years of Sedimentology it was thought that low rates of bed-load sedimentation would result in *foreset* laminae with *angular* lower boundaries. Large amounts of suspended material produce *tangential* or *concave* lower contacts ([Figure 3.11](#)). Very high sedimentation rates may give rise to *sigmoidal* foreset laminae, showing part of the sediments deposited in the area between the summit point and the brink-point preserved ([Plate 8](#)). Cross-strata are visible due to spatial variations in texture and/ or composition that are due to a number of processes:

- variations in the texture, composition and transport rate of bed load arriving at the brink-point of the dune or ripple. As a result of this, deposits of successive avalanches show a different grain size;
- *grain sorting* during the process of grain flow in avalanches down the steep leeside slope. Kinetic sieving produces reverse grading in individual avalanche deposits and
- settling of suspended, relatively fine, sediments on the lee side. In between two avalanches, a thin drape of fines is laid down.

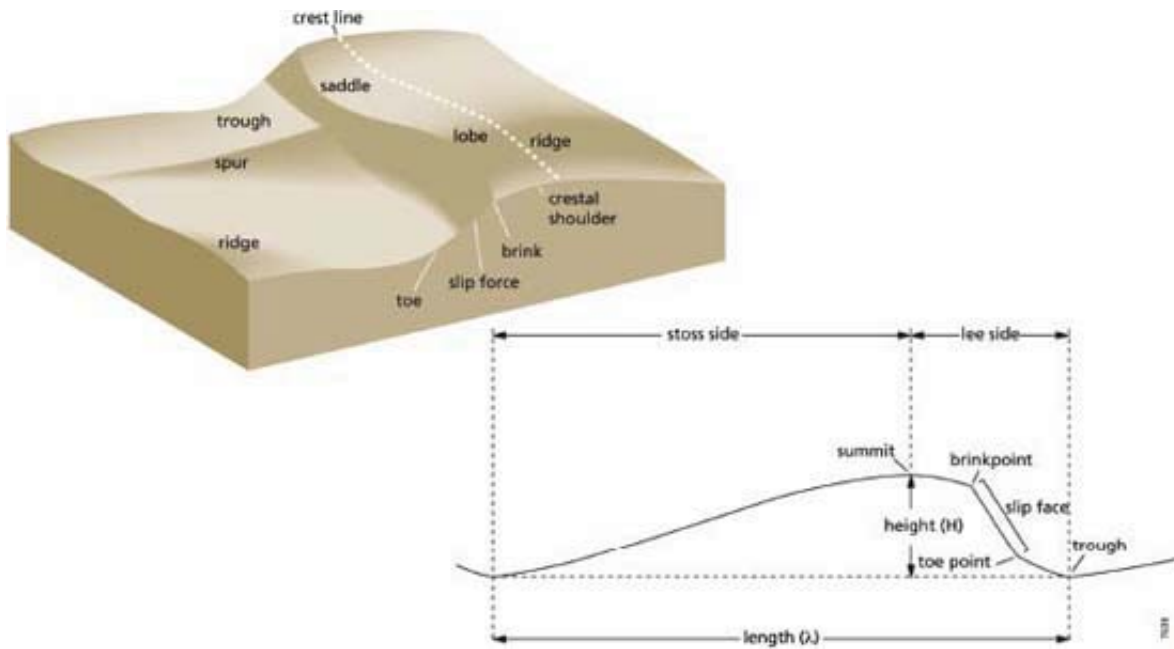


Figure 3.8. Dune morphology (Allen, 1984)

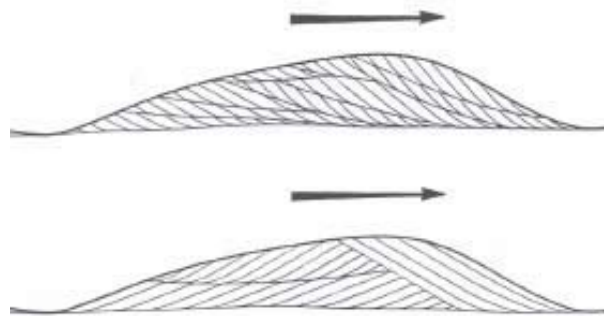


Figure 3.9. Dunes with form-concordant and form-discordant internal structure. Cross-stratification in the lowermost dune was formed in a period with opposite flow direction (Reineck and Singh, 1973).

Flow-separation and back flow

Flow separation occurs at the leeward side of all actively migrating ripples and dunes (Figure 3.12). The upper portion of the flow retains its forward position, while a *separation vortex* (or *eddy*) develops in the lower part. The flow pattern in the trough between two dunes can thus be divided into a zone of *co-flow* and a zone of *backflow*, where the current moves in a direction more or less opposite to the main flow. The relatively fine-grained deposits produced by backflow and *coflow* that accumulate in the dune trough is termed the *bottomset*, which is somewhat misleading as it is not a separate set but part of the crossbedded set. The difference in grain size between bottomset and *foreset* is generally quite obvious, especially when the bed load consists of coarse sand (Plate 1).

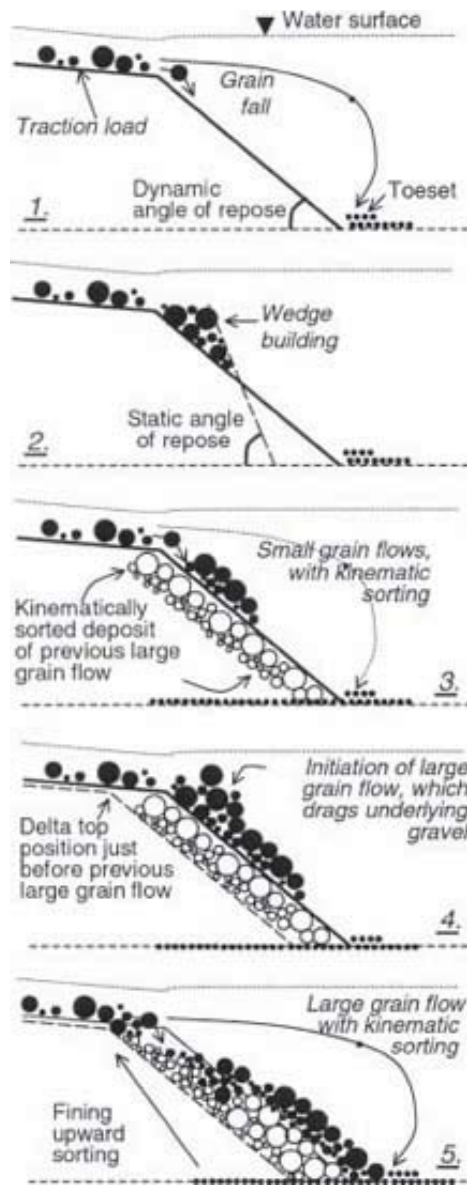


Figure 3.10. Deposition on the slip face of a sandy experimental delta, in case of no suspended load. Three stages are distinguished:

- A. (pictures 1,2): grain fall creating the sediment wedge and the toeset;
- B. (picture 3): small grain flows with kinetic sieving, generating a reverse graded stratum, and
- C. (pictures 4,5): large grain flow deposit that drag the top of the previous grain flow deposit downslope, leading to a fining upwards (Kleinmans, 2005a).

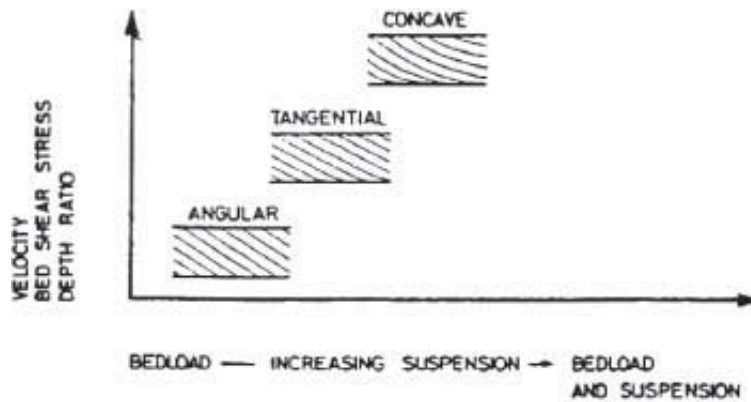


Figure 3.11. Scheme showing factors controlling the shape of foreset strata as suggested by Jopling (1965). Close inspection of the strata however learns that in the tangential or concave cross-bedding often an (angular) foreset and a bottomset layer can be distinguished (see Figure 3.13).

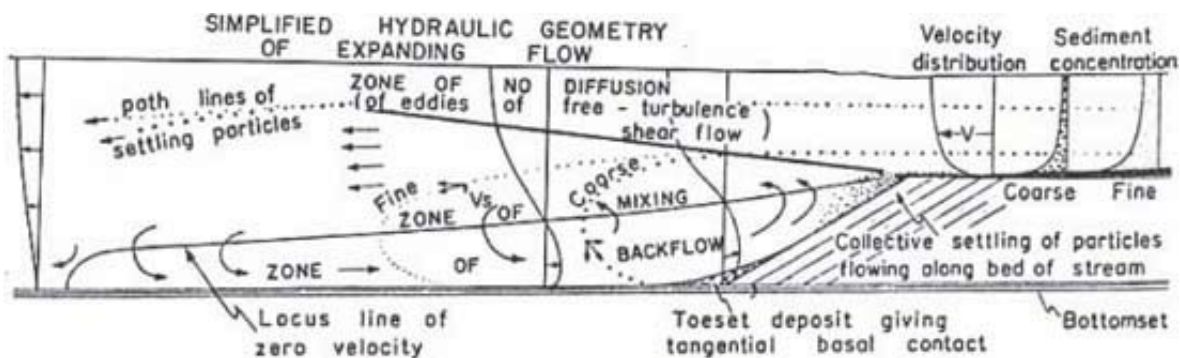


Figure 3.12. Geometry of flow over a dune with a long stoss side and accompanying change in suspended sediment and its effect on sedimentation on the dune's lee side (Jopling, 1963).

Bars

Ripples and dunes form fields of bed forms of about the same shape and size. Their occurrence is related to the flow strength and their size is small compared to the channel width. Bars are related to the flow pattern in plan view. They may or may not be arranged in a regular pattern. In a given environment, bars are generally larger than dunes and have a smaller height-to-length ratio. The surface of a bar may be covered by repetitive bed forms (dunes or ripples). The length of bars often is comparable to the channel width. Figure 3.14 shows examples of regular bar patterns. In plan view, some regular bed form patterns bear characteristics of bars and dunes: case C in Figure 3.14 could also be classified as a pattern of linguoid dunes depending on the length of the bed forms relative to channel width. Bars are not generally arranged in a regular pattern. The most typical example of a single bar is the elongated, streamlined accumulation that is formed in the shelter of an obstruction in the flow, such as a bunch of stranded tree stumps. Such a 'shelter' or *tail bar* is a special case of a *longitudinal bar*. Other types of single bars or *unit bars* are *transverse bars*, *medial bars*, *point bars* and *diagonal bars*. The latter three bar types may evolve from longitudinal bars or transverse bars, as

indicated in Figures 3.15 and 3.16. Point bars form accumulations on the inside of river bends. They are also referred to as *side bars* and *lateral bars* and may evolve from *alternate bars* (Figure 3.17 A and B). The types of bars that form within the channel are grouped together in the term *braid bars*. The overall geometry of point and braid bars is controlled by channel-forming (\cong bank full) discharge. At lower flow stages, bars may be dissected or remoulded (Figure 3.17 B and D). Bar erosion and bar deposition create changing gradients of the bed and water surfaces, which in turn may lead to the formation of new channels or *chutes*, which cut across braid bars and point bars.

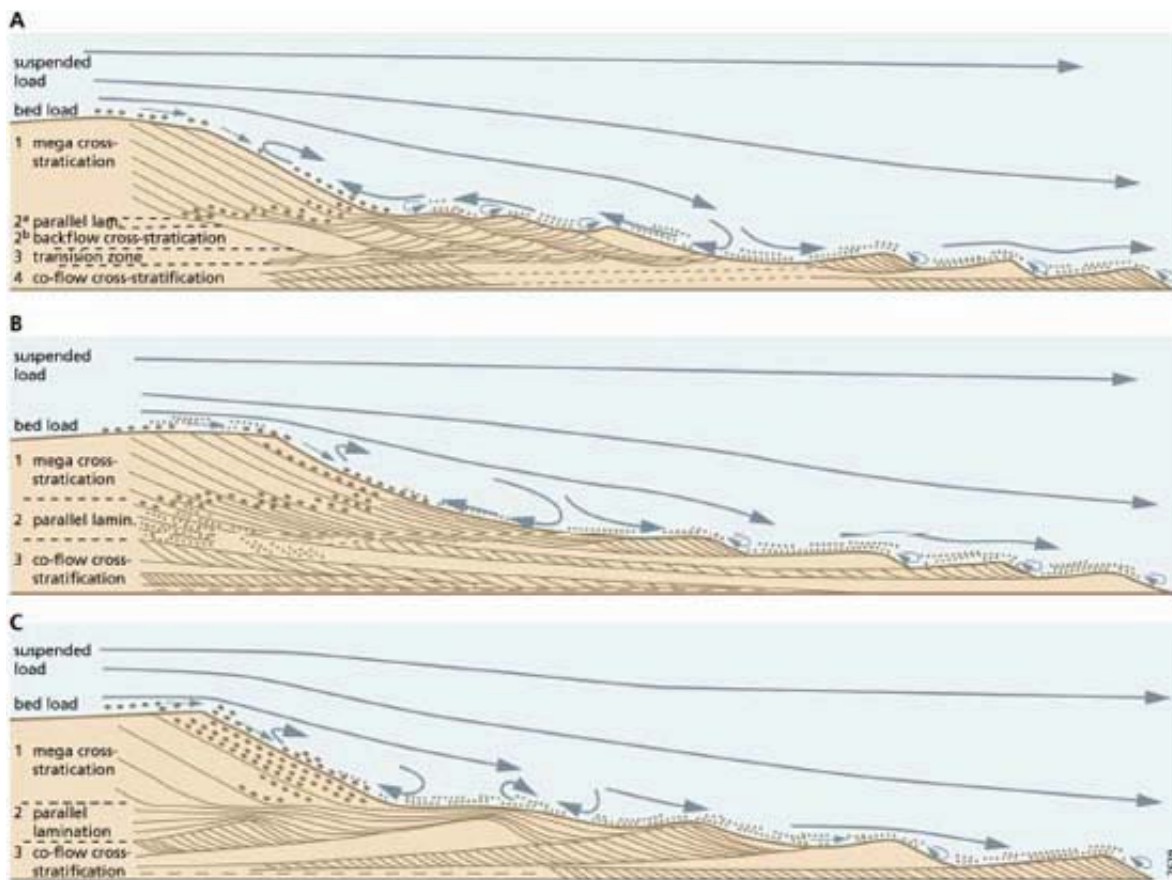


Figure 3.13. Three sedimentation models to visualize the generation of bottomsets in dune troughs. Flow strength decreases from A to C. A. Suspended grains raining down in the vortex area seized by the backflow and moulded into backflow ripples that may finally be capped by some parallel lamination close to the dune front: during periods with constructive backflow, the ripples climb the slip face and are eventually covered by grain flow avalanches. Under periodic less competent vortex activity, the backflow slows down and backflow ripples tend to degenerate and may be draped by some parallel lamination. B. Backflow incapable of forming ripples. The parallel lamination of the backflow merges away from the dune front into coflow cross-lamination. C. No well-developed vortex. Dune degenerates and the rough area starts to fill in. Coflow sets climb under the influence of the outfall of suspended sand and incompetence of the flow to transport it. Coflow ripples climb, with an increasing angle when nearing the dune slip face and eventually degenerate into parallel lamination before being covered by grain flows avalanching down the dune slip face (modified after Boersma, 1967).

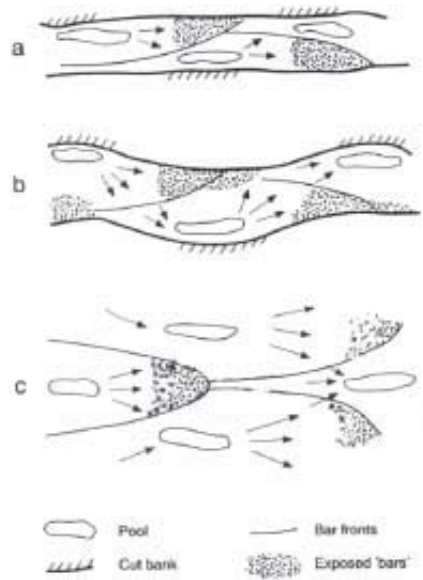


Figure 3.14. Regular bar patterns (modified after Knighton, 1998).

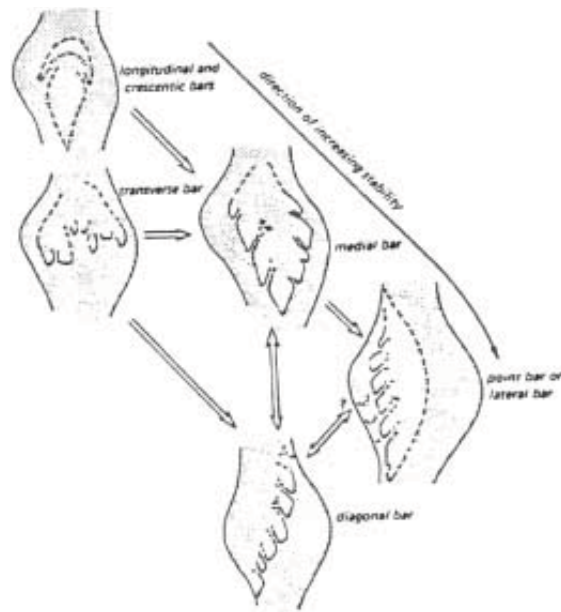


Figure 3.15. Unit bars, types and evolution (Church and Jones, 1982).

In cross-bedded sets it is often difficult or simply not possible to differentiate dune or bar origins. As the occurrence of bars is not related to the vertical flow structure, vortices in front of these bed forms are generally weak, as compared to conditions in front of dunes. Therefore, evidence of an incompetent backflow – such as in case C of Figure 3.14 – may point to a bar origin. However, degenerating dunes in decelerating flows also result in the same weak vortex conditions. Bars in rivers often reflect strongly depositional conditions. Therefore, preserved cross-stratified sets are probably

produced more often by bars rather than by dunes.

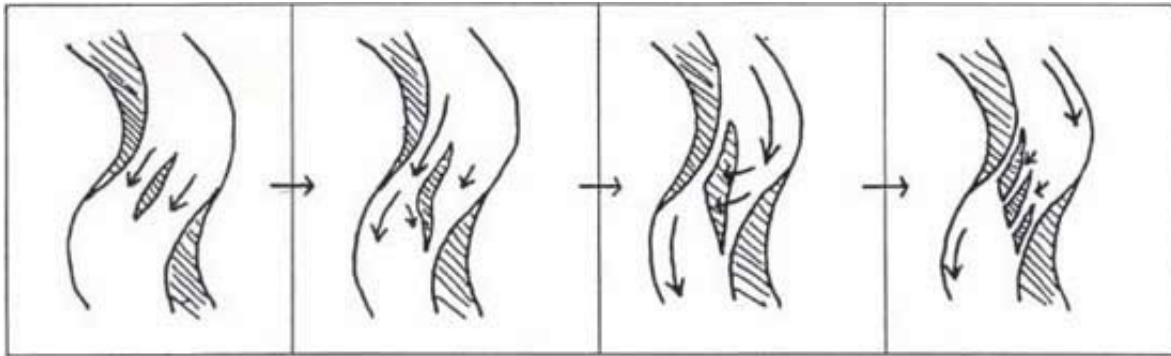


Figure 3.16. Evolution of longitudinal to diagonal bar.

At an outcrop, a large number of measurements of directions of maximum cross-bed inclinations produced by dunes is necessary to provide a good indication of the (palaeo) flow direction. As the front of bars is generally not perpendicular to the flow direction, measurements of the dip directions of bar cross-strata are less reliable flow direction indicators.

Terminology of cross-stratification

The internal structure produced migrating bed forms, regardless of their size, is called *cross-stratification*. The thickness of individual cross-strata depends largely on the size of the avalanches. Therefore, it is often possible to decide whether a ripple or a dune bed form produces a small-scale set. Many authors make a distinction between *cross-bedding* (here abbreviated as X-bedding) and *cross-lamination* (x-lamination). X-bedding is used for mm-cm strata produced by large-scale structures, produced by migrating dunes (mega-ripples) or bars; cross-lamination is used for strata of one mm or less than a mm thickness, which are produced by migrating ripples.

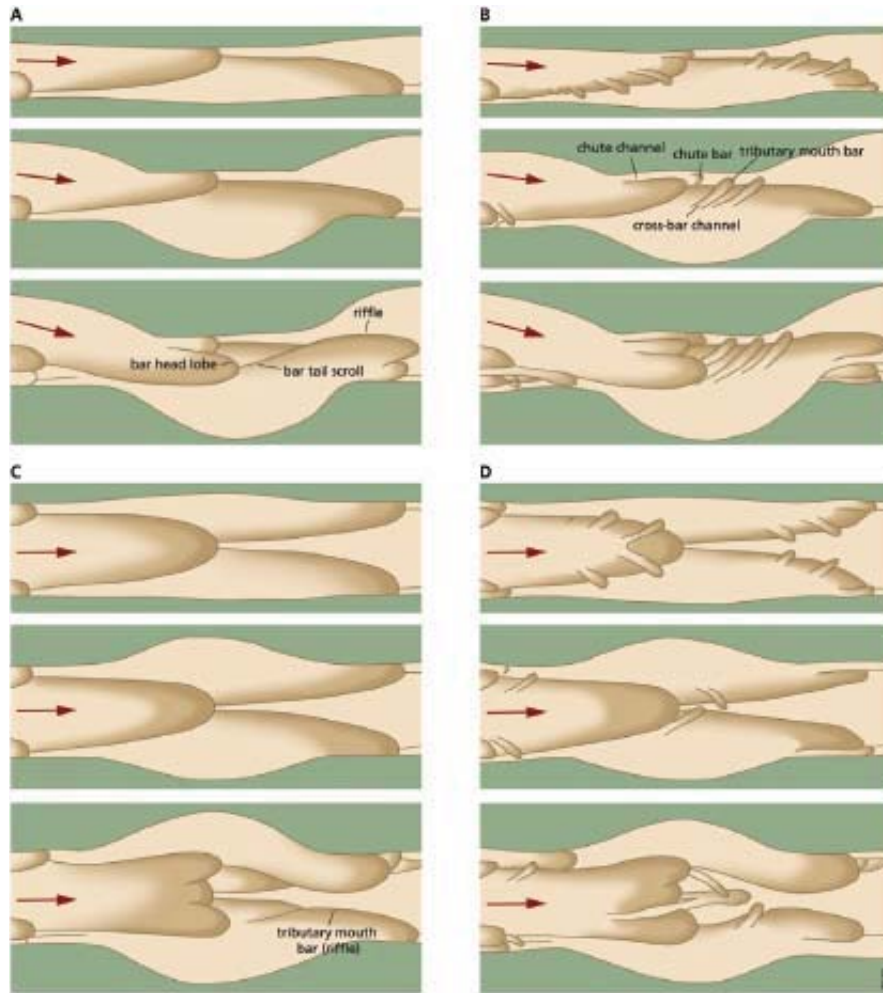


Figure 3.17. Idealized evolution of bar patterns resulting from bank erosion and channel widening. The crest lines of unit bars (represented by solid or dashed lines) may or may not be associated with angle-of-repose avalanche faces. Arrows represent flow directions and stippled areas are topographical highs.

- A. alternate bars (top) evolving to point bars (bottom);
- B. As for A, but with cross-bar channels (chutes) and associated channel mouth bars (*chute* bars), which may form a during the falling stage;
- C. Double-row alternate (linguoid) bars (top), evolving into more complex braid bars (bottom);
- D. As for C, but with chutes and chute bars, which may form during the falling stage (modified after [Bridge, 1996](#)).

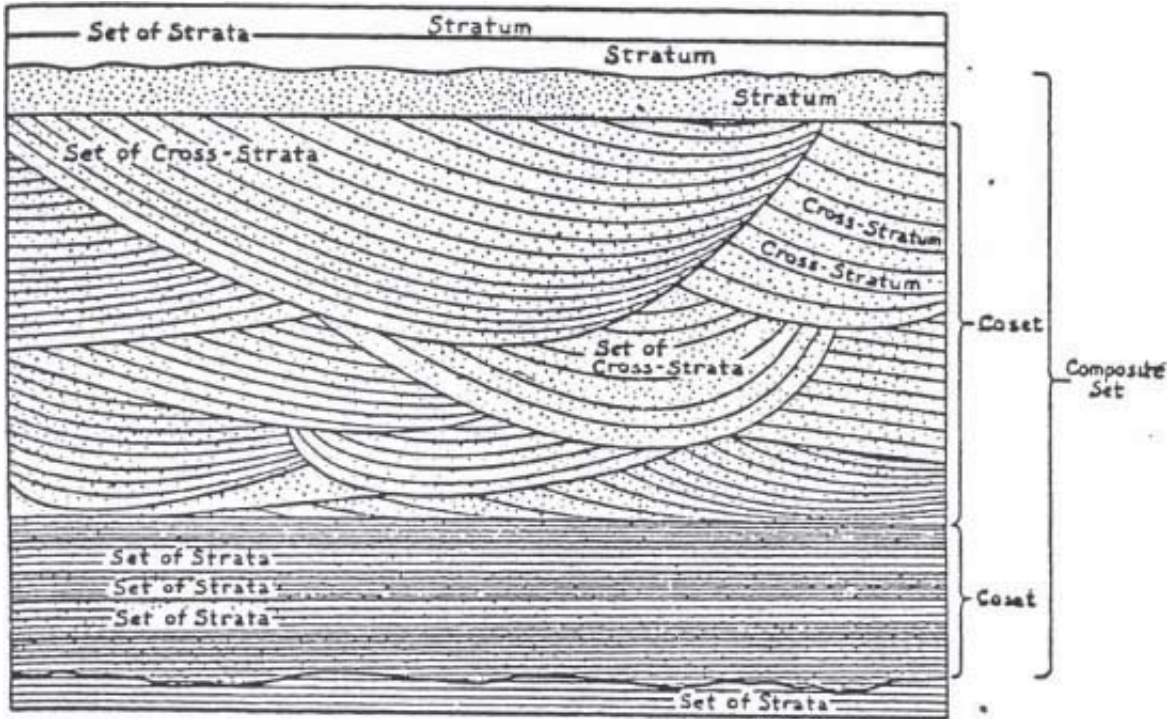


Figure 3.18. Bedding terminology according to McKee and Weir (1953).

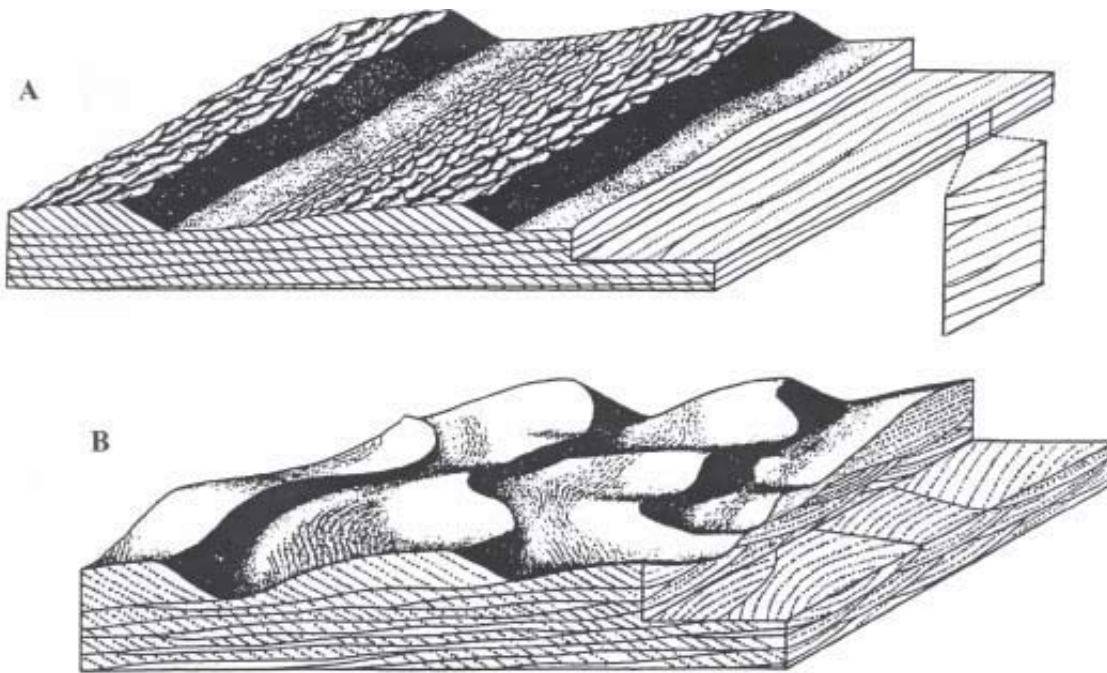


Figure 3.19. Block diagram showing X-bedding (A) produced by migration of straight-crested current dunes (the X-bedded sets are tabular in dip and strike section) and (B) produced by migration of linguoid dunes (the X-bedded sets are wedge-shaped in dip section and trough-shaped in strike section (Harms et al., 1982)). Similar set shapes are formed by 3D ripples (Plate 2)). Note that the presence of ripples on top of the bed forms in (A) indicates that in the presented situation the dunes are not stable and would disappear if the flow strength does not change in time!

The maximum thickness of a set of x-lamination is limited by the ripple height and therefore, does not exceed 4 cm. In cases where confusion might arise, it is advisable to add the adjectives large-scale or small-scale when referring to the size of the cross-stratified sets. The terminology of McKee & Weir (1953) is commonly used for the description of compound forms of cross-stratification (Figure 3.18). The basic unit is the *set*, which is a group of essentially conformable cross-strata, separated by surfaces of (slight) erosion, non-deposition or change in character. At the base of an X-bedded set an x-laminated suspension unit may be present (Figure 3.13 and Plate 1) and at the upper part a low-angle unit may be preserved, representing the area between brink-point and summit (see also Figure Plate 4 and 8). Although somewhat conflicting with the McKee and Weir terminology, it has become common practice to differentiate in a depositional unit produced by the migration of a dune a *topset*, representing the area between summit and brink-point, a *foreset* and a *bottomset* or *toeset* (Figure 3.13). Successive sets of similar character, which were apparently deposited by the same processes, are grouped together as *cosets*.

Three-dimensional form of cross-stratification

The appearance of cross-stratification in two-dimensional sections varies not only with the bed forms concerned, but also with the orientation of the section, with respect to the generating process. For a correct three-dimensional reconstruction of the original bed form type, it is therefore advisable to study several different. Three main types of sectioning are distinguished:

1. The *dip* section, which is more or less parallel to the main current direction. The largest and most consistent angles of dip of the cross-stratification can be observed in this section.
2. The *strike* section, which is parallel to the main elongation of the ripple crests, and therefore perpendicular to the general flow direction.
3. The *principal bedding-plane* section, which is cut parallel to the overall (palaeo) depositional surface.

The lower boundary of sets of cross-stratification may be *planar* or *curved* in dip section. In three-dimensional view, *tabular*, *wedge-shaped* or *trough-shaped* (festoon-shaped) sets may be distinguished. These set shapes usually represent different types of ripples or dunes (Figure 3.19).

Climbing cross-lamination

Whether or not the x-stratification produced by ripples is preserved, as well as its final appearance, depends on the rate of net sedimentation. At very small sedimentation rates only relatively thin sets will be preserved that may be too small to see any x-lamination. Although at first sight the structure might resemble upper plane bed (Figure 3.23) lamination, it can be distinguished by its faint and less straight appearance. At higher rates of net deposition, set thickness increases and x-lamination becomes visible. At still higher rates, the sets may adopt an inclined position with the foresets climbing in a down-current direction. This implies that the path followed by the crest of the ripple was no longer parallel to the depositional surface but ascending (Figure 3.20). This is understandable if we consider that the whole bed is subject to extensive net aggradation due to settling out from suspension. The above reasoning makes it clear that the angle of climb represents the ratio of vertical sedimentation versus ripple celerity. Thus a change in angle of climbing does not necessarily imply a change in sedimentation rate, it may also reflect a change of flow velocity and related ripple celerity.

At the highest values of this relative sedimentation ratio, the stoss-sides of the ripples are no longer swept clean by the current, thus leaving behind stoss-side laminae (Figure 3.21 and Plate 3). Climbing x-lamination is also known as: *ripple-drift* x-lamination. Note that a continuous package of ripple-drift lamination forms one set. Because of the relatively small volume of sediment in a ripple, the aggradation rates required to cause these bedforms to climb at relatively steep angles are not difficult to achieve in nature. In dunes with increasing aggradation, much similar structures are formed (Fig. 3.22). However, large dunes contain such large volumes of sediment that it is only rare that aggradation rates are large enough to cause the bedforms to climb at such a rate that part of the area above the brink-point is preserved and so-called *sigmoidal* strata are produced. In case of dunes made up of particles coarser than medium sand, a high aggradation rate is simply not possible, as bed material is transported in the bed-load mode and suspension outfall is negligible. Therefore, co-sets of X-stratification with large set-heights composed of coarse sand or gravel can only be attributed to deposition by successive (single) bars.

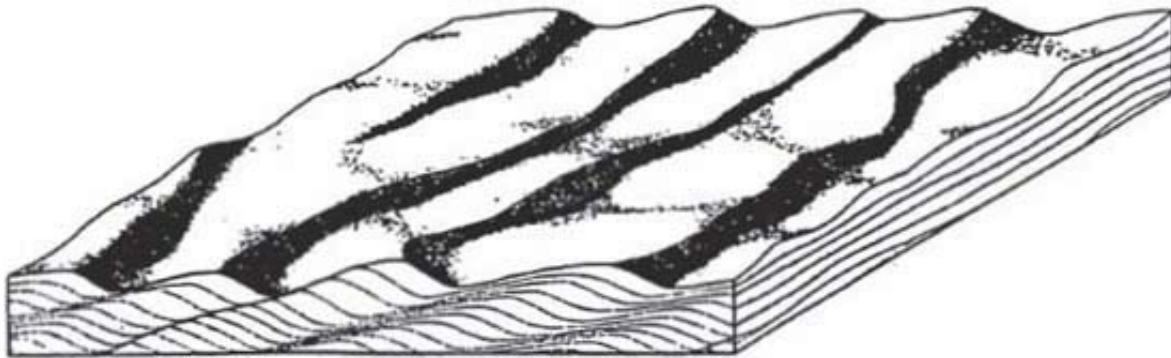


Figure 3.20. Climbing x-lamination produced by small current ripples receiving high quantities of sand from suspension.

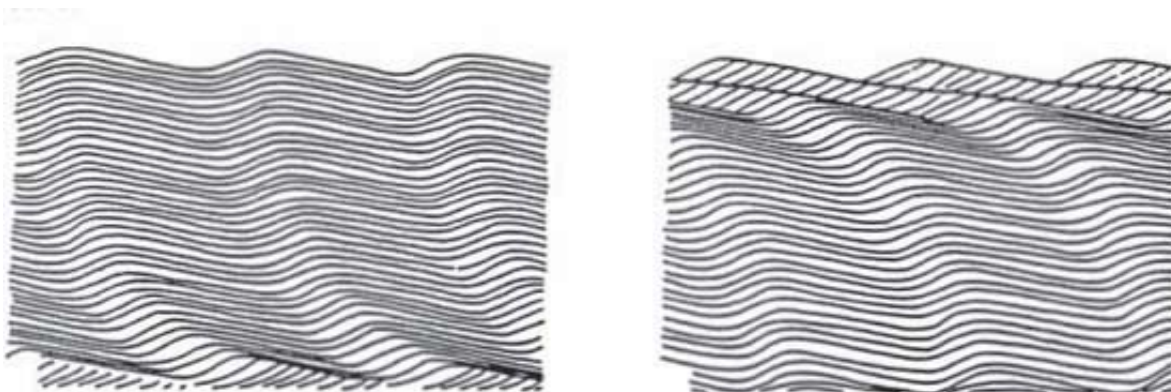


Figure 3.21. Transitions between x-lamination and ripple drift lamination, due to increase in time of spatial flow deceleration and or increasing suspension fall-out (left) and decrease in time of spatial flow deceleration and/or decreasing suspension fall-out (right).

Even lamination/bedding

Even lamination/bedding is also called *horizontal* or *planar lamination/bedding* in the geological literature. A large variety of genetically different stratification types are included in this class, all of which have in common that they have been deposited on a flat, more or less horizontal surface. Very good sorting of the original material and low relief of the bed forms may prevent the recognition of internal cross-lamination, as is often the case in eolian deposits. Four genetically distinct categories of even lamination generated by unidirectional flow may thus be distinguished (see also [Figure 3.5](#)):

1. High mobility plane beds (in any grain size of non-cohesive particles);
2. Low mobility plane beds (in sediments coarser than 0.7 mm);
3. 'False' plane beds: ripple migration without leaving traces of foreset lamination;
4. No mobility plane beds: settling from suspension without traction.

Even lamination can also be generated, as can certain types of cross-stratification by oscillatory (bidirectional, wave-generated) flow. Deciding on which genetic implication should be attached to even lamination is not an easy matter. Category 2 is probably rare, since it seems unlikely that thick deposits of this type will be preserved because of the low transport rates in this regime. Category 3 can sometimes be recognized by its association with small-scale cross-lamination. Category 4 occurs mostly in fine-grained sediments. When this lamination drapes over and fills pre-existing relief it is called *parallel* lamination. Category 1 is probably the most common. Bounding surfaces of planar laminae normally have discontinuous ridges and troughs, with a relief of a few grain diameters, that extend parallel with the flow for decimetres and have transverse spacing of millimetres to a centimetre or so. If outcrop conditions are favourable, this *current lineation* (also *parting lineation*) can be seen on bedding planes of this upper plane bed type structure ([Figure 3.23](#)). Also, thin (< 1 mm) lag deposits of concentrations of heavy minerals are a very characteristic feature of this type of planar stratification. Such heavy mineral patches, sometimes called *heavy mineral shadows*, may display a downstream decreasing gradient in the concentration of heavy minerals, which can be used, in conjunction with current lineation, to determine the paleoflow direction ([Cheel, 1984](#)). A typical feature of upper plane bed is the preferred orientation of sand grains with their long axes oriented parallel to the flow and dip, termed *imbrication* consistently into the current. In the case of pebbles the same imbrication is found, with the important difference that the long axes of the stones are preferentially not oriented parallel to the flow but perpendicular to it. Shells transported under upper plane bed conditions are deposited preferentially with their convex side upwards ([Plate 9](#)). It is stressed that even lamination produced during the upper plane bed state does not necessarily refer to (near) supercritical flow conditions ([Figure 3.5](#)).

Backsets

The upstream migration of antidunes, chute-and-pools and cyclic steps results in upstream directed cross-stratification, which is called *backset bedding*. The repeated growth and decay in a slightly different position of antidune trains means that there is some tendency for backset laminae for being accumulated in bundled, overlapping lenses. Rarely also downstream oriented laminae are formed ([Figure 3.24](#)). Backset lamination is of the low angle type and much less regular in spacing and slope than "normal" cross-stratification. The length of antidunes is proportional to the square of depth-averaged velocity ([Kennedy, 1963](#)), which in a general sense also means a proportionality with flow depth. Thus, in very shallow water antidunes are small and produce small sets. For instance, thin sheets of swash or backwash on a beach produces very small backsets that generally can not be

discriminated from the surrounding even (swash) lamination. Chute-and-pools and cyclic steps are more stable bedforms and their backsets are therefore more persistent. Backset stratification is rarely preserved as it represents high energy conditions and therefore generally areas of net erosion. As backset bedding is produced at conditions with supercritical conditions its presence in subaerial environments indicates shallow water. As will be shown later, backset bedding can also be produced by hydraulic jump related bedforms generated by turbidity currents.

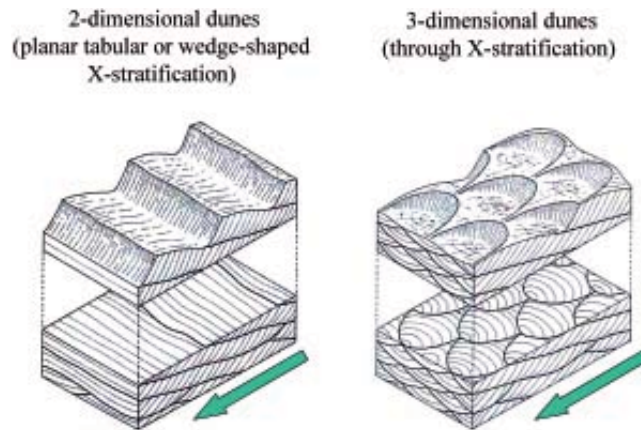


Figure 3.22. X-bedding produced by 2D and 3D dunes in dip and strike section (modified after Allen,1984). Note that climbing dune structures can only be generated by dunes of fine sand.

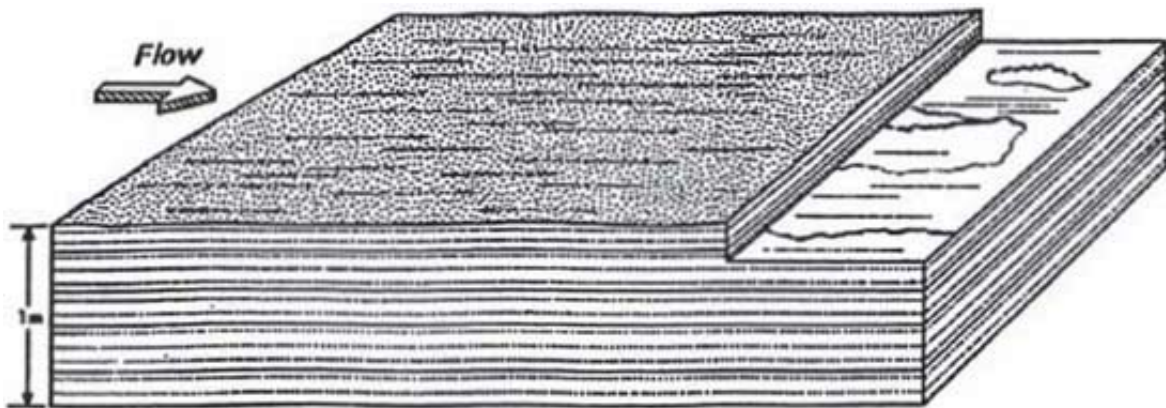


Figure 3.23. Planar lamination (also called even or horizontal lamination) produced by net deposition during upper plane bed conditions (see also Plate 4, 6 and 10). Note transport surfaces with current lineation and its counterpart on internal surfaces: parting lineation.

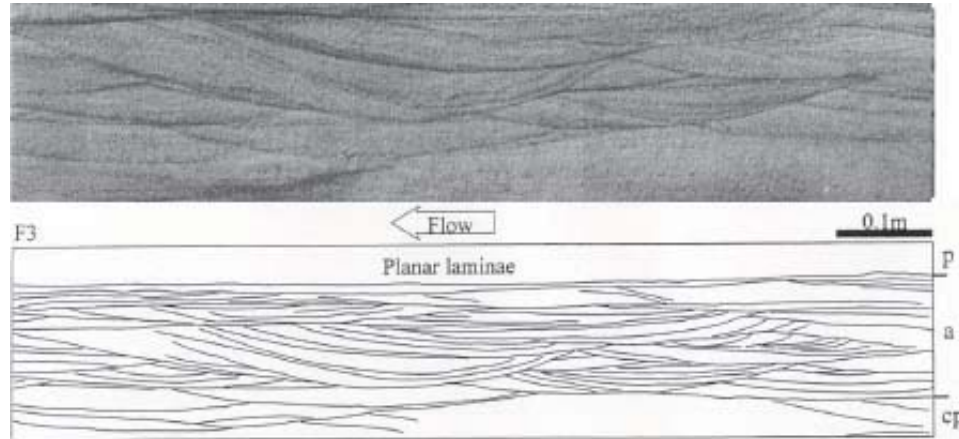


Figure 3.24. Sedimentary structures associated with plane bed (p), antidunes (a) and chute-and-pools (cp) in a flume experiment (flow depth 0.073–0.086 m, mean flow velocity $1.16\text{--}1.5\text{ ms}^{-1}$, median grain size 0.42 mm; after Alexander *et al.*, 2001).

Stratification types in unsteady unidirectional flow

If a flow decelerates, stops temporarily or reverses direction, distinctive bedding types may form. Circumstances under which this happens range in time from that of a pulsating unidirectional current in a river to regularly reversing tidal currents in marginal marine environments, such as estuaries and tidal flats. Pulsating uni- and bi-directional currents can be of three kinds:

- a. normal flow – deceleration – normal flow,
- b. normal flow – stop – normal flow, and
- c. normal flow – stop – reversed flow.

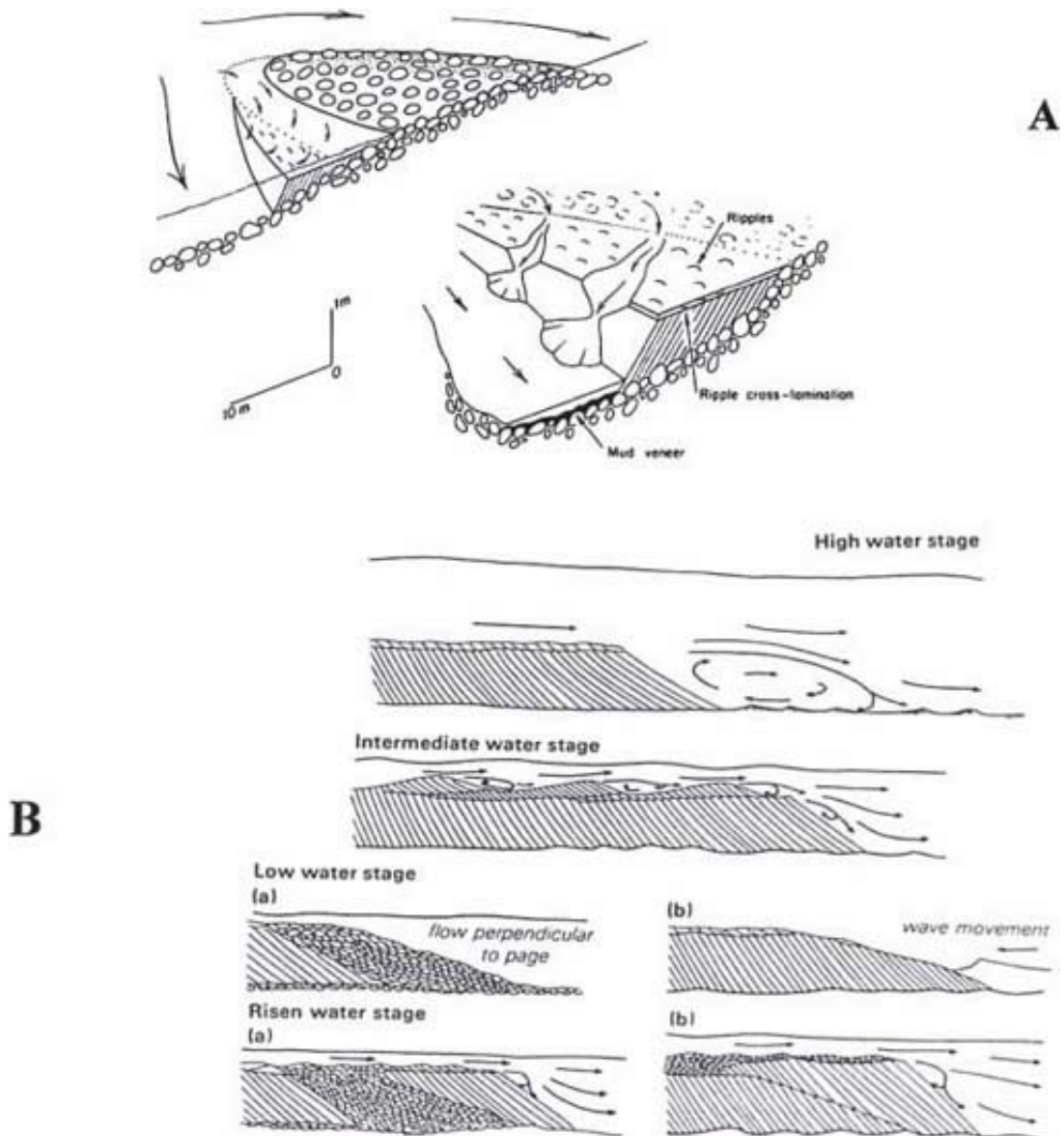


Figure 3.25. Structures formed along and in front of bars during a combination of deceleration of flow and lowering of water level. A: along the side of a gravel bar. Note the change in flow direction related to the emergence of the bar (Rust, 1971); B: in front and along the sides of sand bars (Collinson, 1970).

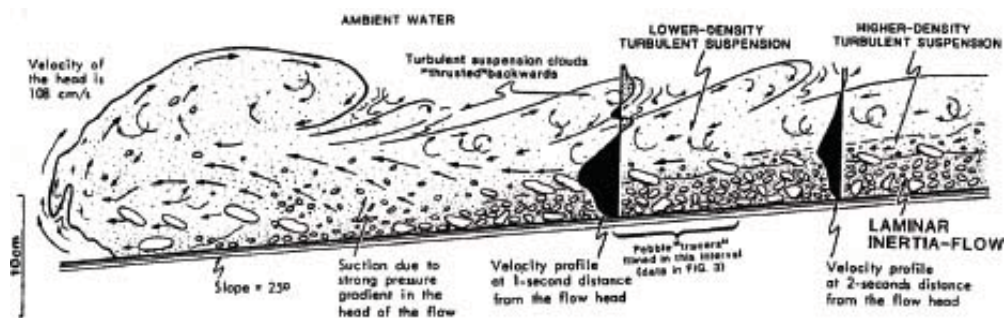


Figure 3.26. A profile of the head of an experimental density-stratified turbidity current. Laminar inertia flow = basal laminar layer (Postma *et al.*, 1988).

These types of flow are most prominent where the resident bed form is of a large scale, meaning that average flow strength exceeds the ripple phase. A current of type (a) produces cross-strata in front of a large-scale bed form (dune or bar) during conditions of normal flow. Toward the end of this episode, grain size may decrease and small ripples may start to descend the lee-side slope. Doing so, these ripples may locally erode the lee-side of the bed form, especially its upper portion. The resultant surface, which at least locally is non-concordant with the underlying cross-strata, is known by different terms: *discontinuity plane*, *set-interruption plane*, *pause plane* or, most frequently though less appropriate, *reactivation surface*. If current velocity drops sufficiently, this reactivation surface may be covered by mud settling from suspension. During this ‘slack’ stage, a thin mud drape may be formed. As the flow resumes its normal flow-strength, i.e., the acceleration stage, at first the lee-side slope may again be a site of erosion before full-height foreset construction resumes. During this acceleration of flow, the mud-drape is often partially or wholly eroded, especially the upper part of the lee-face (see also Figure 4.16). If the current comes to a complete stop, mud deposition is likely to produce thicker drapes that more readily resist successive erosion. In rivers, a stop-phase often means a low discharge at which bars are partly exposed. The bar front slope may then be eroded by gullies or waves and a reactivation surface is produced, as lateral growth increment of the bar at high flow resumes (Figure 3.25 B). In the case of a gravel-bed river during the waning flood, sand transport may continue for some time while gravel transport is ceased and a wedge-shaped cross-stratified sand accumulation is formed (Figure 3.25 A).

Influence of excessive suspended load on bedforms and sedimentary structures

Evidence from a large amount of data from medium to large sand-bed rivers indicates that with increasing flow strength, the hydraulic roughness of fluvial dunes diminishes, whereas dune height hardly changes (Van Rijn, 1984; Julien and Klaassen, 1995). This points to a reduction of the size and shape of the flow vortex downstream of dunes with increasing flow strength. This in turn can only be caused by a lowering of the brink-point, at the start of flow separation at the lee-side of dunes (see Figure 3.13). A lowering of the brink-point during an increase in flow strength was assumed for preserved sedimentary structures in ancient deposits of fluvial dunes by Røe (1987) and Fielding (2006) and established for recent intertidal dunes of the Scheldt estuary (i.e., Boersma and Terwindt, 1971; Van den Berg *et al.*, 1995). This lowering of the brink can be considered as an initial stage in a transition of dunes to upper-plane bed, caused by damping of turbulence by suspended bed material (Bridge and Best, 1988), due to several mechanisms, i.e., buoyancy caused by a high near-bed gradient of suspended bed-material and in the moving bedload layer (Allen and Leeder, 1980). However, a full understanding of the phenomenon, which was already noticed in flume experiments by Jopling (1966), is still not available. The lowering of the brink-point is followed by a lowering of the bedform height but this process lags far behind and even after virtual disappearance of the vortex and the avalanche slip face, more or less sinusoidal dunes may last for a long period. Flood waves in large sand-bed rivers such as the Mississippi are generally too short to completely transform the sinuous bedforms into plane beds. The resultant structure is known as *sinusoidal (cross)-stratification* and, in its extreme form, *large-scale wavy stratification*.

The consequence of the above reasoning is that if a flow with near-bed *hyperconcentrated flow* (i.e.,

suspended load concentration typically larger than 1–3 % by volume) passes over a plane bed, no dunes will be formed. Such is the case in *turbidity* currents, in which the driving force is created by the density difference between the near-bed suspension flow and the overlying fluid on a sloping bed surface. The suspension of sediment in a turbidity current is, like flow in a river, mainly sustained by fluid turbulence. This turbulent Newtonian flow often drives a much slower-moving, several centimetres thick basal laminar layer (Fig. 3.26) with a plastic behaviour (debris flow) that is often denoted as *traction carpet*. Turbidite currents are the most important transporters of sand and coarser grained sediments into deep-marine environments. Their deposits are called *turbidites*. After the passage of the head of the turbidity current, the flow intensity gradually declines. This is usually reflected in the vertical sedimentary sequence of an individual turbidite, such as the classical *Bouma sequence* (Bouma, 1962); Fig. 3.27). From the base upwards, it consists of a structureless, coarse-tail graded basal unit (Ta) followed by plane bed lamination (Tb), small-scale ripple sets (Tc) and silt lamina formed by low shear and suspension fall-out (Td). The unit is covered by a hemi-pelagic graded mud unit (Te). The sequence demonstrates clearly the absence of a stratal layer, displaying X-bedding in between Tb and Tc. Apart from the influence of buoyancy and related damping of turbulence as a reason for the absence of dune formation, two other factors may be important. The residence time of the turbidity current to generate dunes (possibly several tens of minutes to several hours) may have been too short (Allen and Friend, 1976; Baas, 2004) or the grain size of the suspended sand was beyond the existence field of dunes. The latter is supported by the fact that the hyperconcentration increases the apparent viscosity of a flow. The effect is comparable with a lowering of the water temperature. It results in a reduction of the Bonnefille parameter, D_* , and therefore, a shift of the limit of dune formation to a somewhat larger grain size (see also Fig. 3.5).

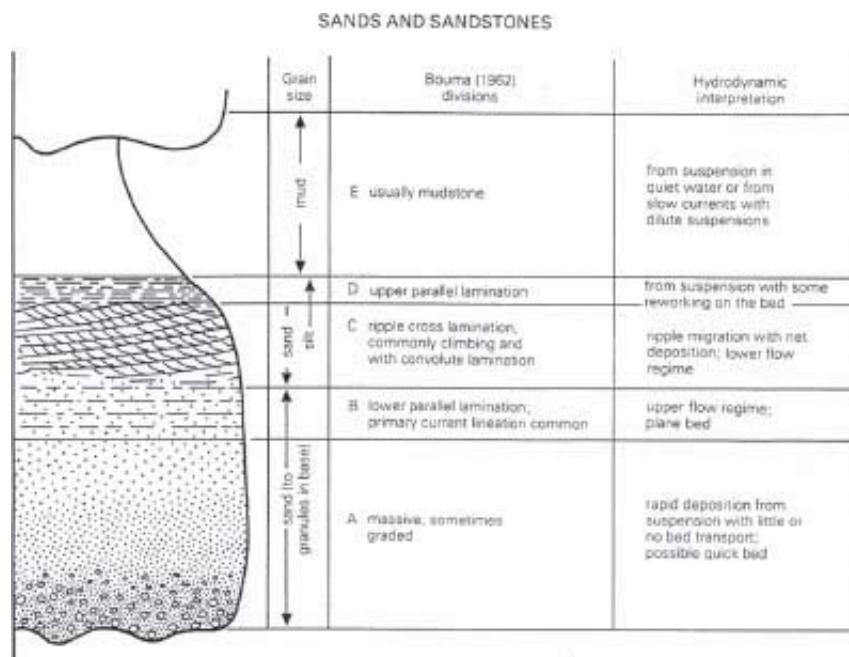


Figure 3.27. The Bouma turbidite sequence and its conventional hydrodynamic interpretation (after Collinson and Thompson, 1989).

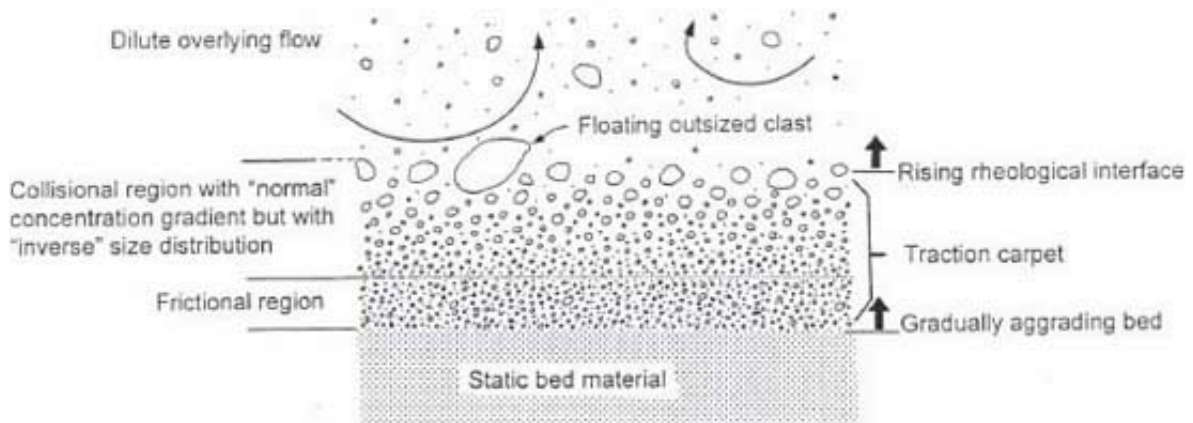


Figure 3.28. Deposition from a traction carpet (Sohn, 1997). The interface between the collisional layer and the overlying fluid is characterized by a sharp drop in the concentration of suspended grain particles.

Traction carpets commonly develop beneath rapidly dissipating turbulent sediment flows. Such conditions are met in turbidites but also in subaerial hyperconcentrated flows and typically show sediment concentrations larger than 9 vol % (ca 15% of the packed-bed; Sohn, 1997). Suspension is supported mainly by grain collisions and *hindered settling*. The latter refers to the reduction of settling velocity of the grains by water that has to “escape” upwards before settling can become effective. Traction carpets can be divided into two regions. In the upper region, grain collisions are important. At a concentration above 80 vol %, particles cannot move freely and independently from their neighbouring particles and collisions between grains are replaced by the rubbing motions of contacting grains in the lower layer (Fig. 3.28). Because greater collisional forces are generated between larger grains (*dispersive stress*), these grains tend to disperse more upwards, resulting in an inverse grading within the upper collisional layer of the traction carpet. Depending on the variation of the grain size of the supplied sediments, deposits of traction carpets may show fining upwards or coarsening upwards trends (Fig. 3.29 C). However, a prominent feature of traction carpet deposits is inverse grading, which seems to result from the vertical density gradient in the collisional region. When deposition occurs directly from the collisional layer, for instance due to large temporal fluctuations in the flow, the inverse grading of this layer may be preserved (Fig. 3.29 D,E). Inverse grading in traction carpets is more common in coarse-grained deposits (Sohn, 1997). Exceptional large clasts relative to the bulk of the grains are preferentially pushed towards the upper part of the traction carpet. They move along the rheological interface, partly submerged in the underlying regions, under intense shear stress and lift force exerted by the overlying fluid (Postma et al., 1988).

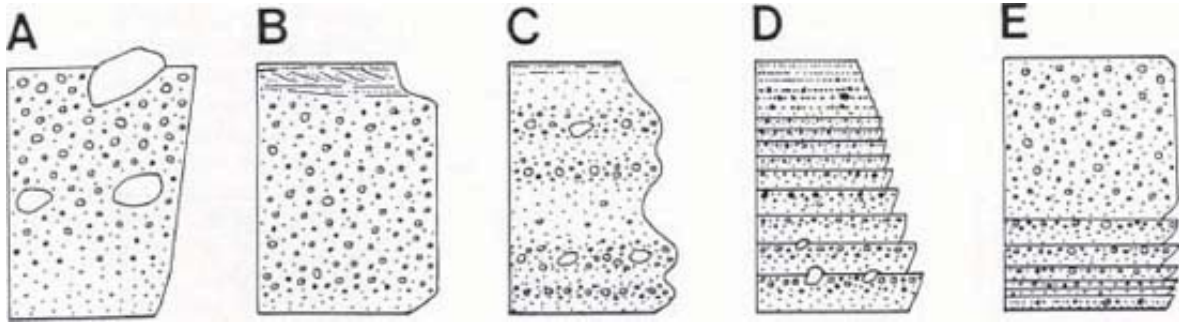


Figure 3.29. Schematic drawings of various deposits that can be produced by traction-carpet sedimentation. A. thick-bedded and inversely graded, B. thick-bedded and massive, with only the basal part inversely graded, C. diffusely stratified, D-E. thinning- or thickening-upward stratified, depending on the duration and character of a traction carpet and the overall flow characteristics. The thicknesses are not to scale and can be very variable (Sohn, 1997).

If the thickness of a turbidity current or a lower part of it, is well defined by a sudden transition to a much more diluted overlying fluid, super- and subcritical flow conditions can be distinguished by the *densimetric* Froude number, Fr' :

$$Fr' = \frac{\bar{u}_f}{\sqrt{g'h_f}} \quad (-) \quad (3.3)$$

where \bar{u}_f and h_f are the velocity and thickness of the flow respectively and g' is the buoyancy-reduced gravitational acceleration,

$$g' = \frac{\rho_f - \rho}{\rho} g \quad (\text{ms}^{-2}) \quad (3.4)$$

ρ_f is the bulk density of the flow, and ρ is the density of the overlying fluid. Many turbidites that originate in submarine canyons will be supercritical, and the densimetric Froude number here may reach the maximum value $Fr' = 2.8$. Above this value Kelvin-Helmholz instabilities develop at the interface of the flow with the overlying fluid, causing an intensive mixing, increasing its flow depth and thereby reducing its Froude number (Mastbergen and Van den Berg, 2003). Reduction of the slope at some point brings the densimetric Froude number close to unity, which will force the flow to pass through a hydraulic jump in order to reach the subcritical state. In the case of a long persisting steep slope relative to the thickness of the turbidity current, it is suggested that after a hydraulic jump, the flow may accelerate and return to supercritical (Massari, 1996), which might result in a series of chute-and-pools or cyclic steps (Van den Berg *et al.*, 2002). Evidence of the existence of such trains of cyclic step bedforms was provided by successive side-scan sonar views of the seabed of Monterey submarine canyon, Pacific coast of California, which clearly showed the upslope migration of cyclic-step type bedforms that could only be formed and reactivated by turbidity currents (Fig. 3.30).

It is not known how cyclic steps in turbidity currents are initiated but the analogy with their subaerial occurrence and some evidence from flume experiments (Spinewine *et al.*, 2009) suggests an evolution starting from antidunes. Small-scale hummocky cross-stratified units (see page 57) that are sometimes

found in Bouma Tb and Tc divisions are generally attributed to antidunes (e.g., [Prave and Duke, 1990](#); [Mulder *et al.*, 2009](#)). So far, evidence of gravity flow-related backset bedding produced by cyclic steps or chute-and-pools from detailed sedimentological descriptions is restricted to small channelized turbidites that were generated on a steeply sloping Gilbert-type delta ([Massari, 1996](#)) or the steep face of a barrier spit-platform front ([Nielsen *et al.*, 1988](#)). The structures are an order of magnitude larger than backsets produced in subaerial conditions and consist in convex upward stratified sets with an irregular erosive base that cuts into the giant avalanche foresets of the delta or barrier spit structure ([Fig. 3.31](#)).

Backset strata show a remarkably strong downstream fining, which can be explained by the sudden reduction of flow competence after the passage of the hydraulic jump. Imbricated gravel particles provide evidence of the flow that climbs the chute or step on which the backsets are deposited. At present, there are no criteria to decide whether these backsets are produced in a (single) chute- and-pool or cyclic step morphology.

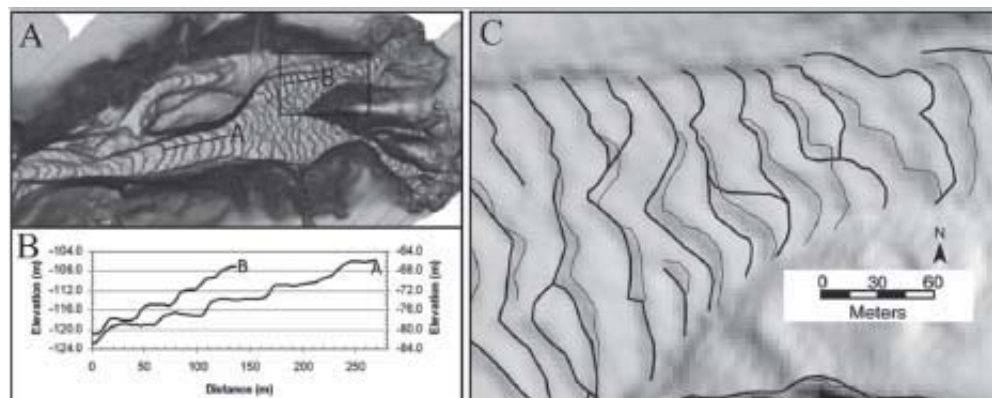


Figure 3.30. A. Bathymetry of the upper reach of Monterey Canyon, USA; B. Bedform profiles; C. Plan view of cyclic step terrace edges. Dark and grey lines indicate their position on September 17, 2004 and on November 19, 2004, respectively (after [Cartigny *et al.*, 2010](#), modified after [Smith *et al.*, 2005; 2007](#)).

Close inspection of Bouma Ta teaches us that in many cases this division is not completely structureless but contains some vague stratification. In case of the absence of any lamination, this indicates that flow traction was lacking ([Baas, 2004](#)). Based on a comparison of sedimentary structures produced in flume experiments, [Postma *et al.* \(2009\)](#) postulated that normally graded, structureless Ta units represent the sudden deposition at the hydraulic jump, where near-bed flow velocities are low. This interpretation is supported by the rip-up clasts and flame structures that may be found at the base of Ta, which can be explained by strong under-pressures at the bed that accompany the hydraulic jump ([Fig. 3.32](#)).



Figure 3.31. Backsets generated downstream of a hydraulic jump in turbidity current on the steep front of a prograding spit platform, Northern Jylland, Denmark (see also [Nielsen *et al.*, 1988](#)).



Figure 3.32. Flame (red arrows) and antidune structures (dotted lines) in the Bouma Ta interval of a turbidite sequence ([Postma *et al.*, 2009](#)).

4 Influence of Wave Action on Bed Forms and Sedimentary Structures

Wave action

Waves on seas or lakes are generated by wind. The size and shape of the resulting wave pattern depends on strength and duration of the wind and on the *fetch*, the length over which the waves are generated. When initially formed, the waves have a large variety of sizes, shapes and periods. Large ocean waves can travel over distances of thousands of kilometres away from the source of wave generation with no significant loss of energy. After some time and with increasing distance from the area of formation, the waves are sorted out into a more regular, long-period pattern called *swells*. Where surface waves travel through deep water, the water column is set into an orbital motion. In approximately sinusoidal (swell) waves, each water particle essentially describes a closed orbit. At the surface, the amplitude of orbital motion is equal to the wave height. From the average water surface, the orbital velocity and orbital diameter decrease exponentially downwards (Figure 4.1). Approaching shallow waters, e.g., where reaching a coastline, at a certain point, the *wave base* starts to ‘feel bottom’. Although the wave base is usually taken at a relative depth $h/L = 0.5$, wave – bottom interaction does not occur until $h/L < 0.25$. Figure 4.4 shows the change of near-bed maximum orbital velocity \hat{U} , as computed for irregular, natural waves that approach the SW part of the Dutch shore (Ribberink and Al-Salem, 1991). The solid lines in Figure 4.4 show the change if near-bed oscillation remained symmetrical. However, as the waves move into shallower water, the wave profile changes from sinusoidal to a shape characterized by a broad shallow trough and a narrow, peaked crest, termed a *solitary* wave. In addition, the orbital motion of the wave, after first touching bottom, changes from a harmonic orbital motion to an increasingly disharmonic elliptical motion (Figure 4.2). At the water sediment interface, the circular movement is reduced to a disharmonic to-and-fro motion with a short-lasting strong forward stroke and a longer but weaker backward stroke, which, in case of a horizontal bed, results in a sand transport in the direction of wave propagation (Figure 4.3).

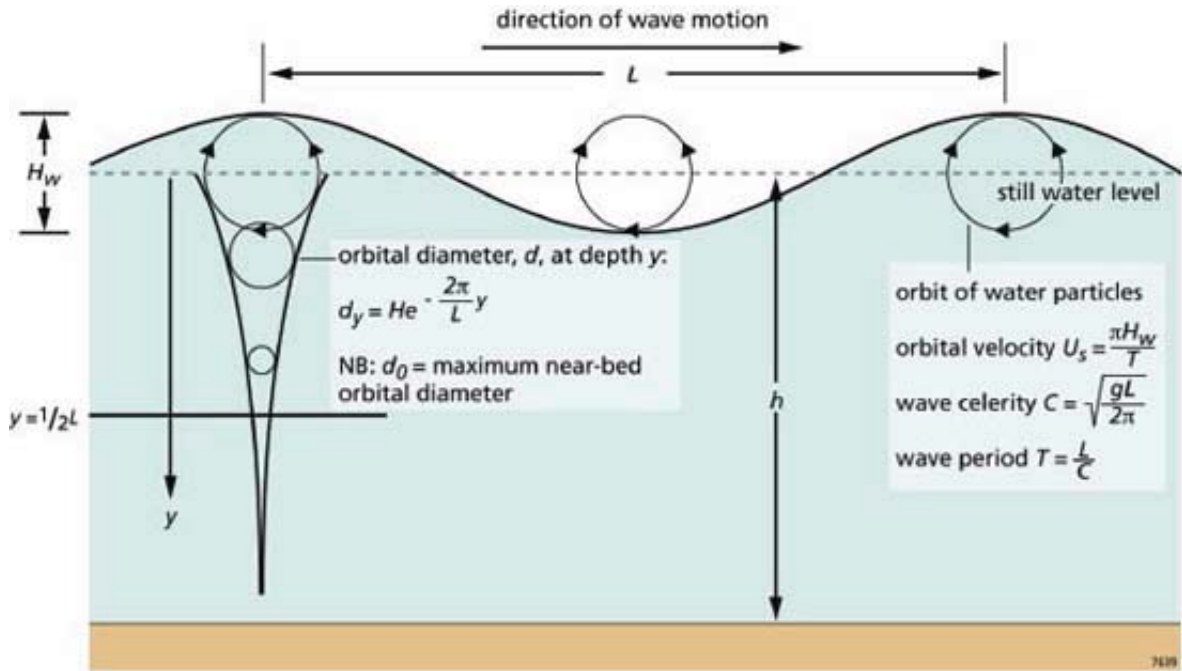


Figure 4.1. Definition diagram for oscillating sinusoidal wave in deep water ($h > 1/2 L$).

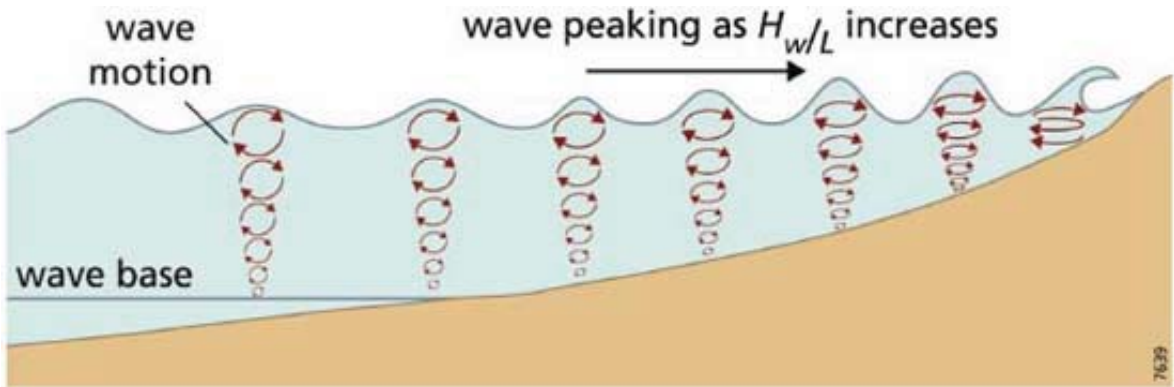


Figure 4.2. Waves approaching the shoreline (modified after Carter, 1988).

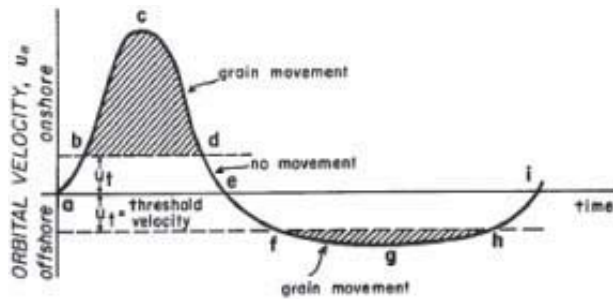


Figure 4.3. Asymmetric near-bed oscillation and grain movement due to wave deformation in shallow water (Komar, 1976).

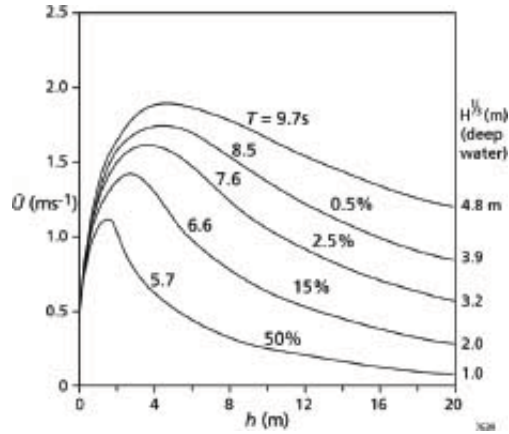


Figure 4.4. Near-bed orbital velocity amplitude, \hat{U} of shoaling propagation increases waves at several values of deep-water significant wave height, according to linear wave theory, modified after (Ribberink and Al-Salem, 1991). Percentages refer to depth. In very shallow annual occurrence along the Dutch coast. water, the propagation.

In shallow water, e.g., when $h/L < 0.25$, the propagation velocity (celerity) of waves decreases with water depth. In very shallow water the wave celerity, as seen from an observer from a fixed point, C , is determined by the *Surge Froude Number*, Fr^* :

$$Fr^* = \frac{C + \bar{u}}{\sqrt{g(h_t + H_w)}} = 1 \quad (4.1)$$

where h_t = water depth below the wave trough and \bar{u} = depth-averaged velocity of the oppositely directed current. With increasing opposed flow velocity, the propagation velocity of the waves decreases, i.e., as long as the waves do not become unstable and break, the sum $C + \bar{u} \cong$ constant.

Shoaling waves increase in height, H_w , until they break at a value in the range of $1.3 < H_w/h_t < 0.4$. Shoaling waves generate positive surges or bores after breaking. The Froude number, Fr^* , of *bores* is somewhat larger than unity. On shallow shoaling slopes, *spilling* precedes the actual breaking. Spilling starts at the wave crest and gradually envelops the whole wave front. Spilling continues over distances of up to several wave lengths. In this case, little of the turbulence created reaches the bed. On steeper slopes, *plunging* waves are found (Figure 4.5). Plunging is a far more violent process, energy dissipation is concentrated in a smaller zone and much more turbulence reaches the bed. The type of breaker partly depends on the grain size of the bed material, as the slope of the beach face is generally steeper in coarser sediments. Not all the energy of waves is dissipated and transformed into heat during breaking. Part of it is transformed into *wave-induced* currents, such as longshore and rip currents in the nearshore zone. As a matter of fact, waves occur generally superimposed on the practically omnipresent unidirectional flow, producing *combined* flow. Even in lakes, wave action without a flow component is rare, as currents are likely to be formed simultaneously with waves by wind shear and transformation of wave energy into (unsteady) flow within the breaker zone. In the case of a steep

beach face and plunging being the dominant breaker type, a relative large part of the wave energy is reflected back to the sea (*reflective* beach); in the opposite case, with surging breakers on a gently sloping surface, the beach condition is called *dissipative*.

Bed forms generated by waves and combined flows

The oscillatory motion of water over a bed of loose granular material produces ripples as soon as the boundary shear stress (or near-bed velocity) is large enough to move sand-sized particles. For particles < 600 μm , the critical threshold condition is given by (see also [Figure 4.11](#); Komar and Miller, 1973):

$$\frac{\rho \bar{U}^2}{(\rho_s - \rho)gD_{50}} = 0.21 \left(\frac{d_0}{D_{50}} \right)^{0.5} \quad (4.2)$$

where d_0 is near-bed oscillation length.

The first bed forms that appear are *rolling grain* ripples. Rolling grain ripples are small straight-crested patterns with gentle slopes. The crests are oscillating with the flow. They are transient patterns that after some time ([Figure 4.6](#)) grow into *vortex* ripples (the ‘classical’ wave ripples, see also [Figures 4.7](#) and [4.8](#); Rousseaux, 2006). These have steeper sides, with characteristic lee-side eddies where the flow separates. Each time the flow reverses direction, the vortex moves to the other side of the ripple. Coarse sediment avalanches over the lee-side, while finer sediment may be taken in suspension by the vortex, which rises into the higher parts of the flow, each time the flow reverses direction ([Figure 4.7](#)). The height of these sand fountains may be several dms and is proportional to the shear velocity related to the maximum orbital velocity. With long oscillation periods (swell waves), asymmetrical ripples, comparable to current ripples, may develop. They alternately change their direction of migration when the orbital velocities in both directions are large enough (*reversing crest* ripples), but may also migrate essentially in one direction when the velocity distribution is unequal, due to wave asymmetry or a superimposed unidirectional current. The latter ripples are generally called *asymmetrical* wave ripples. *Symmetric* wave ripples have a vertical form index, λ/H , generally between 2.5 and 5, asymmetrical ripples are more flat, with an index between 5 and 10, which is still much steeper than current and wind ripples, which generally have indexes between 10 and 40 (see also [Figure 7.4](#)). With a further increase in the intensity of the oscillatory flow, the vortex ripples become flattened off, forming low-steepness bed forms with rounded profiles, known as *post-vortex* ripples. They appear to form a transition between vortex ripples and a plane bed characterized by very high sediment transport rates. ([Figure 4.10](#))

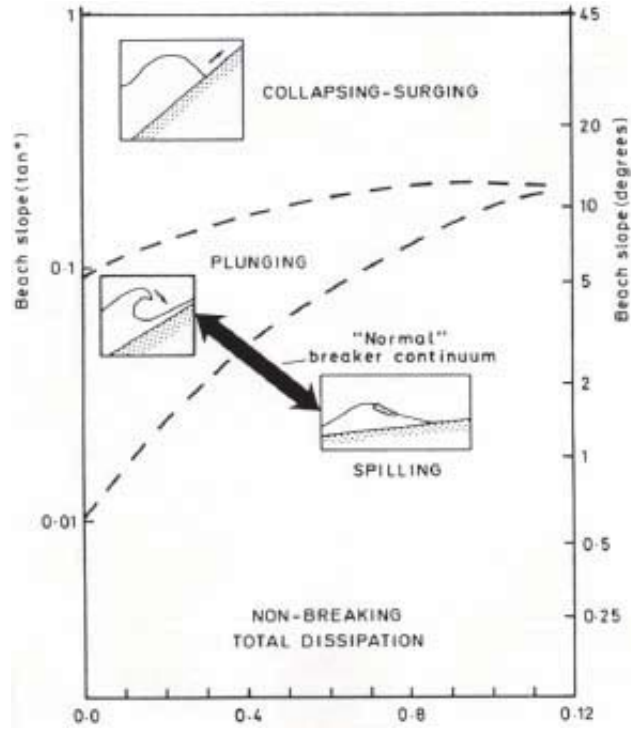


Figure 4.5. Breaker types as related to beach slope (Carter, 1989).

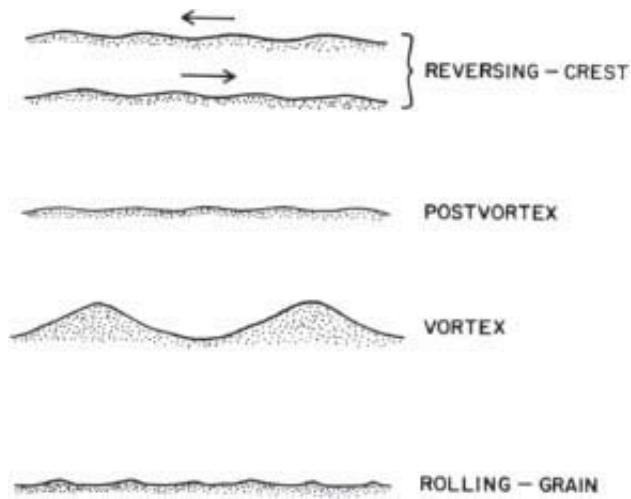


Figure 4.6. Typical normal-to-flow profiles of the various types of oscillation ripples (Harms *et al.*, 1982).

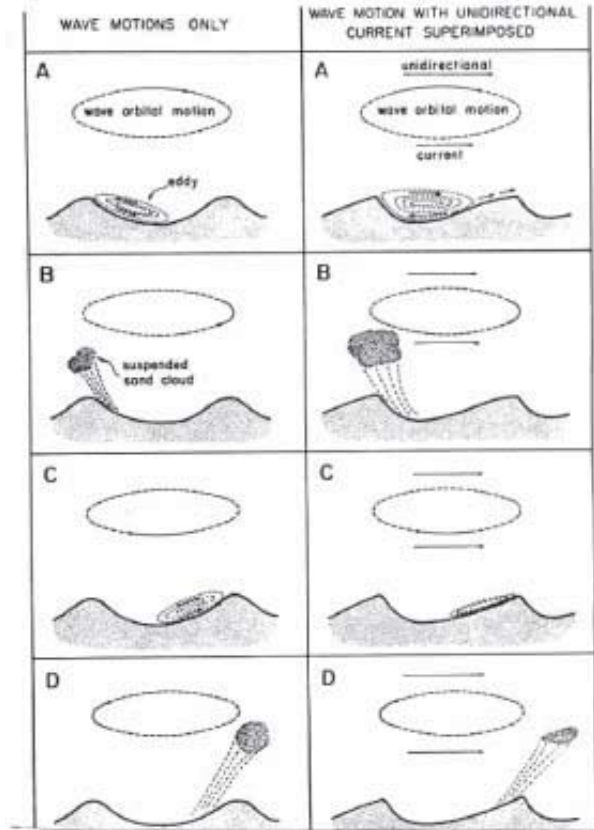


Figure 4.7. Sediment suspension due to eddies formed behind ripple crests, without and with unidirectional currents superimposed on the wave motions (Komar, 1976).

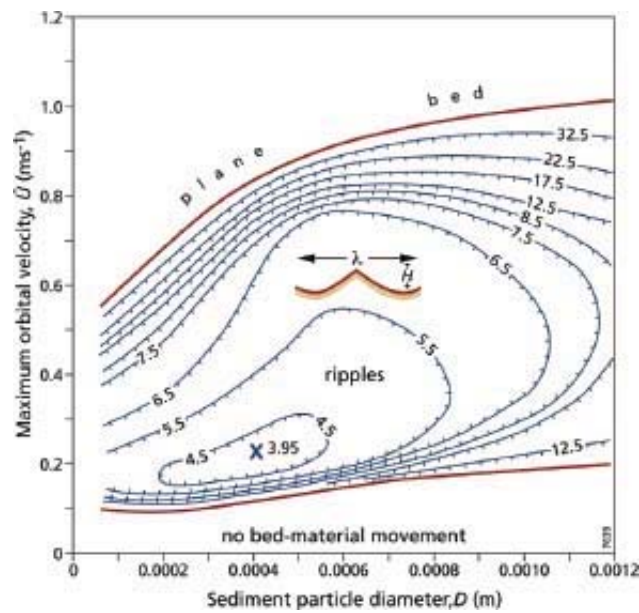


Figure 4.8. Maximum *ripple steepness* (λ/H) of symmetrical ripple marks, as a function of \hat{U} and D_{50} (modified after Allen, 1984).

In their simplest form, vortex ripples are symmetrical in profile and straight or parallel-crested in plan view. In places, Y-shape bifurcations appear at regular distances along the crest line. Small secondary crests sitting in the trough or on the crest are common features as well. Such straight, long-crested wave ripples are generated by unidirectional waves. When a broad spectrum of wave direction is present, as is often the case in offshore, relatively deep water, this superposition produces an irregular pattern of short-crested wave ripples.

A number of attempts have been made to bring together the various types of bed forms in oscillatory flows into one stability diagram. An analogy of the diagram of Shields (Figure 2.6A) that formed the basis of successful diagram for unidirectional flow (Figure 3.5) is shown in Figure 4.11. In the domain of higher current velocities, especially if associated with long periods of oscillation (long duration of the current!), the ripple crests may show a periodically reversing asymmetry and curving crest line (3D) pattern. With a prevailing long period of oscillation and increasing near-bed orbital velocity, the 3D ripples are transformed into large-scale, rounded *hummocky* features, separated by broad troughs or hollows. The height and length of these *hummocks* may be up to several decimetres and meters respectively. A further increase of the near-bed velocity leads to a (upper) plane bed.

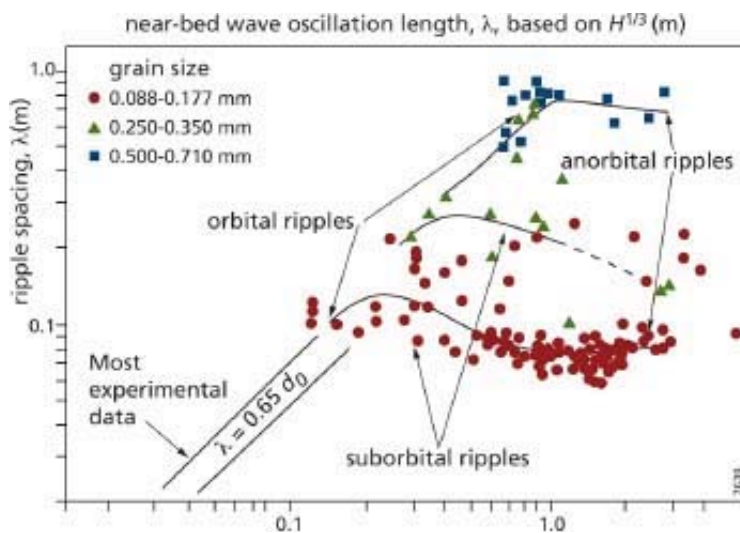


Figure 4.9. Relation between ripple wavelength, λ , and orbital diameter, d_0 (after Miller and Komar, 1980, modified by Allen, 1997).

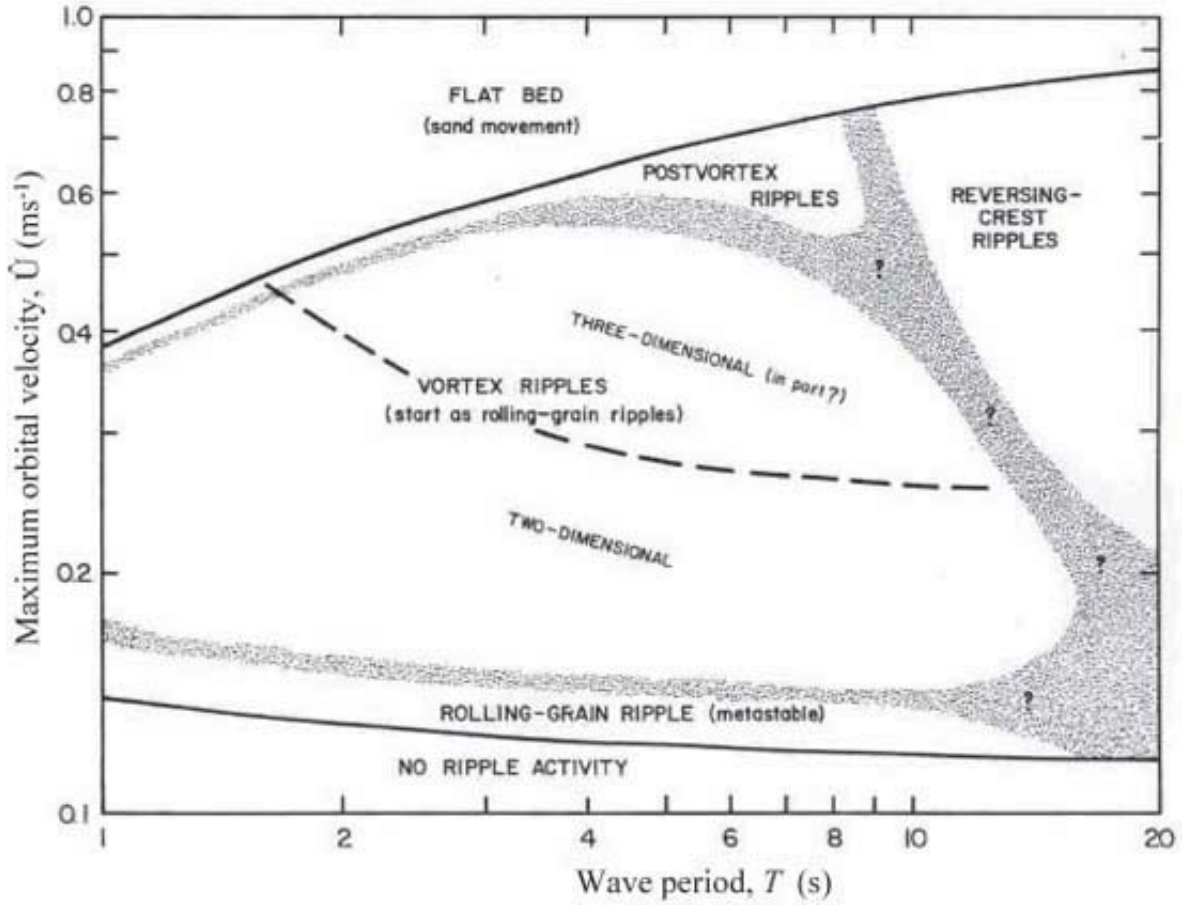


Figure 4.10. Fields of stability of wave-formed bedforms in fine sand (150-210 μm (Harms *et al.* 1982).

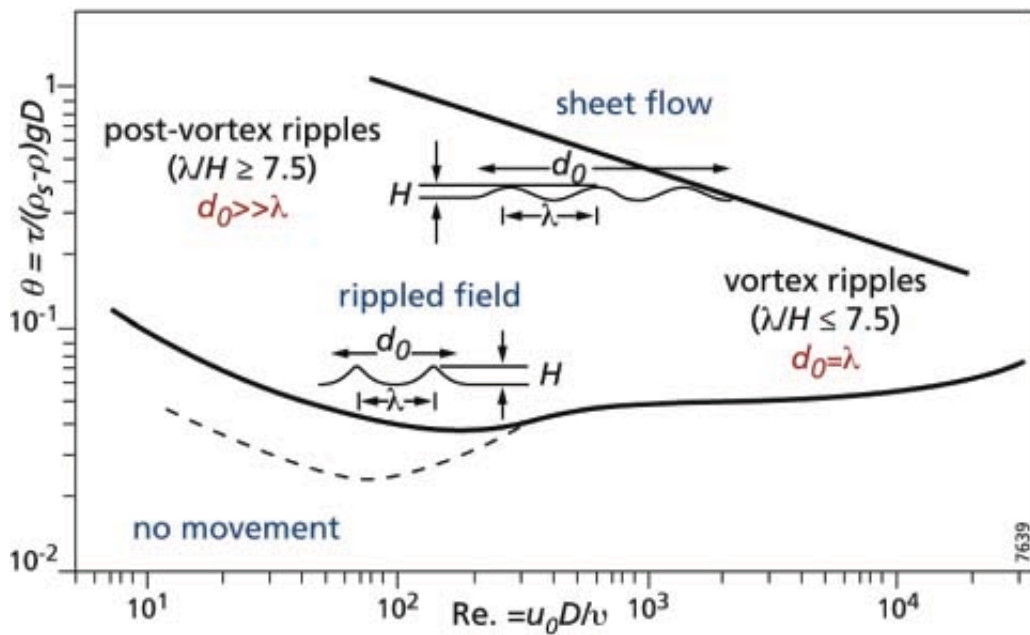


Figure 4.11. The existence of wave ripples as a function of grain mobility related to wave oscillation and the grain

Reynolds Number. The bed shear stress is given by $\tau = 0.5f\rho\hat{U}^2$. For values of the relative near-bed orbital diameter, d_0/D , between 200 and 2, the coefficient f takes the value of 0.01 and 0.03, resp. (modified from Allen, 1997, and Komar and Miller, 1975). Equation 4.2 is valid for the dashed curve and $Re_* < 100$.

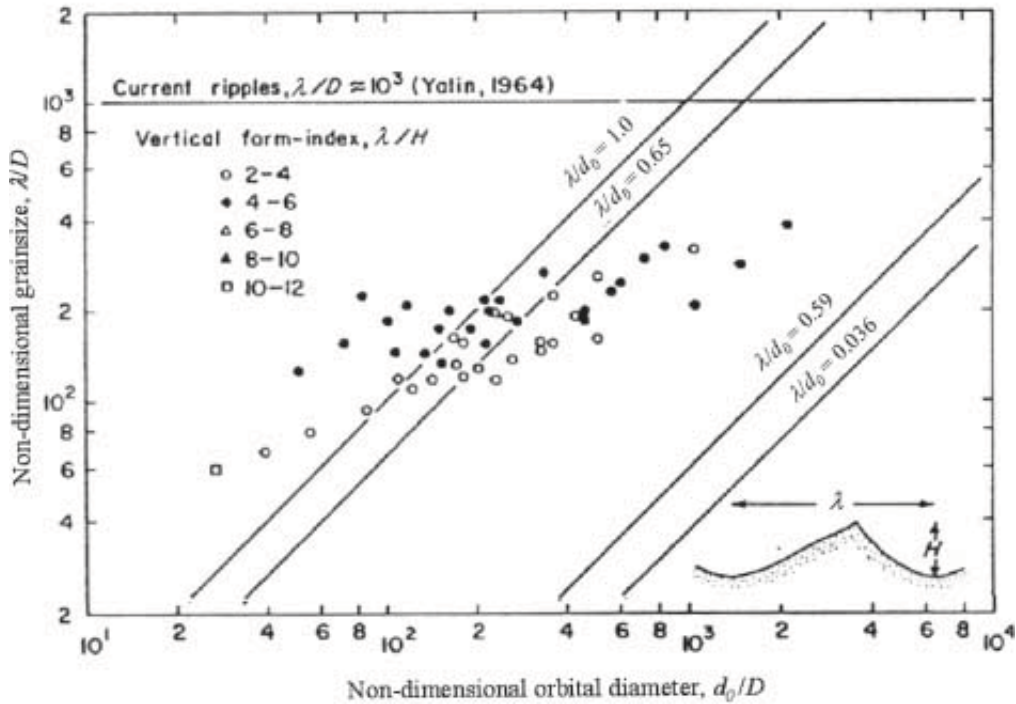


Figure 4.12. Wavelength of wave-related ripple marks relative to particle diameter as a function of near-bed orbital motion (Allen, 1984).

The upper limit of the λ/d_0 ratio for all wave-ripples is represented by an equation proposed by Yang *et al.* (2006):

$$\lambda = 0.75d_0 \quad (\text{m}) \tag{4.3}$$

Ripples that are formed near this limit are termed *orbital* ripples. They form when d_0/D_{50} lies between 100 and 3000. Orbital ripples fit more or less with the traditional view of wave ripples, to think in terms of wave orbitals residing in the troughs of ripples. Examination of wave ripples in natural settings, however, has shown that the near-bed orbital diameter may be much larger than the ripple length. In the case that several ripples per orbital are found, the ripples are called *anorbital*. *Suborbital* ripples are intermediate between orbital and anorbital ripples. As shown in Figure 4.9, the coarser the grain size, the larger the ripples can become. The length of suborbital ripples is negatively related to their orbital diameter. Under larger orbital diameters, when $d_0/D_{50} > 5000$, ripple spacing is dependent only on the grain size. Millar and Komar (1980) obtained for these anorbital ripples the relation

$$\lambda = 147D_{50}^{1.68} \quad (\text{m}) \tag{4.4}$$

The relative wavelength λ/D is well below Yalin's (1964) average value of 1000 for current ripples (Figure 4.12). One might expect a train of wave ripples to be essentially stable with respect to the number and the position of the individual ripples as long as the near-bed wave boundary conditions remain the same. Long-term observations, however, have shown that under such stable conditions: (1) the ripple pattern as a whole may migrate forward or backward; (2) some or several of the individual ripples may disappear in the course of migration, while at other places new ripples are created. The free space left by the disappearing ripples may or may not be filled by new ripples. On the basis of the above observations, the conclusion can be drawn that individual ripples in a ripple train, however uniform and stable conditions seem to be, may perform differential and even opposite movements.

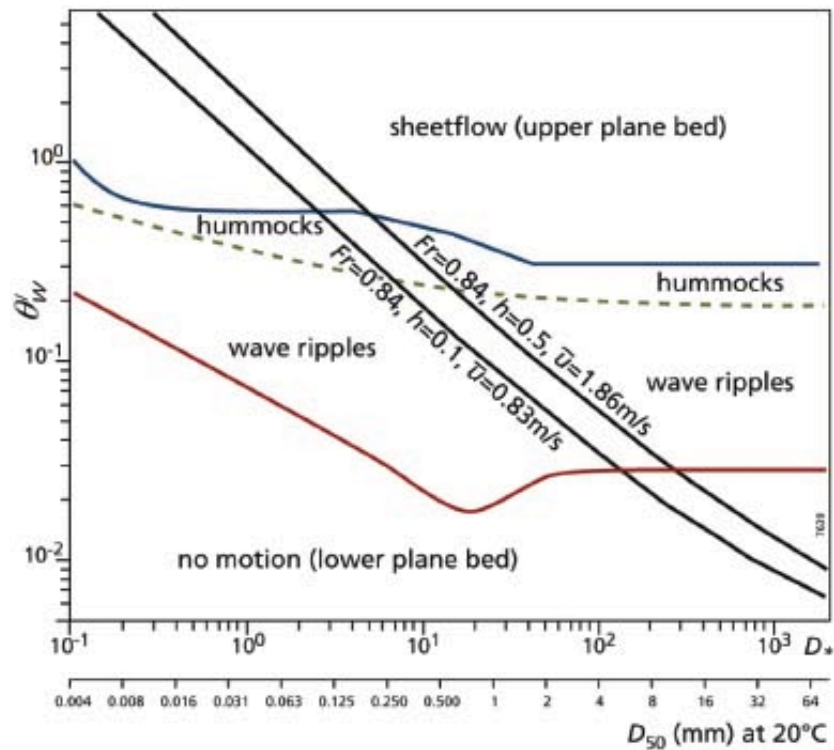


Figure 4.13. Wave bed state diagram based on rational criteria (modified after Kleinhans, 2005b).

Only a few wave bed phase diagrams have been published. The best known is by Allen (1984), which is based on maximum orbital velocity and grain size. However, in this diagram the existence of a field of hummocks is lacking. Based on the rational criteria for the transition to upper-stage plane bed in the lower flow regime (Allen and Leeder, 1980) and the initiation of motion (Shields criterion), Kleinhans (2005b) constructed a bedform phase diagram for waves in a similar mobility-grain parameter plot, as presented for unidirectional flow in Figure 3.5. In this diagram (Figure 4.13) the (wave) grain mobility parameter, is presented by

$$\theta_w = \frac{f_w \hat{U}_0^2}{2gD_{50} \left\{ \frac{\rho_s - \rho}{\rho} \right\}} \quad (-) \quad (4.5)$$

where d_0 and \hat{U}_0 are the near-bed oscillation length and the maximum orbital velocity of the mean 1/3

largest waves, $H^{1/3}$, respectively. is a grain roughness coefficient:

$$f_w' = e^{\left\{ -6 + 5.2 \frac{d_0}{2.5D_{50}} \right\}^{-0.19}} \quad (-) \quad (4.6)$$

with

$$d_0 = \frac{H^{1/3}}{2 \sinh \left\{ \frac{2\pi h}{L^{1/3}} \right\}} \quad (m) \quad (4.7)$$

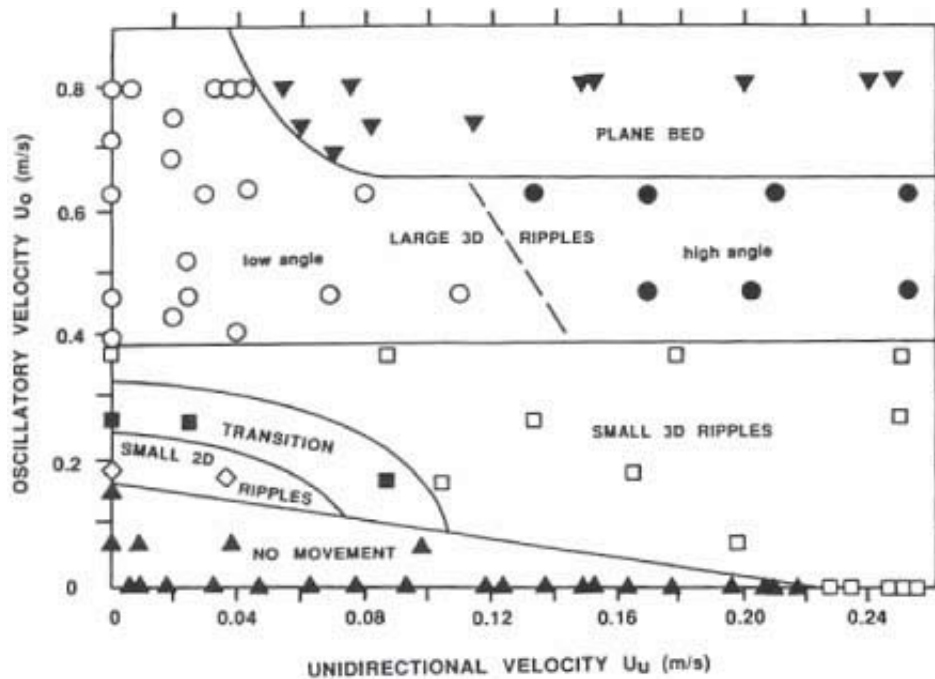


Figure 4.14. Experimental results of bed phases in very fine sand in combined oscillatory and unidirectional flow. Low-angle and high-angle refer to the most steeply dipping flank; low dunes angle $< 10^\circ$. high angle $> 10^\circ$. \blacktriangledown = plane bed; \circ = hummocks; \bullet = 3D dunes; \square = 3D wave ripples; \diamond = 2D wave ripples; \blacksquare = bed forms transitional between 2D ripples and 3D ripples; \blacktriangle = no movement (Arnott and Southard, 1990).

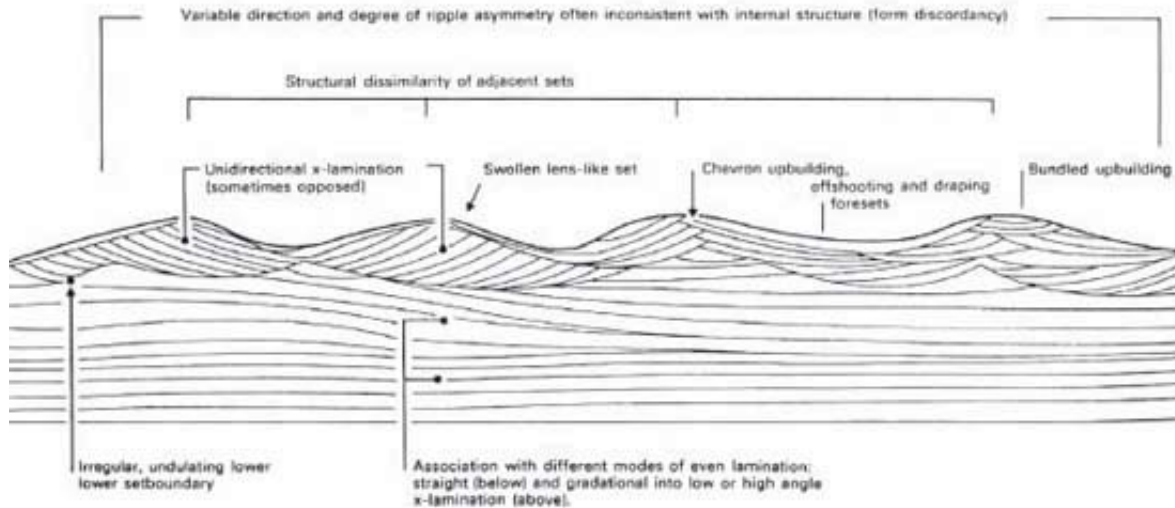


Figure 4.15. The structural dissimilarity of the members of a wave-ripples train and the wave-diagnostic features of planar lamination (De Raaf, Boersma and Van Gelder, 1977).

The bedform phase boundaries of the diagram are largely theoretical and still need verification with more data from nature, especially regarding the transition of wave ripples to hummocks. A serious problem with such a verification is that the conditions in the diagram necessarily refer to monochromatic wave conditions, whereas in reality waves show a spectrum in height, length and direction. As a consequence, all quantitative diagrams in which waves are involved only have an indicative value. The transition to upper-flow regime conditions with Froude-forced upper plane bed ($Fr > 0.84$) is shown in Figure 4.13 for two water depths. Note that such conditions already occur at incipient motion in the swash up- and downrush for gravely beaches.

In combined flows, large 3D bed forms resembling the dunes of purely unidirectional may also be created. The necessary conditions are a relatively high near-bed maximum oscillatory flow with a long oscillation period with only a weak superimposed unidirectional component. In flow duct experiments with an oscillatory period of 8.5 s and using very fine sand as a bed material, it was shown that the rounded, low-angle hummocks generated at oscillation velocities greater than 0.4 ms^{-1} are already transformed into high-angle dunes by applying a unidirectional flow with an average velocity of about 0.15 ms^{-1} (Arnott and Southard, 1990; Figure 4.14).

Stratification produced by oscillatory flows or combined flows

Rolling grain ripples produce thin, sub-parallel laminae that may or may not display some tiny internal cross-lamination. As the bedforms grow to vortex ripples the internal cross-laminae become prevalent. In purely oscillatory flows, with flow and sediment transport strictly symmetrical in the two flow directions and a constant near-bed orbital diameter and velocity, 2D vortex ripples might be expected to remain in one place indefinitely. Then, if sediments are supplied at some rate from suspension to build up the bed, symmetrical oscillation-ripple lamination will be produced. In such a case, minor shifts of ripple crest position back and forth during build-up result in a *chevron*-like interweaving of

laminae at the ripple crest (Figure 4.15). Generally however, migration is not zero because of the omnipresent unidirectional currents or wave conditions. In case of slow migration in one direction relative to build-up velocity, the climb angle is steep and the entire ripple profile is preserved (Figure 4.16 A). Such climbing sets are rather short and very swollen compared to current ripple drift lamination. They often pass vertically into *wavy lamination*, draping the whole ripple train, forming a micro-sequence reflecting conditions of waning wave agitation. If migration is in one direction and rapid relative to aggradation, ripple troughs erode into previously deposited laminae and the stratification involves laminae dipping in one direction only, in sets bound by erosion surfaces. This last type is the most common in the sedimentary record and may be produced by combined flows, or asymmetric oscillatory flows (Figure 4.16 B). Stratification generated by oscillatory flows and weak superimposed flows is often complicated because wave conditions and related wind and wave generated unidirectional flows seldom remain the same for long. Figure 4.15 summarizes some of the diagnostic features of the complex structures formed in such conditions in a condensed and idealized way. Usually, only a few of these features are encountered in wave ripples lying adjacent to each other.

The wave-generated cross-laminations dealt with so far, often appear as (ripple) *form-sets*, i.e., sets that have retained the ripple cross-sectional outline. It is important to note that structures produced by vortex ripples often occur in association with lamination generated during conditions of higher or lower wave agitation; low angle cross-lamination or parallel lamination generated by post-vortex ripples or *hummocks* may be generated during episodes of higher near-bed wave energy; low energy may leave silt or mud drapes concordant with the ripple profile (Figure 4.17).

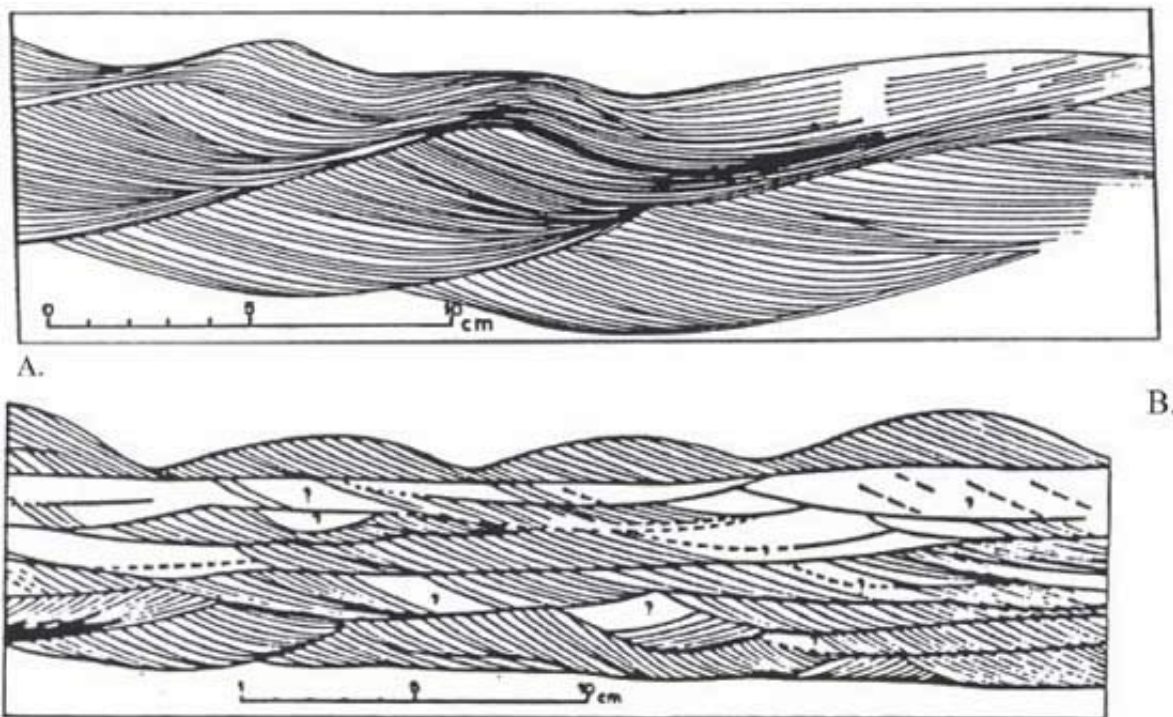


Figure 4.16. Wave-generated x-lamination. A. climbing x-lamination; B. Co-sets of cross-stratification produced by asymmetrical (shoaling!) wave oscillations.

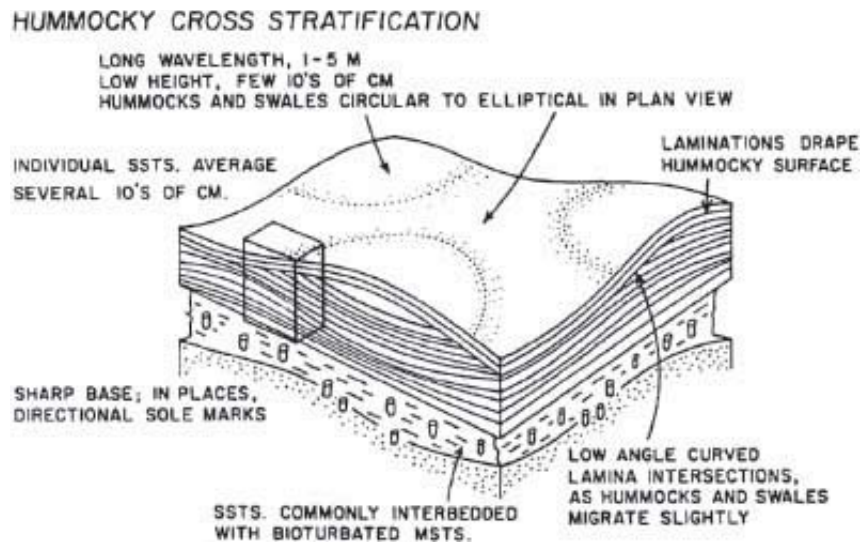


Figure 4.17. Hummocky cross-stratification (Swift *et al.*, 1983).

If the low wave energy conditions prevail and sedimentation continues, wave ripple troughs are filled with laminated silt or clay, gradually obscuring the original relief. Eventually, the infilling laminations pass into horizontal lamination. Instead, higher energy is often witnessed by planar truncation surfaces covered with even or low-angle lamination. High-energy wave-built structures include even (horizontal) lamination and a distinctive type of low-angle bedding with laterally thickening and thinning, slightly undulating laminae. This sedimentary structure, which commonly exhibits slight internal discordances, is widely known as *hummocky* cross-stratification (HCS; Figure 4.17). The closed duct experiments referred to before (Figure 4.14) indicate that HCS is formed under conditions of strong relative harmonic oscillatory currents with a long period and length of oscillation, and a low velocity ‘background’ current. As soon as the latter exceeds a near-bed velocity of about 0.15 ms^{-1} , high-angle cross-bedding develops. This seems to be in accordance with outcrop observations, which often show the two structures merging into each other. The necessary long oscillation length to produce HCS is possibly the reason that this structure occurs most prominently in nearshore deposits of swell dominated oceanic coasts. HCS may be found in typical micro-sequences (Dott and Bourgeois, 1982). Ideally, these start in basal lag, followed by HCS, parallel lamination and or cross-lamination, commonly of the wave type (Figure 4.18). These decimetre to metre-thick sequences may be capped with mud and reflect the waning of storm waves and therefore sometimes also are called *storm sands*. Erosional truncation of these micro-sequences and repeated HCS deposition may lead to thicker, stacked amalgamated sequences. HCS basically consists of bundles of convex up and concave up strata, that truncate and pass into each other, representing respectively humps and swales of the hummocky bed. The term *Swaly Cross Stratification* (SCS) was introduced by Leckie and Walker (1982) for amalgamated sandbodies thicker than 2 m in which concave up bundles dominate. The hump-swale structures of HCS vary enormously in size, with wavelengths, λ , ranging from several meters to perhaps as small as 10-20 cm (compare Plate 11 with Plate 12).

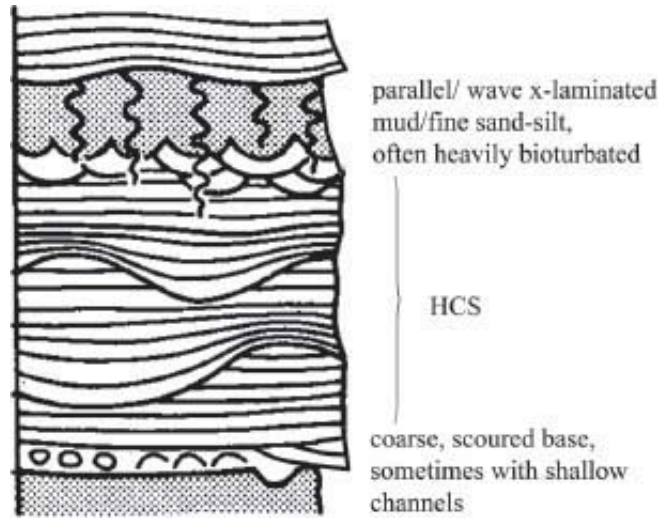


Figure 4.18. Example of typical HCS microsequence (modified after [Dott and Bourgeois, 1982](#)).

5 Influence of Tides on Sedimentary Structures

In this chapter, the origin of the tides will first be treated followed by information on the periodicity of the main tidal constituents, their changes through geological time and how these tidal periods are recorded in some ancient, low-energy deposits. Some attention will then be given to the changes in basic characteristics of the tidal wave when travelling through shallow seas and estuaries. Finally, the main characteristics of sedimentary structures generated by tidal currents in tide-dominated estuaries will be discussed.

Equilibrium tidal theory

The driving forces of tidal processes are the attraction exerted by the Moon and the Sun on the water of oceans and seas around the globe. The Earth and the Moon revolve together around their common centre of mass with a period that is called a *sidereal month* (27.3217 days), or when the lunisolar precession¹ is taken into account, in the slightly shorter time period of the *tropical month* (27.3216 days). It was Pliny the Elder (23–79 AD) who observed that the tides “follow” the Moon. If that were strictly true, we would have diurnal (daily) tides everywhere, whereas semidiurnal tides are the rule. Newton proposed the first explanation for the semidiurnal tides with the *equilibrium tidal theory*. Earth and Moon are held together by gravitational attraction but are simultaneously kept apart by an equal and opposite centrifugal force. At the Earth’s surface, an imbalance between these two forces results in the fact that there exists, on the side of the Earth turned toward the Moon, a net tide producing force, which acts in the direction of the Moon. On the side of the Earth directly opposed to the Moon, the net tide producing force is in the direction of a greater centrifugal force, away from the Moon. Newton envisaged the effects of tide generating forces on a theoretical Earth, covered by an ocean of uniform depth and containing no continents. On such an Earth the ocean waters would respond completely to the directions and magnitudes of the tractive forces and two tidal bulges would be produced on opposite sides of the Earth, propagating with the velocity imposed by the rotation of the Earth-Moon couple (Figure 5.1). The plane of the Moon’s orbit is inclined about 5° to the plane of the Earth’s orbit and thus the Moon in its monthly revolution around the Earth remains close to the ecliptic. The ecliptic is the intersection plane of the Earth’s solar orbit with the celestial sphere and is inclined 23.5° to the Earth’s equator, north and south of which the Sun moves once each half year to produce the seasons. The Moon’s inclination causes two maxima of the tidal bulges on either side of the equator. A point at a middle latitude to be located north or south of the equator therefore experiences different magnitudes of the two tidal waves. The diurnal inequality is at a maximum when the Moon is at its maximum declination and disappears twice during a tropical month, when the Moon’s ecliptic coincides with the Earth’s equatorial plane. Therefore, the maximum number of successive diurnal inequalities of the tide cannot extend longer than contained in half a tropical month (26.4 ebb-flood cycles). Tides that experience a significant diurnal inequality are referred to as mixed tides.

Since the gravitational forces of both the Moon and the Sun act upon the waters of the Earth, the

Moon's changing position with respect to the Earth and the Sun, during its monthly cycle of phases, affects the tidal range. The phase cycle is called a lunar month or *synodic month*. A synodic month has a period of about 29.53 days. Tides are higher at *syzygy*, when Earth, Moon and Sun are nearly aligned. The highest tides, at new and full Moon, are known as *spring tides*. The tide-raising force of the Sun is approximately 2.5 times smaller than that of the Moon, resulting in spring tidal ranges that are usually 20% higher than the mean tidal range. At the first and third-quarter phase of the Moon, the gravitational attraction of the Moon and Sun are exerted at right angles to each other. The resultant tidal force is thereby reduced and tidal ranges are less than average. These tides are called *neap tides*. One synodic month contains 28.53 *lunar days*. In view of the simultaneous presence of two tidal bulges, this means that one neap-spring tidal cycle contains on average 14.27 semi-diurnal tides. A lunar day lasts 24 hours and 50 minutes. This is longer than 24 hours because the Moon orbits in the same direction as the Earth rotates, which requires a little bit more than one revolution for the Earth during a *solar day* (24 hours) to “catch up” to the Moon. Since the Earth rotates through two tidal “bulges”, we experience two high and two low tides every lunar day.

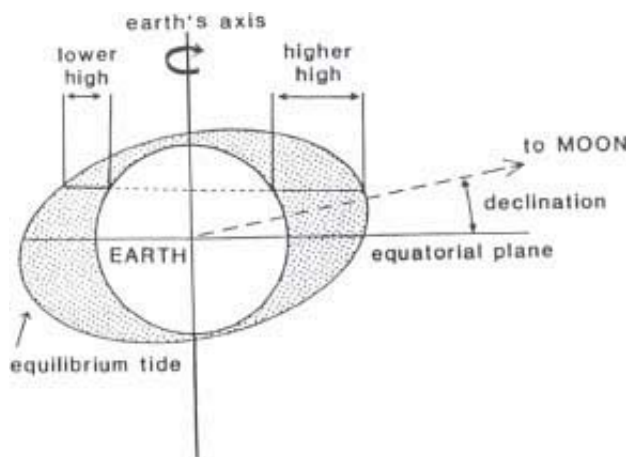


Figure 5.1. Schematic representation of the tidal bulges on a theoretical Earth, covered by an ocean of uniform depth (after De Boer *et al.*, 1989).

The Moon follows an elliptical, eccentric path around the Earth, with a 27,55 day periodicity, a period known as the *anomalistic month*. As a result, the gravitational attraction changes. Therefore, slightly lower tides occur at *apogee*, when the Moon is farthest from the Earth and higher tides half a month later, at *perigee*. Similarly, in the Sun-Earth system, when the Earth is closest to the Sun, at *perihelion*, about January 2nd of each year, the tidal range is enhanced, and when the Earth is farthest from the Sun, at *aphelion*, around July 2nd, the tidal ranges will be reduced. When perigee, perihelion and either new or full Moon occur at approximately the same time, considerably increased tidal ranges result. When apogee, aphelion and first or third-quarter Moon coincide at approximately the same time, considerably reduced tidal ranges will occur. However, near the *equinoxes*, when moon, Earth and Sun lie along an almost straight line (September 21 and March 21), spring tides are highest. The moon, in making a revolution around the Earth once each sidereal month, passes from a position of maximum angular distance north ($23.5^\circ \pm 5^\circ$) of the equator to a position of maximum angular distance south ($23.5^\circ \pm 5^\circ$) of the equator during each half month and *vice versa*. This cyclic variation from 18.5° to 28.5° of the lunar orbit and the ecliptic is called the 18.61 years *lunar node cycle*. It accounts for a small cyclic temporal change in tidal range of spatially varying magnitude.

Along the Dutch coast the amplitude of the lunar node cycle is about 4% of the average semidiurnal tide (De Ronde, 1983). The Earth-moon system contains one more orbital variation, the *lunar apse cycle*, 8.85 years, determined by the rotation of the long axis of the moon's elliptical orbit. However, its influence on the tide is weak, only 0.21% of the mean tidal amplitude (Fairbridge and Sanders, 1987). For a more elaborate description of astronomically induced tidal periods, the reader is referred to Pugh (1987) and Kvale *et al.* (1999).

Change in tidal periods since the Proterozoic

The length of all tidal periods mentioned so far refers to the present day situation. As the energy of the tidal bulges on the Earth is converted to heat, it reduces the energy incorporated in the axial rotation of the Earth and the orbital motion of the Moon. This results in a slowing of the Earth's rotation, a slowing of the Moon's rotation around the Earth and a consequential retreat of the Moon. Several attempts have been made to determine these changes using proxy tidal records from the geological past. First, research was directed to variations in skeletal growth increment in fossils (Wells, 1963; Rosenberg & Runcorn, 1975; Brosche & Wünsch, 1978; Lambeck, 1980). However, the reliability of much of these palaeontological data has met rising doubts (Scrutton, 1978; Lambeck, 1980; Crisp, 1989). A better methodology for tracking the history of the Earth's tidal deceleration and the evolving lunar orbit is offered by sedimentology. Analysis of cyclic rhythmites of low energy tidal origin, i.e., stacked, usually thin, heterolithic strata that display periodic variations in thickness that can be attributed to fluctuations in tidal amplitude, has provided information on this since the Pre-Cambrian. For an overview of this research, which started by the end of the nineteen-eighties, the reader is referred to Williams (2000) and Mazumder & Arima (2005). The leading principle behind the variation in thickness of the rhythmites is that the strength of tidal currents is generally proportional to the tidal amplitude. As suspended bed-material transport is related to about the fourth power of the current velocity (Van den Berg and Van Gelder, 1994), a small increase in tidal amplitude is magnified in the concentration and advective transport of suspended silt and fine sand. This amplification may be documented by varying thicknesses of laminae deposited during successive tides in low-energy depositional sub-environments of the tidal system, such as abandoned tidal channels (Brown *et al.*, 1990; Oost *et al.*, 1993) or distal parts of ebb tidal deltas (Williams, 1989). Based on analyses of several Proterozoic rhythmites, Williams (2000) reconstructed the values of a number of lunar periods for this époque, which are used in Figure 5.2. It should be realized that the validity of the method is still questionable because of difficulties in determining the absolute length of the ancient sidereal month (Mazumder and Arima, 2005).

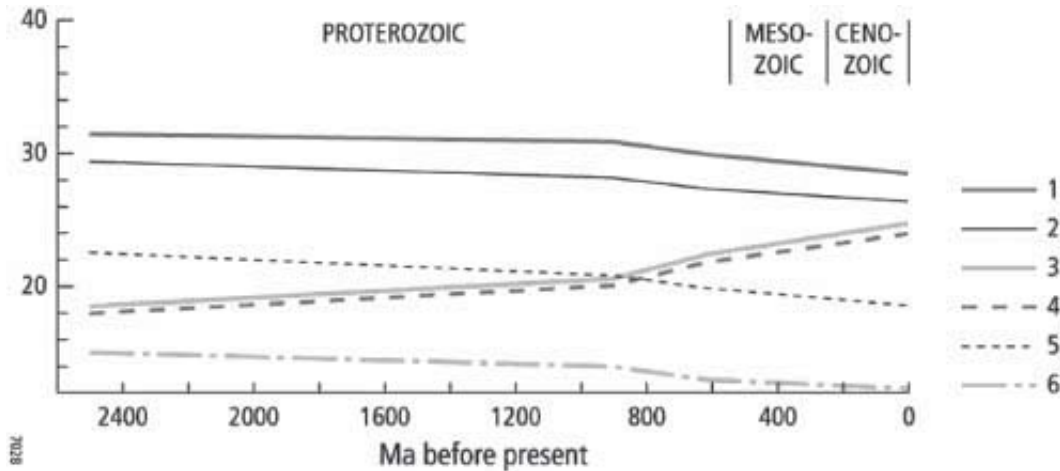


Figure 5.2. Change in length of some lunar and solar periods since the early Proterozoic (derived from Williams, 2000). It is assumed that values calculated for “sidereal” also apply for “tropic”, as suggested by Kvale *et al.*, (1999) and Mazumder and Arima (2005). 1: lunar days per synodic month; 2: lunar days per tropical month; 3: length of lunar day; 4: length of solar day; 5: lunar nodal period; 6: synodic months per year.

Origin	Symbol	Period (hours)	Relative strength
Main lunar, semidiurnal	M2	12.42	100
Main Solar, semidiurnal	S2	12.00	46.6
Lunar elliptic, semidiurnal	N2	12.66	19.2
Lunar-solar, semidiurnal	K2	11.97	12.7
Lunar-solar, diurnal	K1	23.93	58.4
Main lunar, diurnal	O1	25.82	41.5
Main solar, diurnal	P1	24.07	19.4

Table 5.1. Main tidal constituents of present day tide-generating forces, with their strength relative to the main semidiurnal lunar tide (M2). After Van Rijn (1993).

Dynamic tidal theory

While equilibrium tidal theory is fairly straightforward, it understates the complexity of the tides in the real world, as it ignores the fact that ocean basins have irregular shapes, that bulges must respond to friction in moving through basins and that water itself has inertia once it is moving. In the *dynamic tidal theory* the movements and angular speeds of all tidal components are considered (Pugh, 1987). There are over a hundred tidal constituents that can be extracted from harmonic analysis of actual tides. However, only seven of these describe 83% of the variability observed in those tides (Table 5.1).

Because the tide-generating forces are small, only the oceans develop significant tides, and even these tides typically have a range of less than 1 m. Once created, a tidal wave propagates as shallow water waves with a velocity proportional to $(gh)^{0.5}$ through the shelves and shallow seas along the continents, where it reflects, refracts and interferes with waves of other tidal constituents or with

reflections of itself (see also eq. 4.1). A rectangular basin with uniform and shallow depth reflection of a wave with small period would result in standing waves, with nodal lines at a distance of a quarter of the tidal wave length from the reflecting boundary (Figure 5.3). In large basins, where masses of water experience the Coriolis force tidal bulges swing as so-called *Kelvin waves* about the basin margin and the nodal line is reduced to a nodal point, called an *amphidromic point* (Figure 5.4). Kelvin waves rotate counter-clockwise in the Northern Hemisphere and clockwise in the Southern Hemisphere.

The resonance period of oceans is generally rather close to the period of the semi-diurnal M2 tide. Consequently, the amplitude of the semi-diurnal tide is reinforced and generally significantly larger than those of the diurnal tides (Van Rijn, 1993). However, it is stressed that this is not always the case. For instance, at present in some parts of the Pacific and Indian Oceans, and the Gulf of Mexico, the diurnal tide dominates and the neap-spring cycles are synchronized with the 27.32-day tropical month (Kvale, 2006). In mixed tidal systems dominated by the tropical tides, the diurnal inequality goes to zero only at neap tide (Kvale, 2006). This is different from synodically-driven neap-spring cycles, where due to the difference in period of the synodic and tropical month the moment of minimum diurnal inequality – denoted as “crossover” by Kvale *et al.* (1989) – is moving backwards in successive neap-spring cycles (Figure 5.5). The daily inequality is strongest in basins, that resonate at diurnal frequency. This may lead to tropically-driven diurnal tides in areas where the oceanic tide wave is distorted.

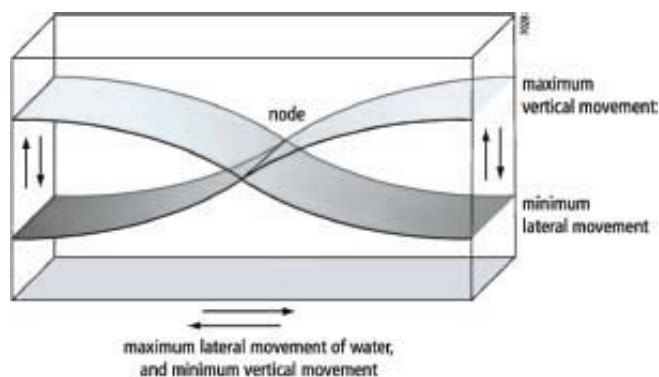


Figure 5.3. Standing wave in a small basin.

During the passage of the wave top, the water depth is relatively large. As a consequence, the wave top progresses with a higher velocity than the wave trough, which results in asymmetry of the wave, increasing with travelling distance. This is demonstrated clearly in the southern North Sea (Figure 5.4): the asymmetry between tidal rise and fall is most pronounced along the coast of central and northern Holland (between III and IV). This asymmetry is mainly due to the relative shallowness of the sea along this part of the coast. Further to the north and along the Wadden Sea, the tidal wave is part of the amphidromic system of the central North Sea, which develops less asymmetry because of the greater water depth (Dronkers, 2005). While propagating in an estuary, the asymmetry of the tidal wave generally further increases (Figure 5.6). At the same time, the bed friction dissipates its energy and converts it to heat. When considering the amplitude of the tidal wave, two other processes are important: (1) landward constriction or convergence in the channel and (2) reflection on shoals or from the estuary head. Although frictional damping decreases the amplitude landward, convergence of the tidal energy and reflection in a funnel-shaped estuary can nevertheless result in an increase of a

landward tidal range. Amplification by reflection is caused when the tidal wave is more or less in phase with the natural wave period of the basin. Three possibilities are distinguished (LeFloch, 1961), as shown in Figure 5.7. When in the course of time the physiography of an estuary changes, its tide characteristics will also change. Many present-day estuaries started with a wide basin shape during the Holocene sea level rise (type c in Figure 5.7) and during the process of filling, gradually transformed into a type 1 funnel-shaped basin (Dalrymple *et al.*, 1992). Thus, such estuaries have changed from *hypochronous* to *hypersynchronous*. A change from type C to type A physiography and the consequential transition from friction-dominated to convergence-dominated tide is documented from the Westerschelde, the Netherlands (Van den Berg *et al.*, 1996). In the beginning of the 17th century, the Westerschelde was a wide basin. Sedimentation along the margins, followed by embankments, quickly led to a much more funnel-shaped estuary (Figure 5.8). In addition, less energy was lost by friction due to a significant deepening of the main ebb channel by dredging. The deepening also resulted in an increase in the propagation velocity of the tidal wave, resulting in a better resonance with the natural wave period of the tidal basin (Van den Berg *et al.*, 1996). As a result, a spectacular increase of tidal amplitude took place (Figure 5.10).

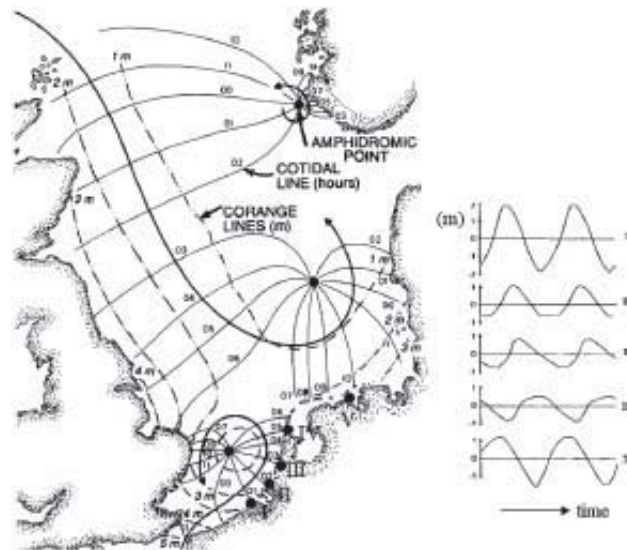


Figure 5.4. North Sea amphidromic tidal system generated by the M2 tide. Lines of equal tidal range are labelled as co-range lines. Co-tidal lines indicate times of high water (after Houbolt, 1968); I – V: distortion of the tidal wave along the Dutch coast (after Dronkers, 2005).

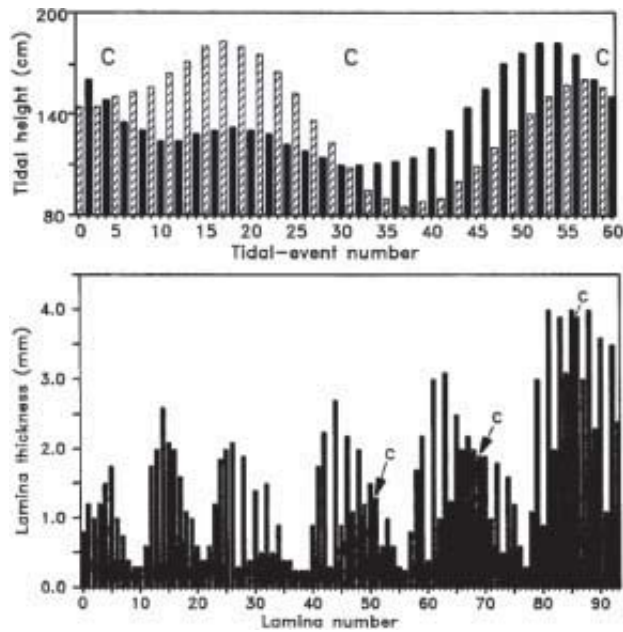


Figure 5.5. Diurnal in equality in synodically-driven neap-spring cycles: A. Predicted tides from Boston, Massachusetts. Tides that are subordinate during the first half of the synodic month (solid) become dominant during the second half. The point at which this occurs (C) corresponds to the crossover point B. Thickness variability of dominant and subordinate laminae in laminated siltstones of the Pennsylvanian Mansfield Formation, Indiana, showing corresponding crossovers moving backwards in phase with respect to the neap-spring cycles (after *Kvale et al.*, 1989; see also [Figure 5.16](#)).

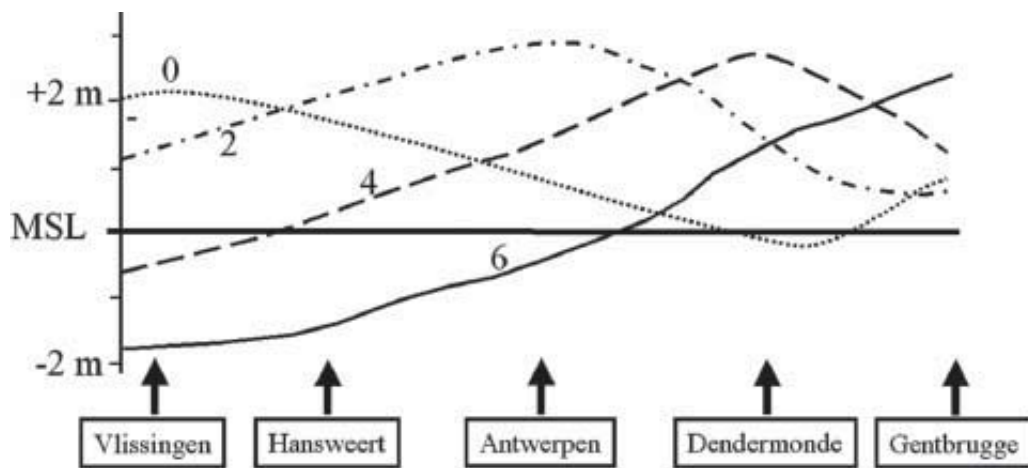


Figure 5.6. Propagation of the tidal wave in the Westerschelde. See also [Figure 5.9](#).

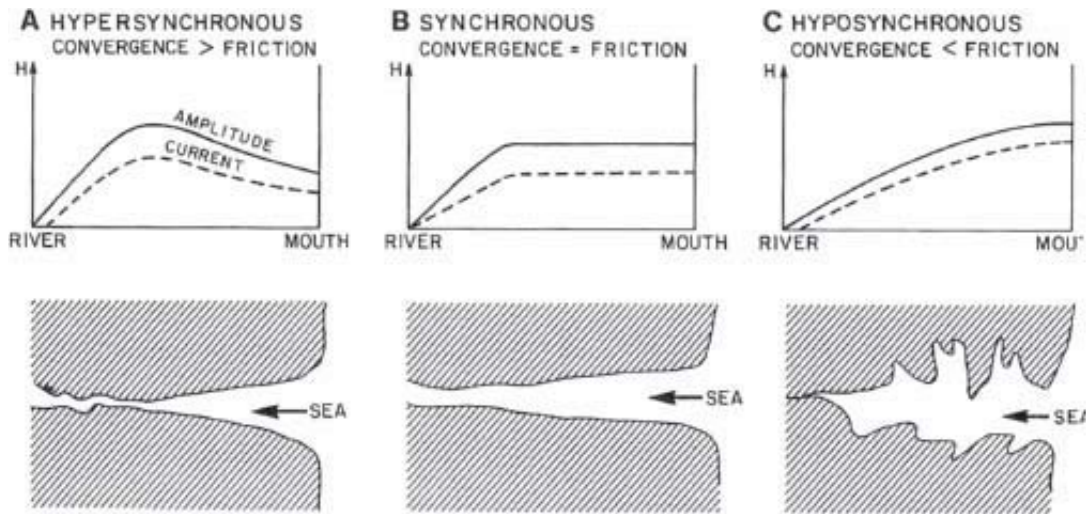


Figure 5.7. Modification of tide range in estuaries with varying ratios of convergence (and reflection) to friction effects (from Salomon and Allen, 1983; modified after LeFloch, 1961).

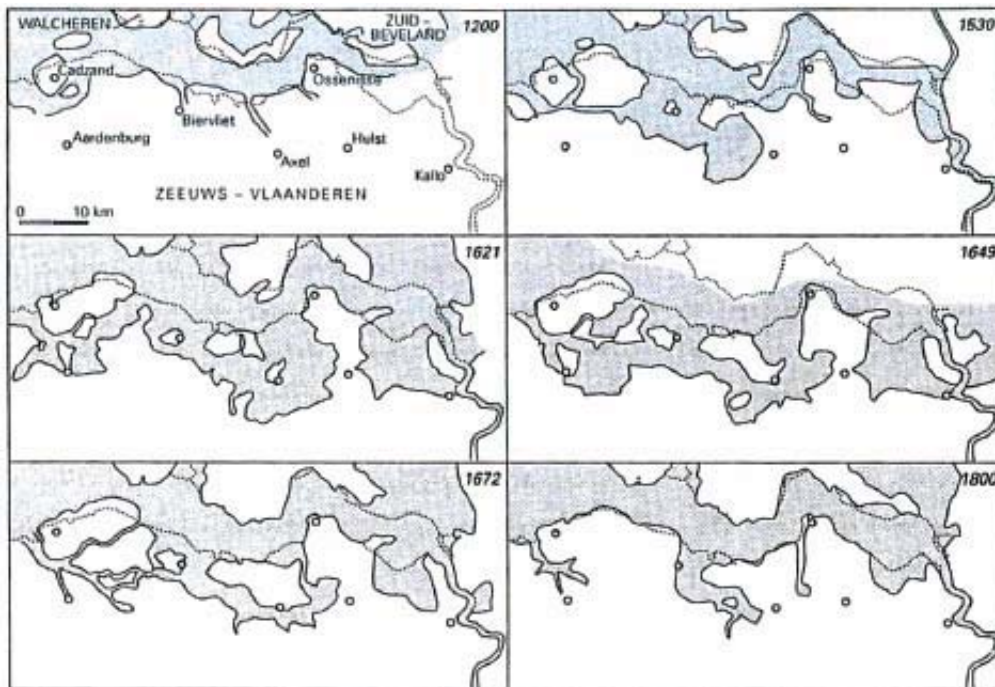


Figure 5.8. Boundaries of the tidal basin of the Westerschelde since AD 1200 (Van den Berg *et al.*, 1996, modified after Brand, 1985).

In case of a high amplitude of the tide and shallow channels, the steepening of the leading edge of the incoming tidal wave may even result in a breaking water front or bore (see also chapter 4). Famous examples are the bore of the Qiantang river (China), the “mascarat” of the Seine river (France), and “pororoca” of the Amazon river (Brazil). The Qiantang bore has a mean height of about 1.5 m and a

maximum height of 3 m, with a propagation velocity of about 10 ms^{-1} (Figure 5.9). Tidal bores may penetrate considerable distances into rivers. For example, the Hoogly tidal bore propagates more than 80 km, flowing past the port of Calcutta (Chanson, 2009). The leading edge of the bore is often followed by a train of bore-related waves, termed *whelps*. In case of steep channel banks, shock waves are generated by the frontal wave and the whelps, which migrate obliquely over the channel. This complicated wave pattern may persist for quite some time. Two types of tidal bores are distinguished; the *undular* bore, with no breaking waves and the *breaking* bore. Undular bores have a surge Froude number, Fr^* , close to unity; the Froude number of breaking bores is larger, which means that their propagation velocity is higher (see also eq. 4.1). Nowadays, bores have reduced in size or disappeared from many places, because of deepening of the main channel by dredging.

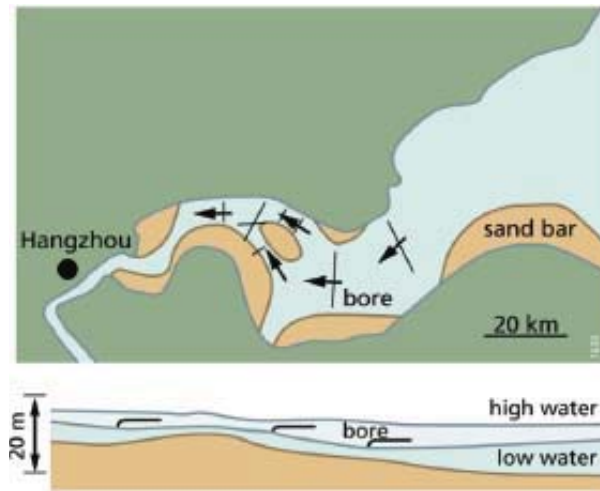


Figure 5.9. The Qiantang tidal bore near Hangzhou, China (Modified after Van Rijn, 1990).

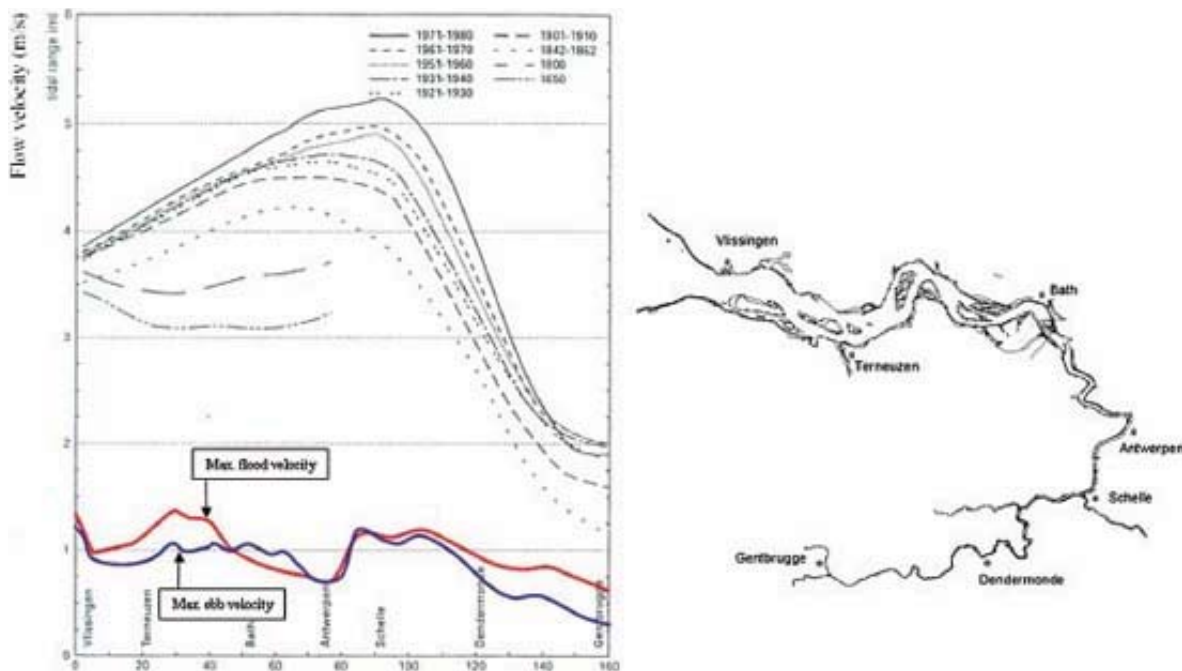


Figure 5.10. Amplitude of the tidal wave in the Westerschelde since AD 1650 (after [Van den Berg *et al.*, 1996](#)) and actual maximum cross-section-averaged tidal current velocities during average tidal conditions. The latter data were kindly provided by Claire Jeuken of Deltares, The Netherlands and were obtained from a one-dimensional SOBEK model using the 2001–2005 hydrography.

Following a terminology proposed by [Davies \(1964\)](#), estuaries are commonly divided into *micro-tidal* (< 2 m tidal range), *meso-tidal* (2 – 4 m) and *macro-tidal* (> 4 m). This classification makes sense, as it provides an indication of the energy level of the tides. In coastal plain estuaries, tides provide the energy for maintaining a funnel-shaped estuary with its characteristic dynamic pattern of ebb and flood channels and shoals. The terminology of Davies has been widely adopted in the sedimentological description of present-day estuaries (i.e., [Boersma and Terwindt, 1981](#); [Allen, 1991](#); [Dalrymple *et al.*, 1990](#); [Nichols *et al.*, 1991](#)). However, the application of the classification to ancient deposits is difficult. [De Vries Klein \(1971\)](#) suggested its determination by measuring the distance between the lowest occurrence of emergence runoff structures and the top of clayey salt marsh deposits. However, evidence of run-off structures or other structures that point to the low water line is rarely found. In ancient deposits intertidal and supratidal deposits generally are also not or only partly preserved. An alternative approach to calculating the tidal range from the increment of dune foreset strata during successive tides was suggested by [Nio *et al.* \(1983\)](#). This approach is based on the assumption that flow velocity in an estuary is proportional to tidal range ([LeFloch, 1961](#); [Siegenthaler, 1982](#); [Dalrymple and Choi, 2007](#)), see also [Figure 5.7](#), which may be true in some cases, such as the Bay of Fundy ([Dalrymple *et al.*, 1990](#)), but unfortunately cannot be generalized. For instance, in the Westerschelde, the (maximum) flow velocity clearly does not correlate with tidal range ([Figure 5.10](#)). For a number of more or less funnel-shaped former estuaries in the SW Netherlands, most of which are now closed by the barriers of the Dutch Delta Project, the highest flow velocities were found in the estuarine mouth ([Van der Kreeke and Haring, 1979](#)). The reconstruction of the palaeotidal range is further complicated by spatial variations in flow velocity ([Lacombe and Jago, 1996](#)). In fact, the palaeotidal range may only be calculated with some confidence when deposits allow a detailed reconstruction of the tidal system, by applying numerical model simulations, as executed by [Van der Spek \(1994\)](#) for a former Holocene estuary in the Netherlands.

Tidal currents and sediment import mechanisms

During periods of low sea level, river valleys become incised. With the succeeding transgression, the lower reaches of these valleys become inundated and start to trap sediment supplied by the river as well as from the coastal areas and the sea. As a result of the Holocene sea-level rise, such estuaries are very common along modern coasts throughout the world. When the accommodation space created by sea-level rise is greater than the sediment supply, a *wave-dominated estuary* sensu [Dalrymple *et al.* \(1992\)](#) is formed. During the first part of the Holocene, rapid sea-level rise contributed to the presence of many wave-dominated estuaries. Later on, many of these transformed into *tide-dominated estuaries*, notwithstanding the fact that sea level continued to rise, though at a slower rate. This illustrates the fact that estuaries are very efficient sediment traps. Sediment enters the estuary both from river sources and from the sea. The latter import is supported by a number of processes. Basically, three mechanisms can be distinguished, asymmetry of the tidal wave at the entrance of the basin, settling lag effects and estuarine circulation. The first mechanism accounts for the import of sand, the latter two apply to the import of mud. The steeper water level gradient at flood (see [Figure 5.4](#)) causes higher inshore-directed tidal flow velocities during flood as compared to ebb. In the case of a wave-dominated estuary, this tidal asymmetry results in a net import of sand. Because the transport of sand is

proportional to the third (or higher) power of the depth-averaged flow velocity, sand import into the basin during flood is not compensated by sand export during ebb. When this import outweighs the creation of accommodation space by sea-level rise, it eventually results in the generation of tidal channels and intertidal shoals. The maximum of the flood discharge will shift gradually to higher water levels at a later stage in the flood period, during which the shoals become flooded when an increasing part of the tidal basin is occupied by shoals. Such a shift means an increase in the wet cross-sectional area of the main channels at the estuary entrance for the moment of maximum discharge, implying a reduction in flow velocities. The presence of large tidal flats also delays the moment of maximum ebb, as the lowering of water levels on the shoals lags behind the fall in the larger channels (Dronkers, 1986; Speer and Aubrey, 1985). As a consequence, the maximum ebb discharge at the estuary mouth shifts to a lower water level. The effect is, as shown by model computations of Friedrichs *et al.* (1990), that the ratio of flood to ebb sand transport decreases with increasing shoal coverage. Thus, in a tide-dominated estuary, the import effect due to the asymmetry of the incoming tidal wave is counteracted by a delaying effect on the ebb and flood discharge peaks caused by the emerging shoals. The results of the simulations by the latter authors apply to small basins, as they ignore spatial differences in water level, but the basic mechanisms are valid for small as well as large basins, such as the Westerschelde (Van der Spek, 1994; Wang *et al.*, 2002). The analysis of Speer and Aubrey (1985) suggests the existence of an equilibrium condition of the extent of intertidal area in a tidal basin at which no net import or export of sediment would occur. However, such an equilibrium is not to be expected, as the analysis refers to sand. When considering mud, other mechanisms are important. Among these, the most important are the well-known settling lag and scour lag effects, as described by Postma (1967) and Van Straaten and Keunen (1957) and the density-driven estuarine circulation. Both processes favour a net landward transport of mud particles into a tidal basin and into the salt marshes along its margins. Therefore, after the drowning of an alluvial river valley by sea-level rise, two morphology-related stages of infilling can be distinguished (Van den Berg *et al.*, 1996; Figure 5.11). The rate of infilling in stage II depends of course on the availability of mud from river and marine sources and the presence of estuarine circulation. The Oosterschelde and Westerschelde (for location see Figure 5.12) – both mature stage tidal basins in the sense of the model – show remarkable differences in suspended mud concentrations. During 1972 –1975, the mean mud concentration measured in the Oosterschelde was about 30 mg l⁻¹; in the Westerschelde the concentrations were about twice as much. The difference is caused by the fact that the Oosterschelde lost its river connection and therefore lacks an estuarine circulation. The difference in the suspended mud concentration on supratidal marsh growth is reflected in their embankments. In the period 1880–1950, the size of the Oosterschelde basin reduced at an annual rate of 0.18 %, the rate of reduction of the Westerschelde basin was 6 times greater.

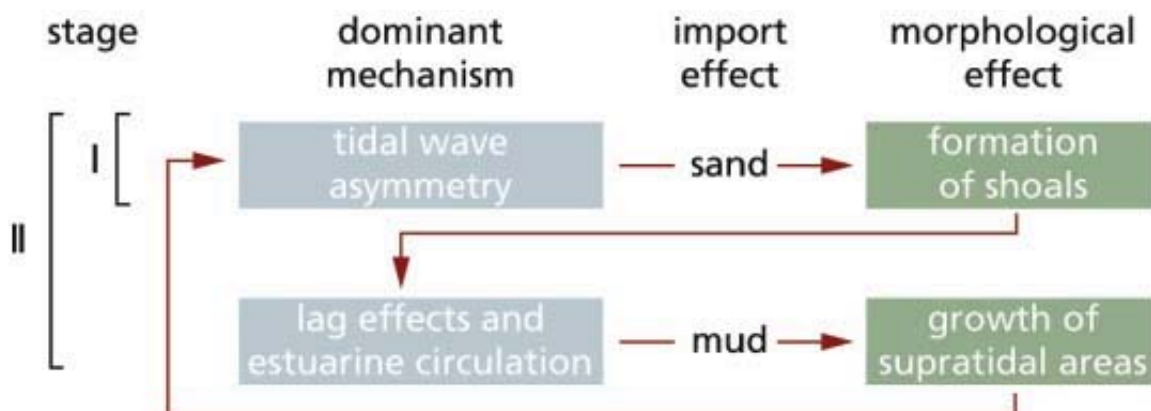


Figure 5.11. Fill processes in meso- and macro-tidal estuarine basins along alluvial coastal plains in the case of a relatively low sediment input from rivers. I. Initial stage: infilling dominated by import of sand due to tidal asymmetry. The imported sand contributes to the formation and expansion of intertidal shoals. As a result, the maximum of flood and ebb discharge shifts to a later stage in the tidal cycle, resulting in a gradual reduction of the sand import. II mature stage: the ratio of channel and shoal areas is “dynamic equilibrium”. Further infilling with sediment from marine sources is caused by lag effects related to mud. This effect is enhanced in case of increased suspended mud concentrations due to estuarine circulation. A large part of the mud deposition contributes to the growth of supratidal marshes, resulting in a reduction of the intertidal area and thus restoring some of the tidal wave asymmetry effect. Note that in stage I, an originally wave-dominated estuary is transformed into a tide-dominated estuary (modified after [Van den Berg *et al.*, 1996](#)).



Figure 5.12. The Ooster- and Westerschelde.

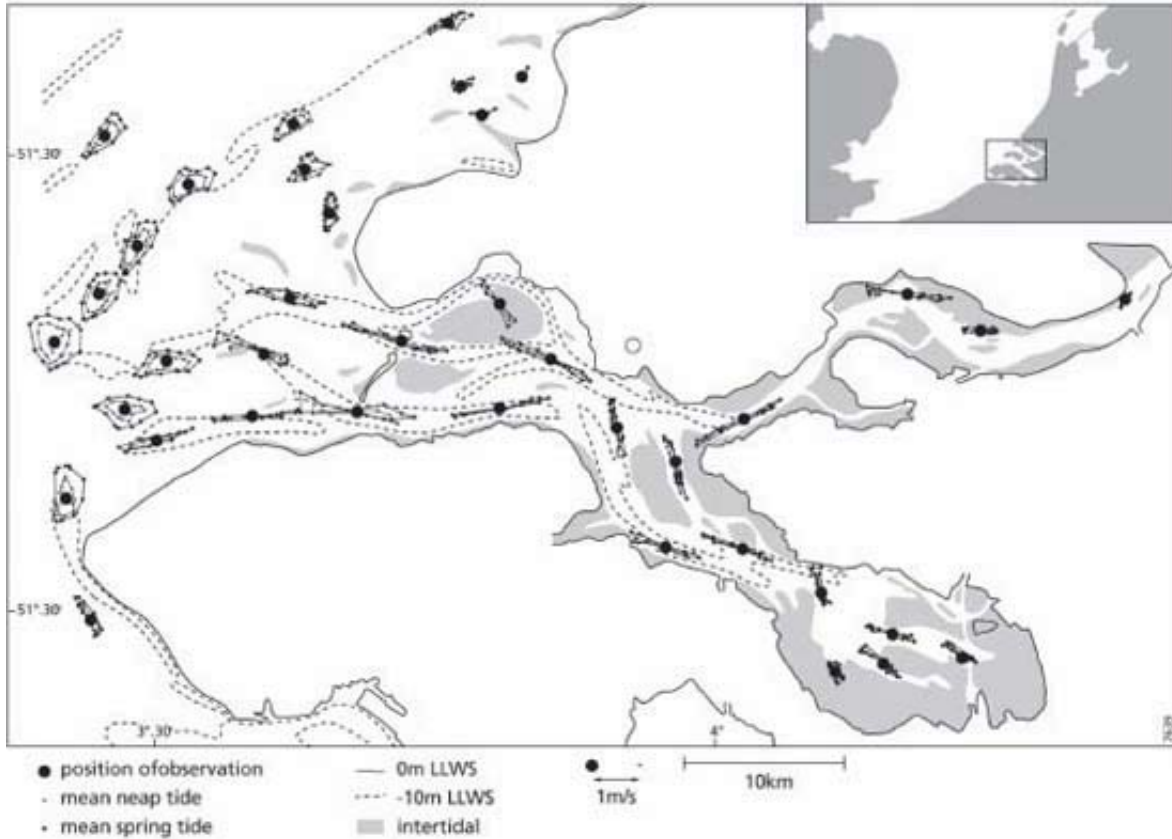


Figure 5.13. Offshore tidal ellipses and inshore reversing rectilinear flow paths in the Oosterschelde during mean neap and spring tide conditions (modified after Siegenthaler, 1982).

In coastal plain estuaries and mud-flat areas, the main part of the flow is concentrated in channels in which the flow reverses from a stable flood direction to an oppositely directed ebb direction. In between flow reversals, slack water periods occur. Offshore rotary tides do not have such slack water periods (Figure 5.13). As a consequence, sedimentological features related to slack water, such as the systematic deposition of mud drapes in subtidal settings at high and low water slack, are restricted to inshore tidal areas. Due to the bi-directionality of the flow inshore, tidal environments have much better developed channels and their size scales nicely with the water volume transported by the dominant tide (Figure 5.14).

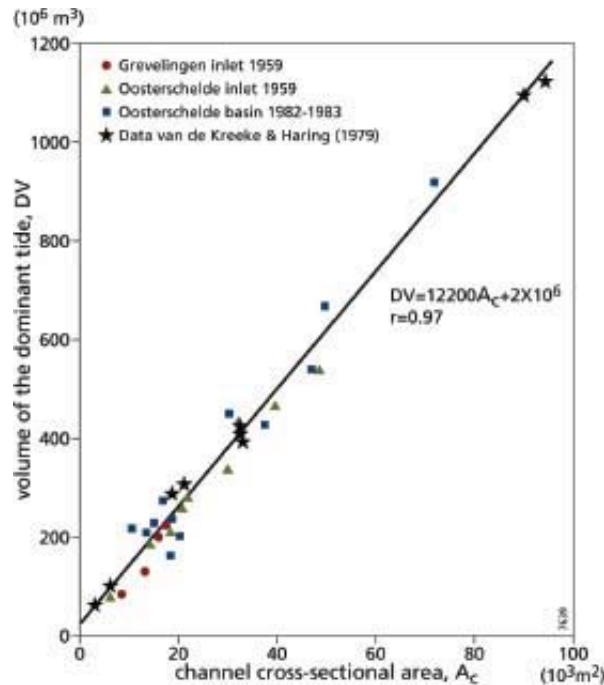


Figure 5.14. Channel cross-sectional area below mean sea level, A_c , as related to the volume of water passing through the channel during the dominant tide, DV (Modified after Van den Berg, 1986).

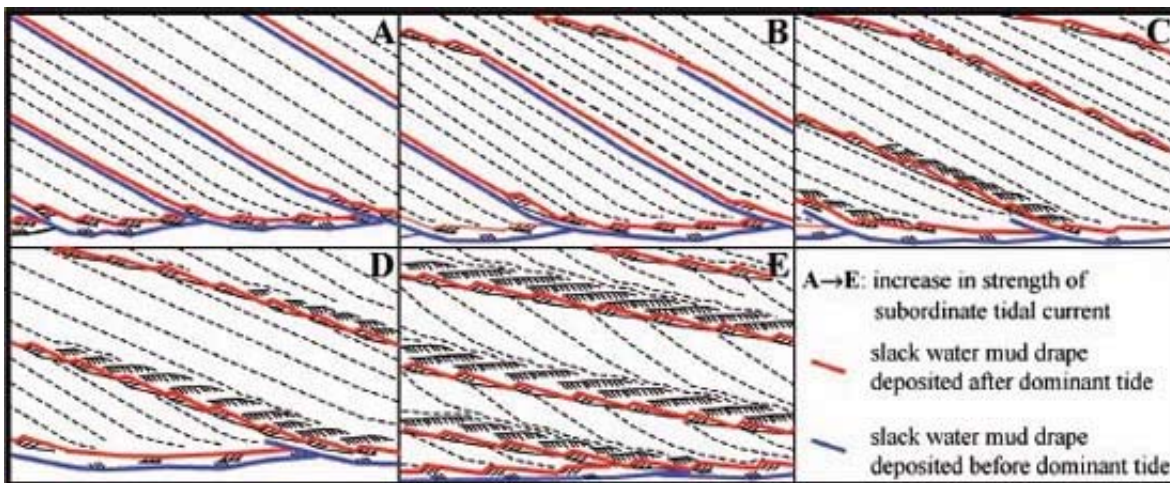


Figure 5.15. Effect of increasing strength of subordinate tidal current on the internal sedimentary structure of subtidal dunes in case of bi-directional tidal currents in deep estuarine channels (modified after Nio and Yang, 1991 and De Mowbray and Visser, 1984; Plate 6):

- A. Incompetent subordinate tide: both slack water mud drapes (*double mud drape*) completely preserved (see also Plate 5).
- B. Subordinate tide capable of eroding the uppermost part of the slip face and the lower drape of the double mud layer.
- C. Subordinate tide capable of eroding most the uppermost part of the slip face and lower drape of the double mud layer, creating a discontinuity surface. On this surface, a train of ripples form

sets formed by the subordinate, draped with mud deposited during the slack water after the subordinate tide. Before a high angle avalanche slope is restored by the dominant tide, a coset of ripple-drift lamination is formed on the mud-draped discontinuity plane.

D-E. Similar to C but with more pronounced discontinuity planes and better developed ripple-drift layers.

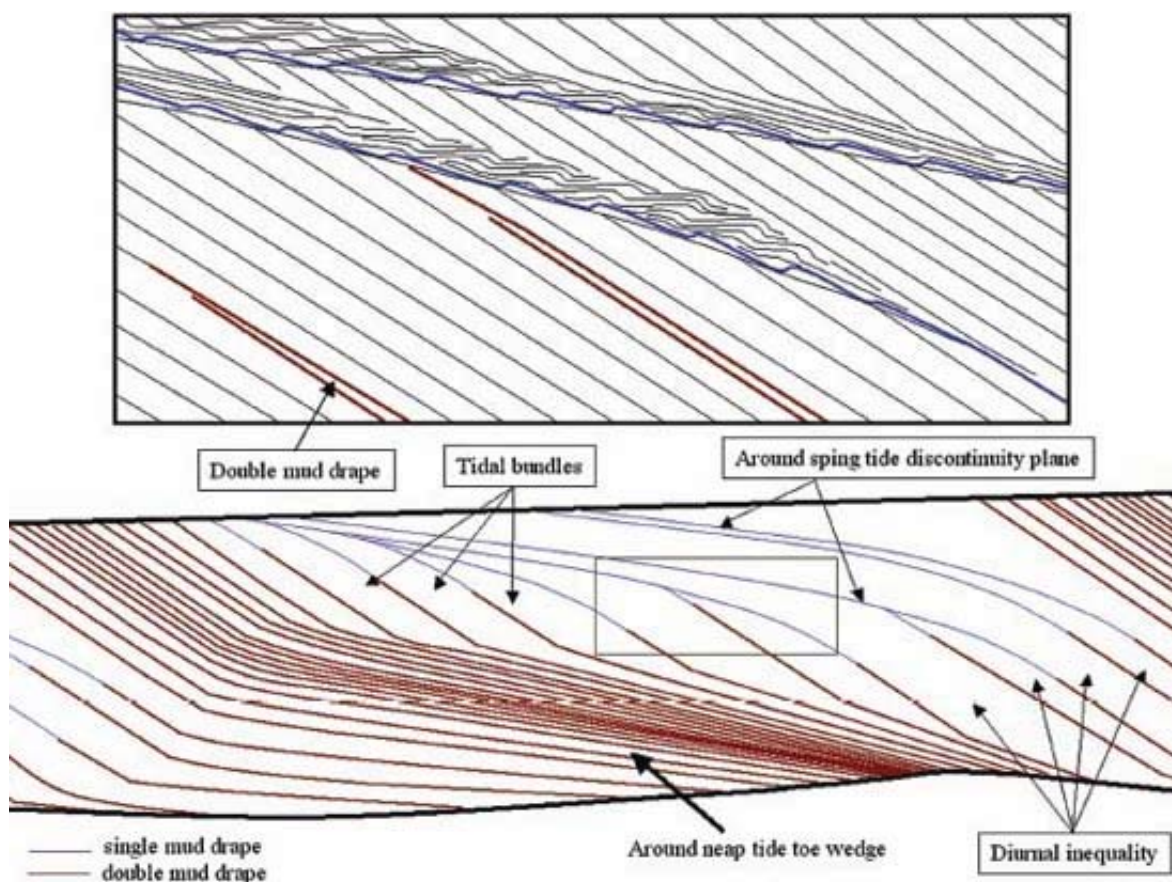


Figure 5.16. Tidal cyclicity in dune deposits in case of a rather strong tidal asymmetry (B and C in Figure 5.15; Plate 7).

Stratification types in unsteady unidirectional and bi-directional (tidal) flows

What sedimentary structures will be formed by tidal currents depends largely upon the flow energy, availability of mud and degree of current asymmetry, i.e., the difference in strength between the dominant and the subordinate tidal currents. In case the dominant tidal current, ebb or flood, is strong enough to generate dunes, it is important whether or not the subordinate tidal velocity exceeds the threshold for sand movement, ripple movement or dune movement. If this threshold is not surpassed and large quantities of mud are present (estuarine conditions), the effect will very likely be a mud drape that marks the pause. The increment of the X-stratified bed between two successive tidal cycles is called a *tidal bundle*. The principal sedimentary features of bidirectional flow in the dune domain are illustrated in Figure 5.15. In the extreme situation that the subordinate tidal current is almost as

strong as the dominant tidal flow, very complex bedding structures with oppositely directed X-bedded sets or bundles of cross-strata are formed. If both tidal currents are of roughly equal strength and are in the ripple domain, an x-laminated coset with oppositely directed semi-tabular sets will develop. The strength of the tidal current varies within the neap-spring tidal cycle. Therefore, during this cycle the produced sedimentary structure may change, for example, in Figure 5.15 from situation A at neap tide to situation D at spring tide. These changes are accompanied by a variation of the dune height, expressed in the partial fill of the dune toe by a thick wedge-shaped bottomset or *toeset* deposit (Figure 5.16).

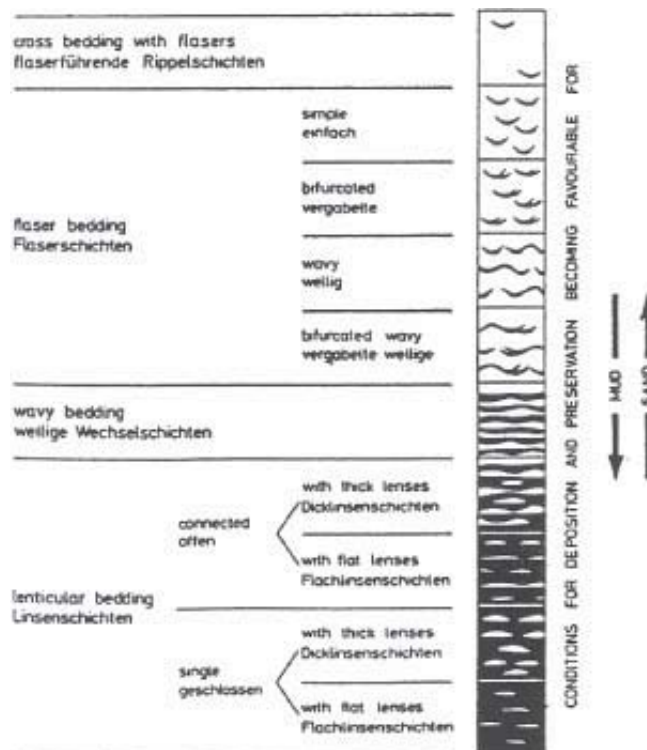


Figure 5.17. Different types of sand-mud alternations, also known as heterolithic bedding. Flaser bedding consists of x-laminated sand with mud drapes. The mud drapes are usually thin and line the former ripple trough or cover the whole ripple. *Wavy bedding* usually refers to continuous sand-bands separated by equally continuous mud bands. The ripple-form preserved along the upper boundary of the sand-bands gives them a wavy appearance. In lenticular bedding, the sand is concentrated in separate lenses, completely embedded in mud (Reineck & Singh, 1973).

Very little is known about the sedimentary structures produced by tidal bores. Only the breaking type of tidal bore seems to be able to cause some erosion of the bed (Bartsch-Winkler and Ovenshine, 1984; Chanson, 2009). As tidal bores differ in size and character, with or without whelps, possibly their reflection in sedimentary structures will show much variation. Martinius pers. comm. attributed some dm thick beds composed of vague, irregular low-angle cross-stratified beds on top of undulating erosional surfaces in the Late Jurassic Lourinhã Formation, Portugal, as a product of tidal bores (Plate 13).

Flaser and lenticular (= ‘linsen’) bedding

Flaser and *lenticular* bedding are end members of a continuum of sand/mud alternations (heterolithic

bedding), in which the proportion of sand and mud vary. Flaser bedding is characterized by thin, curved clay drapes in a usually x-laminated sand body. These clay drapes follow the ripple outline and are thickest in the ripple trough (Figure 5.17). Lenticular bedding (German: *linsen*) consists of sand lenses embedded in a clay layer. These sand lenses may be isolated or connected and represent ripples, which have migrated across a compacted clay-substrate. If, during ripple migration, only a limited amount of sand is available, the ripples build isolated sand heaps and they are said to be 'incomplete'. Flaser and lenticular (*linsen*) beddings are formed in environments with either a start-stop or a reversing flow characteristic and high mud concentrations. Although look-alike heterolithic beds may be found in fluvial sediments, they are most commonly formed in the tidal domain.

1 The lunisolar precession refers to the very slow rotation of the axis of the Earth causing the axis to trace out a full circle against the fixed stars every 25776 years.

6 Soft-Sediment Deformation Structures

Any sediment may be disturbed after deposition but disturbance is most common in sands and finer grained materials. Earlier structures may be disrupted and distinctive new structures may form as a result of physical, chemical and biological processes. In this chapter, only the generation of deformation structures by physical processes is treated.

Reduction of sediment strength

Many types of physical disturbance, commonly gravitationally induced by inverse density gradients, occur in unconsolidated sediments in a weak condition. According to the Coulomb law, the resistance of sediment to physical disturbance can be expressed by its shear stress, τ , being a function of grain cohesion, C_g , intergranular friction and the effective pressure between the grains:

$$\tau = C_g + (\sigma - p)\tan\phi \quad (\text{Nm}^{-2}) \quad (6.1)$$

in which σ is pressure normal to shear, p is excess pore-fluid pressure and ϕ is the angle of internal friction (in loose sands without pore water flow ϕ equals the “angle of repose”). For sediment to fail and be deformed after deposition, it should behave like a fluid. Consequently, its shear strength must be very small. Exceptionally, mud with a high water content behaves as a *plastic* (Bingham) fluid. Examples are sling mud in harbours or fluid mud of biogenic origin: up to several dm thick ‘*crème de vase*’ covering part of the intertidal flats of the Bay of St Michel, France. Generally, however, a substantial reduction of the shear strength — to practically zero — is needed to obtain a fluid-like behaviour of the sediment. Such a rheologic change can be achieved by a loss of cohesion, by a readjustment of packing to reduce $\tan\phi$, or by increasing the pore pressure. Cohesion is controlled by grain size and mineralogical properties and therefore not readily changed by mechanical forcing. Changes of pore pressure or internal friction angle, ϕ , are easily produced in an over-pressured or under-compacted state of the waterlogged sediment, thus making it susceptible to losing its strength. If a certain critical shear value is surpassed, the fabric of loosely packed grains is destroyed, the grains lose their mutual contacts and collapse into more tightly packed structures. During the process of compaction, the sediment changes from a solid-like state into a fluid-like state and back again.

Even if all factors act in the same direction creating a potential instability, the dislocation may not take place unless mechanical triggering takes place, bringing the sediment into a temporary fluid-like state. Potential triggers are an earthquake or cyclical normal stresses exerted on the seabed by large swell waves. The critical shear condition may be reached by sediment loading at the top of a sub-aqueous slope, loading due to emergence or erosion at the base of a slope. Current traction on top of a loosely packed sand-bed may also trigger deformations.

The change from a solid-like to a liquid-like state may be due to *liquefaction*, *fluidization*, or a combination of these processes. A pure liquefied flow is generated without an external source of water, whereas the existence of a pure fluidized flow exactly depends on it. Liquefaction may occur in cohesionless materials as well as in clay, though the process in clay is more complex. In case of a sand deposit, the two mechanisms exclude each other. In cohesionless materials, the liquefaction process is only possible in water-saturated, loosely packed, fine sands (pore space > 43 %). Tightly packed sands (pore space < 43 %) tend to expand under shear, a process known as *dilatancy*, for which reason it can only operate with an influx of water from an external source (=fluidization). In sand, a liquefied flow *sensu stricto* can only exist for a very short time: the process of settling into tighter structures takes only a few seconds or tens of seconds at maximum. Liquefaction of clay results from the collapse of grains into more tightly packed structures but is also related to changes in the structure of clay aggregates. Freshly deposited marine clays often show a very open, flocculated structure. An attempt to change from an open structure with high porosity and water content to a denser structure results in an increase in pore pressure as well as a lowering of porosity and permeability. Due to this, the over-pressure of the pore water is released only slowly. A liquefied state in clay may therefore last much longer than a liquefied state in sand. Fluidization, like liquefaction, occurs in mud as well as in sands. The upward flow may be caused by over-pressured groundwater, by the presence of an artesian aquifer or as the result of compaction due to increased loading because of (rapid) sediment accumulation or glacier advance (!). Whereas the time available for the deformation of liquefied sand is short, that for a fluidized state may be so prolonged that complete mixing of the sediment occurs. In the latter case, the sediment may become massive throughout. A liquefied flow on a slope may be fluidized by absorbing ambient water and pass into a *debris* flow or even a high-density *turbidity* current. It is important to realize that the fluidization process can be more effective when a debris flow is turbulent, implying the necessity for a relatively high Reynolds number, thus a high velocity of the debris flow (steep bed slope) or a great thickness. In other words, a small debris flow on a gently sloping surface is unlikely to be transformed into a turbidity current.

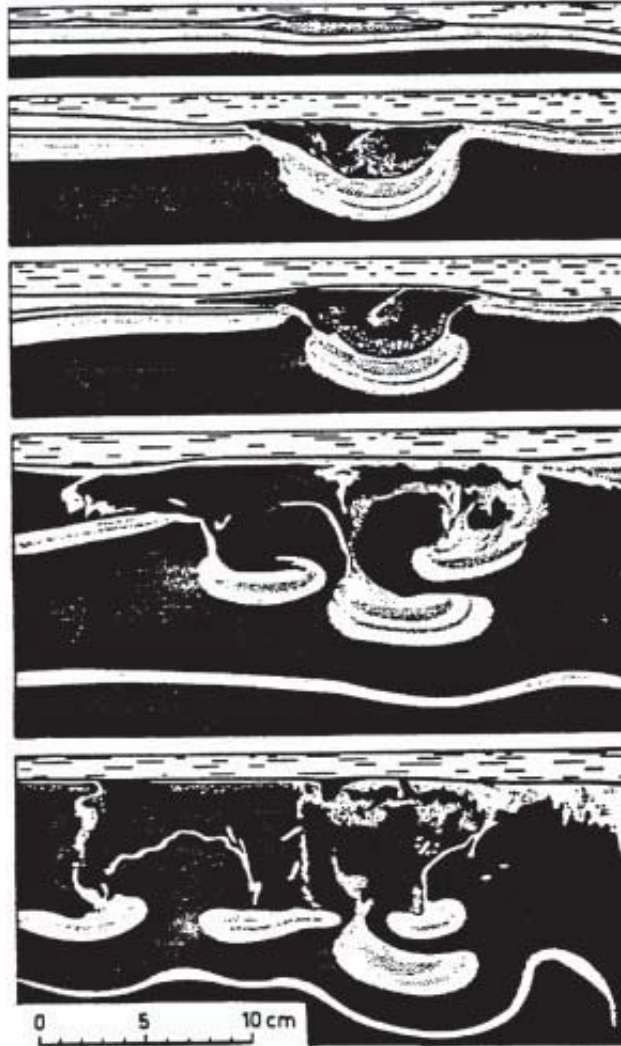


Figure 6.1. Load casting produced in a laboratory tank. Part of a sand layer overlying clay sinks down (Keunen, 1965).

Terminology, classification and occurrence of deformation structures

Deformation structures are often limited in a vertical and lateral sense. The depth of deformation depends on the number of layers involved as well as their thickness. The thicker and more numerous the layers participating in the dislocation, the more penetrative and more voluminous the resultant structures will be. The classification of deformation structures on the basis of a hierarchal system of parameters is virtually impossible, due to the difficulty of assessing objective criteria for the description of the often complex, 3D configurations. In addition, the configurations may change considerably over a short distance. As a consequence, deformation structures are usually described and grouped in a rather artistic way, on the basis of style and intuition concerning their generation.

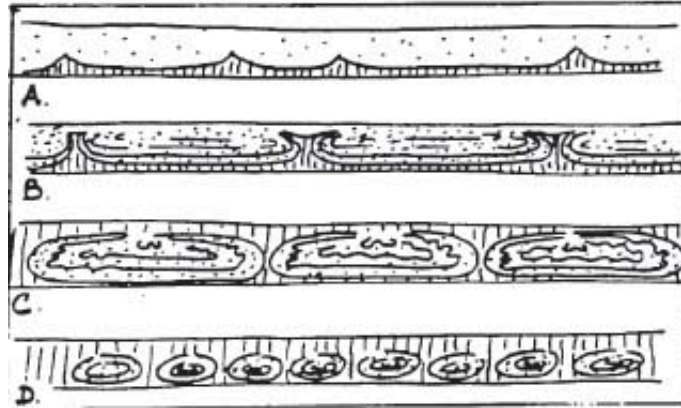


Figure 6.2. Four types of load casting largely dependent on relative thickness of the competent layers.

The value of the deformation structures for environmental interpretation is rather limited, as their implication is largely rheological, pointing to a failure in the strength of the sediment during or shortly after deposition. Strength failure of this kind, caused by excessive pore fluid pressure or the compactional instability of an underlying (clay) layer, can be expected to occur in almost every environment, although fine-grained, rapidly deposited sediments are more susceptible than others. Low-energy environments in which loosely packed heterolithic strata are deposited from suspension are vulnerable to deformation. On the other hand, strong wave action on the seabed likely produces sands with a dense fabric, which is unfavourable to the generation of deformation structures.

Load casts

Load structures or *load casts* form when a bed of relatively high density sinks into a less dense one (Figure 6.1). The contrast in density may have to do with a difference in mineralogical composition and grain size of the beds, but more often, with only a slight difference in their water-filled pore volume: mud commonly has a high depositional porosity of 60–70%, which result in a relatively small bulk density compared to sands, which have a depositional porosity of about 40–42%. Mineralogy and grain size may influence the compaction of a bed. As such, a clay bed is retarded in its compaction compared to a sand bed, since the former's water escape is hindered by the sheet-like structure of the clay minerals. Mineralogy may also influence the stability of a bed in a more direct fashion. Certain minerals such as micas tend to act as a lubricant between the more equi-dimensional grains of a sand bed. The shape and size of the load-cast largely depend on the thickness of the pile of strata involved and their bedding characteristics. A relatively thick sand bed that sinks into a thin clay layer will produce long *pillows* with edges that are hardly pulled-up (Figure 6.2 A,B). The clay layer builds regularly-spaced *flames*, protruding into the overlying sand. If sand and clay beds are of about equal thickness, the pillows will subside further into the underlying clay and be squeezed into more or less closed *balls* enveloped by clay (Figure 6.2 C). Where the sand bed is relatively thin, the subsiding balls may become tilted. If the sense of tilting is erratic, it usually implies that the beds were originally in a horizontal position. If the tilting shows a pronounced preference in direction, a depositional slope may have been the case. Numerous, small load casts 'swimming' in a clay layer usually point to a succession of loading events in which thin and laterally limited beds participate. These thin beds may come from the successive detachment of thin sub-beds or bundles of laminae from the base of a thicker bed or from successive ripples travelling across and subsiding into a clay surface. Usually, the

different stages of loading can then be distinguished.



Figure 6.3. Slump structures produced in a laboratory tank.

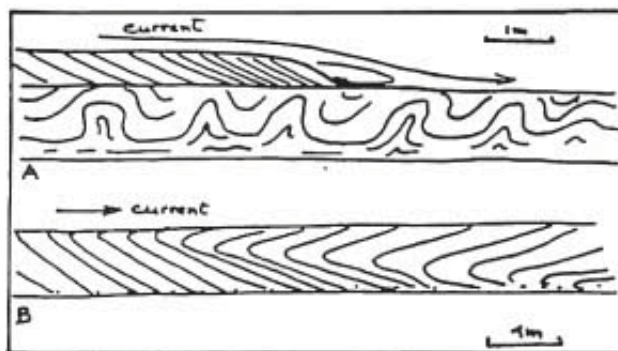


Figure 6.4. Convolute structures and overturned cross-bedding.

Slump structures

These constitute erratically contorted, usually variably sized and shaped slabs of sediment with a 'floating' appearance. The sediment participating in these slabs may be pure sand but very often is a sand-mud alternation. Slumps are produced by a lateral displacement under gravitational forces together with a loading into the underlying sediment. Usually, the slump-slabs have completely lost their mutual connections. Mixing with overlying water may dilute the sediment flow to a debris flow or even a turbidity current. Therefore, all sorts of transition can be observed between load-casts with a slight lateral movement and completely disordered, slump deposits or deposits of debris flows, with great lateral displacement. The direction of the palaeo-slope is often difficult to deduce from well-

developed slumps. Examples of slump structures are depicted in [Figure 6.3](#).

Convolute lamination and deformed cross-bedding

Convolute lamination is characterized by a complex of intricate folding in a laterally more or less continuous fashion ([Figure 6.4](#)). Relatively broad and gently curved synforms are connected by sharper and narrower antiforms (*pitch and swell*).

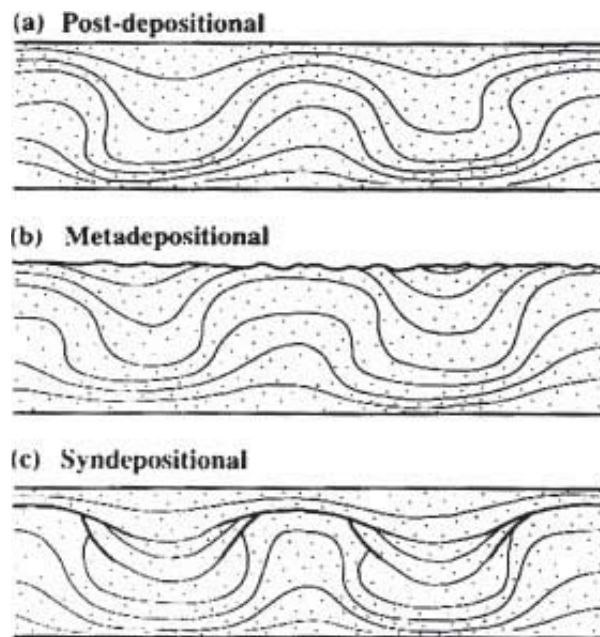


Figure 6.5. Schematic types of convolute laminations ([Allen, 1985](#)).

The individual beds or laminae participating in this kind of deformation structure may be traceable over considerable distances, often showing local thinning and thickening, apparently by stretching and contraction. Convolution is commonly attributed to the interaction of the following processes: (1) rapid deposition and liquefaction of the sediment, (2) drag exerted by the overlying current, which causes flow of the sediment, and (3) water escape in beds of fine-grained sand or silt. Because such types of sediments are often produced by turbidity currents and river overbank flows, these environments are especially prone to the evolution of convolute lamination. Many eolian deposits contain load casts and other deformation structures that may be the result of liquefaction after being soaked with water during a rain storm ([Schwan, 1991](#); [Plate 14](#)). Some caution is necessary, however, because similar structures are formed by animal feet imprints. In niveo-eolian deposits water escape and resulting liquefaction may occur during melting of buried snow. Three varieties of convolute lamination can be distinguished, depending on the inferred relative timing of deposition and deformation ([Figure 6.5](#)). Deformed cross-bedding often appears as over-steepened or even overturned upper portions of the foresets ([Figure 6.4](#)). Towards the lower levels of the cross-bedded set, the cross-strata may be undulating or even crumpled. Deformation structures include (shrinkage or mud) cracks and rain spots, formed through the impact of raindrops on soft, fine-grained sediment ([Plate 14](#)). Also, some of the sole marks discussed earlier (see [Figure 3.2](#)) belong to this category of structures.

Fluidization structures

Fluidization of sand bodies devoid of clay layers usually produces an almost complete obliteration of stratification and a massive, structureless appearance. If mud, even in small quantities, is admixed as a matrix or as thin drapes, the force of water expulsion during deposition of the fluidized sand body may develop a *dish and pillar* structure (Figure 6.6). The dishes consist of rather vague, upwardly concave, pseudo laminations remotely resembling flasers. The ‘tails’ of these dishes may be upturned. The dishes are attributed to lateral branching of the vertical flow paths of the escaping water around inhomogeneities in the sediment. At these inhomogeneities, clay and silt particles filtered from the water accumulate, thus enhancing and broadening the inhomogeneity. In the upper part of a dish-structured layer, pillar-like structures made of pure, massive sands may be encountered. They seem to represent some kind of exhaust pipe through which water expelled from the lower part is concentrated while moving upwards. As such, the pillars are comparable to clastic dikes but, instead of being sheet-like, the intrusions of sand-water mixtures into adjacent sediments are of a columnar shape.



Figure 6.6. Dish and pillar structure.

7 Eolian Sedimentary Structures

In air the most obvious difference with aqueous flow is the absence of a free surface. An equally important difference has to do with the easy compressibility of air, in contrast to the incompressibility of water. Despite these differences, it is fortunate that gasses like air and liquids like water are both fluids in the sense of their mechanical behaviour and the fundamental laws of fluid mechanics are applicable to both. In flowing air, just like in water, there are two types of forces that can mobilize grains lying on the bottom: *drag forces*, acting horizontally on the grains in the direction of the main flow and *lift forces*, acting vertically upwards. There are also two forces trying to keep the grains at rest: *gravity*, acting downwards and, if clay particles or water is present in the voids between the grains, *cohesion*, which tries to keep the grain close to its neighbours. As a consequence of some basic physical differences between air and water, the sedimentary morphology, structures and textures are different, to a certain extent. The most important physical difference lies in the much larger density contrast of air and quartz, compared to air and water: $\rho_{air} = 1.23 \text{ kgm}^{-3}$, $\rho_{water} = 1000 \text{ kgm}^{-3}$, and $\rho_{quartz} = 2650 \text{ kgm}^{-3}$. Another important difference is that the dynamic (molecular) viscosity of air, being a gas, is about 56 times lower than that of liquid water. The result of both is that the settling velocity of a quartz grain in air is 60 to 80 times higher than in water and for the transport of a grain in wind, a critical shear velocity of about 30 times higher is required than for the same grain in water. The combination of high velocity and large density contrast leads to an effective transfer of momentum (mass x velocity) when a blown sand grain hits the bottom. As a consequence of this, the process of *saltation* (= 'jumping' of grains) is much more important in the eolian environment than in water. The high energies of falling and impacting grains lead to intense mechanical wear (*abrasion*) of grains during eolian transport and this results in the well-rounded and sometimes *frosted* appearance of eolian grains larger than about $100 \mu\text{m}$. Numerous microscopic impact pits on the grain surface cause this frosted appearance. Smaller grains generally show a larger angularity, for three reasons (Tanner, 1956): (1) because the grain is so light that it is incapable of self-abrasion on impact with other grains; (2) it is transported in suspension and (3) it falls between larger grains and is thus protected from the abrasive action of other saltating grains. A frosted appearance caused by saltation impacts indicates that the grain was subject to a long duration of eolian activity. Frosted quartz grains are therefore typical of desert sands. If, however, quartz grains have been cemented by calcite in fossil sediment, the surface of the grains are corroded by the calcite to give the grain a frosted appearance as well. Under the optical microscope, these corrosion pits appear as light diffraction rings similar to, but often bigger than, those associated with desert frosting.

Sand and silt

Eolian sediments are generally finer grained and better sorted than their water-deposited equivalents. Most of the world's eolian sand deposits are no coarser than $250 \mu\text{m}$. Larger size grades, such as coarse sand and gravel, are sometimes present in distinct layers but then they usually have the meaning

of a *lag deposit* from which the finer fractions have been blown out. Very fine particles, such as silt and clay, are normally not present in active dune sand because they are lifted too high by saltation and are subsequently carried away in suspension.

Eolian silt (=loess) deposits of 10–70 μm grain size are quite common in the world. They form widespread blankets around formerly glaciated areas, high mountain plateaus and, to a lesser extent, around active deserts. The 60-70 μm grain size, which separates the sand and silt fractions, is not an arbitrary boundary but is related to the fact that quartz in plutonic rocks crystallizes with regularly spaced imperfections in its crystal lattice, the so-called *Moss defects*. From these sites small fractures develop, which subsequently form the starting points for disintegration of the quartz into smaller grains. These defects have spacings that are normally not smaller than 60 μm . Sand size grades can therefore easily be produced from plutonic (granite) source rock. Much more energetic processes however, are needed to make smaller grains. Large-scale production of silt is only achieved by glacial grinding or by intense weathering in high, cold, tectonically active mountain regions. At present, the Qinghai/Tibet plateau in Central Asia is the world’s major generator of silt. Classical (Sahara type) deserts do not produce a lot of silt because wind on its own is not powerful enough to comminute the sand. On the other hand, it may be very effective in polishing, rounding and sorting the grains.

After deposition from suspension, loess does not show many sedimentary structures, apart from cryo-/bioturbation and eventually, soil features. In many areas however, the loess is subsequently reworked and redeposited into beautiful aquatic bed forms and structures, as for instance, in the Yellow River and its delta in China.

Mechanics of transport

The threshold of grain movement in wind has been determined in several experiments by various researchers. A pioneer amongst them was *Ralph Bagnold*. In his famous book, “*The physics of blown sand and desert dunes*” he proposed the following simple equation for the critical shear velocity of grain entrainment by wind, also termed the *fluid threshold velocity*:

$$u_{*c} = A \sqrt{\frac{\rho_s - \rho}{\rho_a} gD} \quad (\text{ms}^{-1}) \quad (7.1)$$

where the coefficient A was determined from experiments, and found to be about 0.1 for sand.

Bagnold’s data and those of others have been summarized in [Figure 7.1](#). The strong upturn of the curve for sizes smaller than 0.1 mm is due to cohesive forces.

In wind, in contrast to water, there is an important mechanism capable of lowering the theoretical threshold velocity, which is only related to fluid drag and lift forces. That is the earlier mentioned salation of grains, which results in an effective transfer of kinetic energy from the air to the bed. It is most significant in size ranges larger than 60 μm . Smaller grains do not produce frequent impacts because they are mainly transported in suspension ([Figure 7.2](#)).

There are two fundamentally different modes of sediment transport in eolian environments, just as in water. *Bedload*, which includes the grains moving by *surface traction* plus those mobilized by

saltation. Surface traction load is also sometimes referred to as the *contact load*, since the grains do not lose contact with the surface. The second major mode of transport is suspension. As in aqueous flows there is no sharp boundary between pure suspension (dominated by turbulent diffusion) and saltation (dominated by ballistics). The transitional transport mode is termed *modified saltation*. A distinction between suspended bed-material transport and wash load is normally not made in eolian environments, contrary to the fluvial usage. *Long term suspension* can be considered as equivalent to the term: wash load. An overview of the different transport modes as related to grain size and shear velocity is given in Figure 7.3.

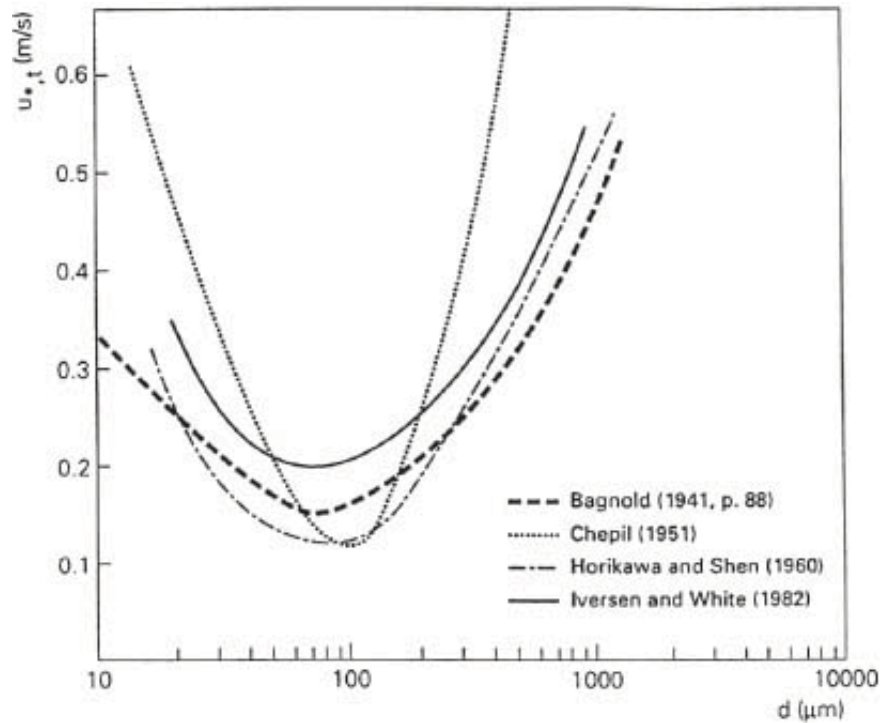


Figure 7.1. Threshold shear velocity curves for quartz grains of different diameter. Iversen & White (1982) take into account variations in cohesive forces. Chepil’s curve relates to an equivalent diameter ($=Dps/\rho$) of sediment that contains a mixture of size fractions (Chepil, 1951; Pye and Tsoar, 1990).

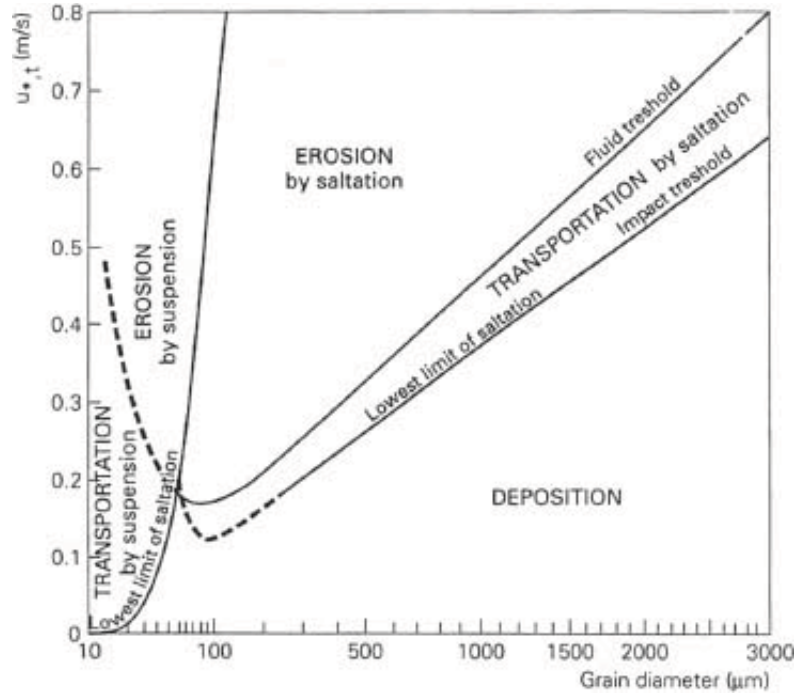


Figure 7.2. Lower limit threshold of the initiation of motion in suspension, in saltation and by the impact of saltating grains (modified after Pye and Tsoar, 1990).

Bed forms

Bed forms under atmospheric flows range over more than four orders of magnitude in size, from the familiar lowly ripples from the action of summer breezes on a dry beach to the gigantic hills of sand captured by aerial and satellite images over deserts. Wilson (1972) defined three distinct bed form groups from the Algerian Erg Oriental by plotting grain size against bed form wavelength. In ascending order, these are *wind (ballistic) ripples*, *dunes* and *draas*. Subsequent studies however, indicate strong overlap between the proposed dune and draa fields, negating the Wilson concept.

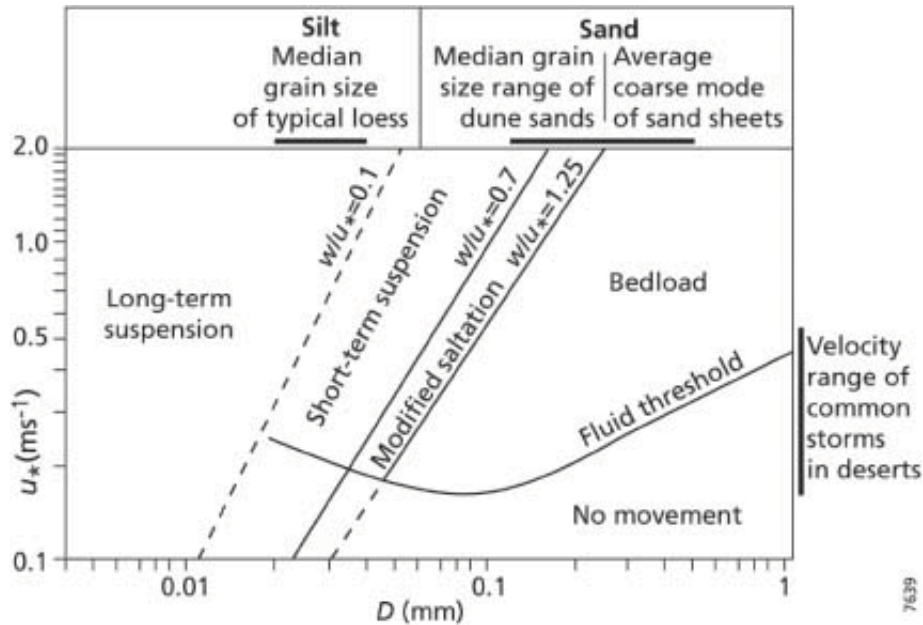


Figure 7.3. Modes of transport of quartz spheres at different wind shear velocities (Allen, 1997, modified after Tsoar and Pye, 1987). w = grain settling velocity and u_* = shear velocity (see table 1 and eq. 1.5).

In case of large bed forms, one or more classes of smaller-sized bed forms are generally found superimposed. Some horizontally layered beds in ancient desert deposits indicate that upper plane beds can occur in eolian conditions (Clemmensen and Abrahamsen, 1983; Schwan, 1988). However, an eolian upper plane bed is probably not an equilibrium bed form as in aqueous conditions. Hunter (1977) saw the development of eolian upper plane beds on a beach at a wind velocity of 18 ms^{-1} . However, within one hour the plane bed was replaced by ripples, while wind speed was not diminished. If plane bed would occur as a stable, equilibrium bed form, it is certain that it would only form at extreme wind speeds and that it would be mobility-forced, as supercritical conditions do not occur in wind and viscosity differences are not influential.

Wind ripples

Wind or *ballistic* ripples form continuous series of equally-shaped and sized bed forms in sand and very fine gravel with wavelengths of 0.02 – 2.0 m and heights from a few millimeters up to 0.3 m (Figure 7.4). The vertical form index, λ/H , is in the order of 20, but can range from 5 to 70 (Allen, 1984). Unfortunately, in current ripples the range of this form of index is about the same. The size of the ripples increases with wind speed and duration (up to a certain limit) and coarseness of the sediment. In contrast to their aqueous counterparts, wind ripples developed in very fine to medium sand show long and weakly sinuous to remarkably straight crests as a stable bed configuration (Figure 7.5). In coarser sediments, the ripples are more three-dimensional. A common attribute of all but the smallest forms in very well-sorted sands is the concentration of coarser grains in the crestal areas.

Concerning the origin of eolian ripples, the superficial resemblance of form to subaqueous ripples hides a fundamental contrast in their mechanism of formation. As discussed earlier, saltating grains in air are much ‘heavier’ than saltating grains in water because of the greatly increased density ratio of

solid to fluid. Conditions on the air-bed interface are thus dominated by grain splashdown effects and not by the small-scale viscous sub layer streaks that control ripple initiation on the water-bed interface. In air, fine sand grains move by saltation and upon impact, their kinetic energy is such that they are capable of nudging coarser grains (up to six times their diameter) by intermittent rolling or sliding (termed *reptation* by some authors) to form part (up to 25 %) of the total sediment transported as creep load. Ripples produced by this ballistic process will increase in wavelength with increasing grain size and decreasing grain sorting, since the saltation jump length of fine particles increases markedly with the size of the bed grains with which they collide. In case of very high wind speeds of long duration and the availability of coarse sand and/or fine gravel, wind ripples may become larger, up to 1 m high. These are also termed *granule ripples*.

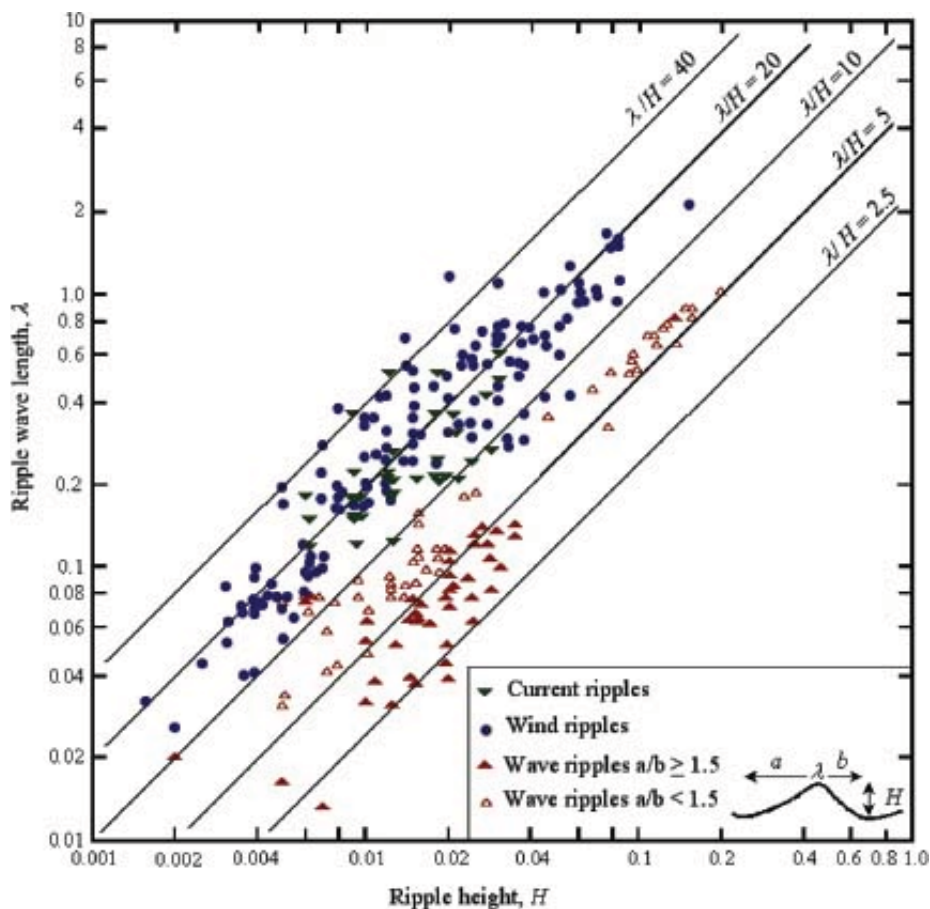


Figure 7.4. Ripple steepness, λ/H of ripples in wind and water. Data obtained from Allen (1984).

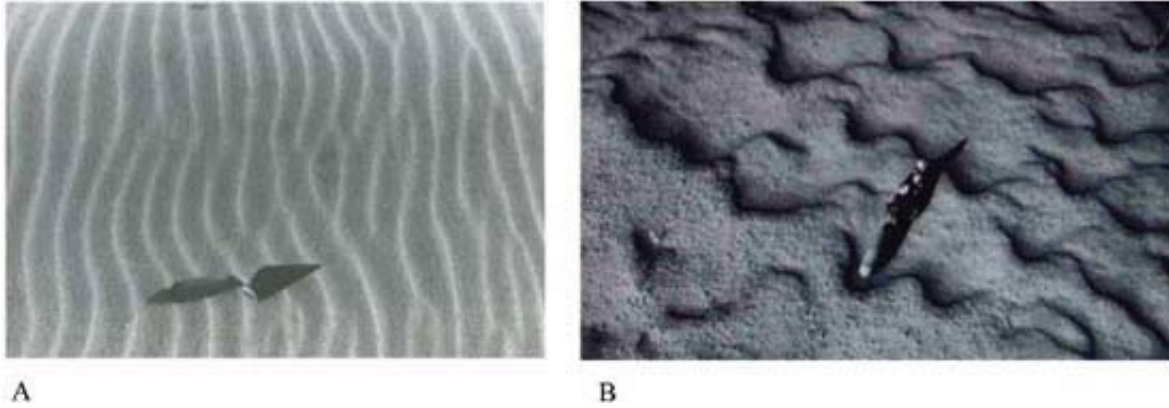


Figure 7.5. Wind (ballistic) ripples: A. in fine sand; B. in ill-sorted medium to coarse sand. Trowel 0.28 m long points to wind direction (Allen, 1984).

Order	Wavelength	Height	Orientation to wind	Possible origin	Suggested name
1st	300– 5500 m	20– 450m*	longitudinal or transverse	primary aero- dynamic instability	draas* (= megadunes)
2nd	3– 600 m	0.1– 100 m	longitudinal or transverse	primary aero- dynamic instability	dunes
3rd	15– 250 cm	0.2– 5 cm	longitudinal or transverse	primary aero- dynamic instability	aerodynamic ripples
4th	0.5– 2,000 cm	0.05– 100 cm	transverse	impact mechanism	impact ripples
	1– 3,000 cm	0.05– 100 cm	longitudinal	secondary horizontal spiral vortices	secondary ripple sinuosity

* Draas can have their own slip faces or may have their lee sides covered in dunes.

Table 7.1. Classification of eolian bed forms by Wilson (1972) and Collinson and Thompson (1987).

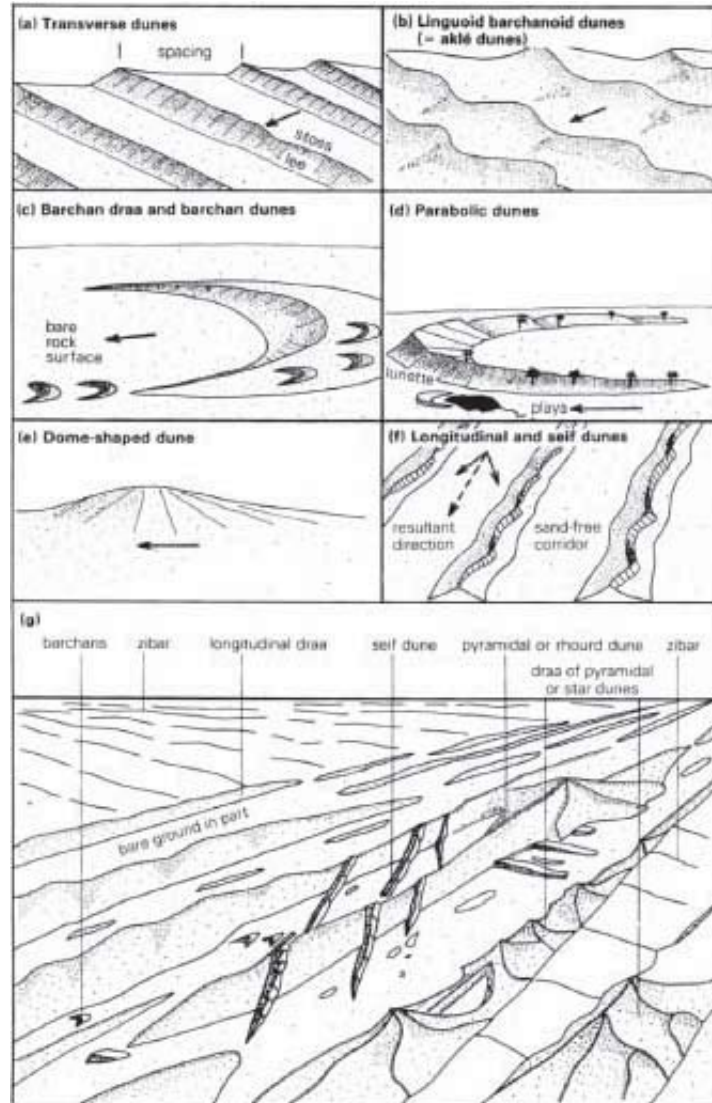


Figure 7.6 Three dimensional forms of some dune types. The arrows mark the dominant direction of the effective winds and, in the case of (f) the dotted arrow is the resultant effective direction. (g) Three dimensional view of draas, dunes and other structures, e.g., zibar. Note that the relationships shown are diagrammatic and such varied close associations are not likely to be found in nature (Cooke and Warren, 1973, modified by Collinson and Thompson, 1987).

Dunes and draas

Eolian dunes show more diverse morphologies than their subaqueous counterparts. A simple division into longitudinal (stream wise), transverse (span wise) and complex forms with respect to the mean resultant wind direction is useful, although transitional forms occur and many dunes commonly show combinations of all elements. Observation of aerial frequency, width, wavelength, height and grain size reveals a hierarchy of bed forms in which similar structures coexist at different sizes and spaces (Table 7.1), suggesting a relation with wind shear. However, a stability diagram analogue of Figure 3.5 does not exist. The reason for this is that wind changes velocity and direction too quickly for dune and draa bed forms to become equilibrium bed forms. Some common associations of desert dune types are

sketched in [Figure 7.6](#). A second control is exerted by the abundance of sand supply. The limited availability of sand leads to barchan types of dune bed forms, which migrate over a stable substrate ([Figure 7.7](#)). Such a substrate does not necessarily consists of hard rock or a gravel (desert) pavement, but can also be related to groundwater (moist or salt covered surface). Vegetation may play an important role in stabilizing and modifying dune forms, for instance, into the parabolic dunes commonly found in coastal dune areas.

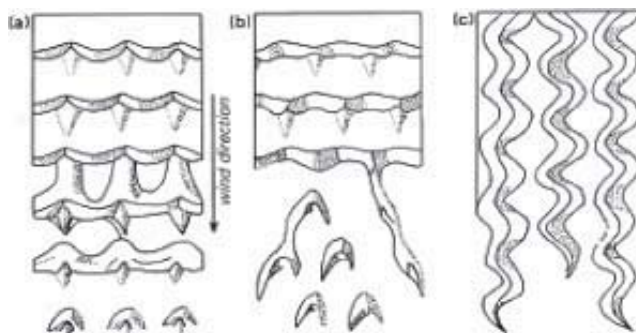


Figure 7.7. Bed form patterns formed by the combinations of longitudinal and transverse elements: (a) grid iron, large transverse in-phase; (b) fish scale, largely transverse out-of-phase; (c) braided, largely longitudinal out-of-phase patterns. A progressive decrease in sand cover is shown towards the bottom of the diagram. Some kinds of barchan and seif dunes form the fish-scale patterns where there is incomplete sand cover ([Collinson and Thompson, 1989](#)).

Sedimentary structures

Detailed studies of sedimentary structures in recent eolian dunes are relatively rare because permanent exposures are hard to make and conserve in dry, unconsolidated sand. The good size sorting combined with the uniform mineralogy is generally responsible for poorly visible structures. Lacquer peels are not easily made for the same reasons. Ancient eolian deposits are relatively better known and studied, at least from cores in the subsurface.

The descriptive terms (cross-bedding, -lamination, even lamination, trough/wedge-shaped sets, etc.) that we have learned for aquatic deposits, can be used equally well for the eolian environment because they are part of an essentially non-genetic classification. A now generally used classification of eolian structures was proposed by [Hunter in 1977](#). He distinguished the sediments on the basis of their main transport mechanisms into: (a) *grain flow*, deposition (b) *grain fall* deposition, and (c) tractional deposition. The structures related to the first two mechanisms are called *grain flow* cross-stratification and grain fall lamination, respectively. Those related to tractional deposition are subdivided into a number of other categories. They are summarized in [Table 7.2](#). The Hunter classification has a genetic implication at its base and it emphasizes stratification types, which can be considered as diagnostic for the eolian environment. An example is the grain flow cross-stratification, which forms long-stretched tongues of sand as a result of intermittent avalanching of sand from the dune's slip face. The lens-shaped deposits ([Figure 7.8](#)) are sometimes clearly recognizable. A grain flow is a plastic flow that "freezes" below a certain critical shear stress. The *freezing* starts at the base of the flow and very quickly migrates upslope. However, at several points the process may be interrupted and the still active part of the grain flow may override the "frozen" cross-stratum, giving rise to in-stratum *flame*

structures, drag folds and breakaparts (Figure 7.9 and Plate 15). The latter structures seem not to form in X-beds of aquatic dunes, which might be explained by the much smaller momentum of aquatic grain flows, which would impede their formation. Eolian X-bedding tends to have a “swoopy” look that is difficult to pin down in detail. This reflects the tendency for the troughs of eolian dunes to be filled by plastering of new trough laminae not just by the mean-upcurrent side, as is usually the case in subaqueous dunes, but on the lateral and mean downcurrent sides as well. Eolian X-bedding is more likely to show a greater dispersion of dip directions of cross-sets, because of the greater variability of wind directions than of subaqueous current directions. If eolian dunes become soaked with rain their steep fronts may destabilize, giving rise to slumps and related deformation structures (Figure 7.10). The thawing of a frozen wet dune surface may also lead to instability and cause sliding of the thawing layer of the dune front over the non-frosted substrate. The originally frozen sand blocks of the fractured superficial sand layer in the slide can be recognized by their angular shape and deviating internal X-stratification (Plate 16).

Depositional process	Character of depositional surface	Type of stratification	Dip angle	Thickness of strata, sharpness of contacts	Segregation of grain types, size grading	Packing	Form of strata
Tractional deposition	Rippled	Subcritically climbing translant stratification	Stratification: low (typically 0–20°, maximum ~30°) Depositional surface: similarly low	thin (typically 1–10 mm, maximum ~5 cm) Sharp, erosional	Distinct Inverse	Close	Tabular planar
		Supercritically climbing translant stratification	Stratification: variable (0–90°) Depositional surface: intermed. (10–25°)	Intermediate (typically 5–15 mm) Gradational	Distinct Inverse except in contact zones	Close	Tabular commonly curved
	Smooth	Ripple-foreset cross-lamination	Relative to translant stratification intermed. (5–20°)	Individual laminae: Thin (typically 1–3 mm) Sharp or gradational, nonerosional	Individual laminae and sets of laminae: Indistinct Normal and inverse, neither greatly predominating	Close	Tabular, concave-up or sigmoidal
		Rippleform lamination	Generalized: intermediate (typically 10–25°) Low (typically 0–15° max?)	Sets of laminae: Intermediate (typically 1–10 cm) Sharp or gradational, nonerosional	Indistinct Normal and inverse, neither greatly predominating	Close	Very tabular, wavy
Largely grainfall deposition	Smooth	Planbed lamination	Intermediate (typically 20–30° min. 0° max. ~40°)	Intermediate (typically 1–10 cm) Sharp or gradational, nonerosional	Indistinct Normal and inverse, neither greatly predominating	Close	Very tabular, planar
Grainflow deposition	Marked by avalanches	Grainfall lamination	High (angle of repose) (typically 28–34°)	Thick (typically 2–5 cm) Sharp, erosional or nonerosional	Distinct to indistinct Inverse except near toe	Intermediate	Very tabular follows pre-existent topography
		Sandflow cross-stratification				Open	Cone-shaped tongue-shaped, or roughly tabular

Table 7.2. Characteristic basic types of eolian stratification (Hunter, 1977).

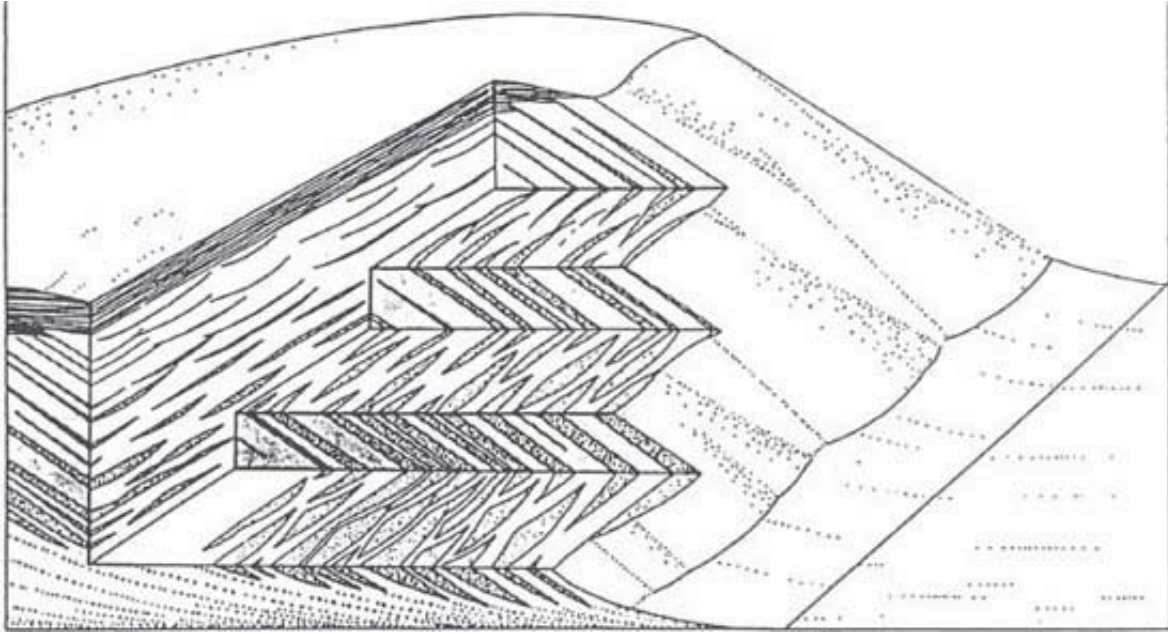


Figure 7.8. Schematic diagram showing the distribution of stratification types in a small dune. Grain flow X-strata heavily stippled, grainfall laminae unshaded (foreset X-strata) or lightly stippled (bottomset strata). Topset climbing translantent strata thin lined (Hunter, 1977).

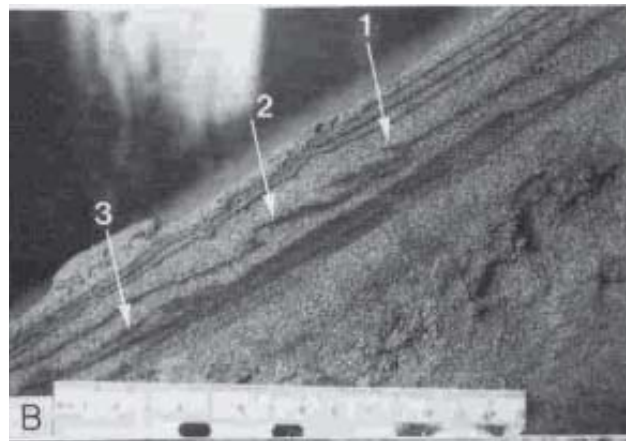


Figure 7.9. In-stratum structures produced at the upslope translation of the freezing front of an eolian grain flow (Fryberger and Schenk, 1981).

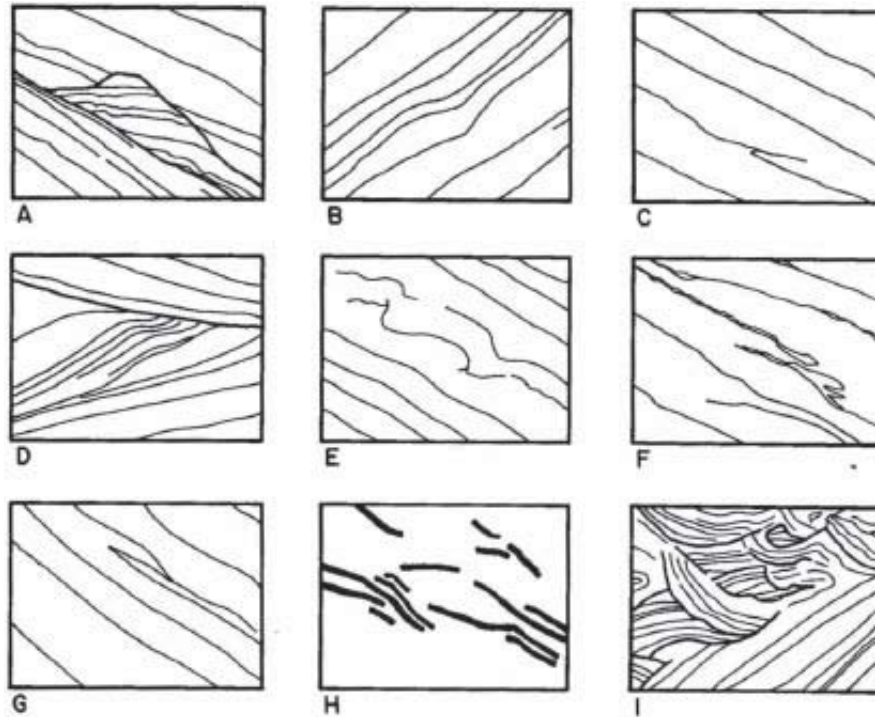


Figure 7.10. Principle types of deformation structures in dune front deposits: A. rotated structures; B. warps or gentle folds; C. flame structures; D. drag folds; E. high-angle asymmetric folds; F. overturned folds; G. overthrusts; H. break-aparts; I. breccias. Each block represents an area of ca. 15×10 cm (after McKee and Bigarella, 1979).

Depending on the sedimentation rate wind ripples form various types of *climbing translantent* strata (Figure 7.11). In contrast to aquatic ripples, x-lamination in eolian ripples is hardly visible, except in rare cases that coarse sand is incorporated (compare Plate 17 with Plate 18). Due to the 2-dimensionality of the ripples, set shapes of subcritically climbing translantent strata generally are rather tabular (Plate 18). The hopping length of large reptating grains is relatively small. As a consequence large grains collect near the brinkpoint of the ripple, while small grains rain down in the ripple trough (Anderson & Bunas, 1993; Makse, 2000; Figure 7.12). Therefore there is a slight tendency to concentrate coarse grains at the crests of the wind ripple, in contrast to the usual coarsening towards the ripple troughs in aquatic environments. Unfortunately this important diagnostic feature of eolian ripples often is not of any use, as many wind ripple deposits consist of well-sorted sand that prevents development of reverse grading. The coarsening upwards in x-laminated sets is best developed in deposits of granule ripples, because they always consist of poorly sorted material and they more often have the set thickness necessary to see reverse grading. *Grain fall lamination* is typically deposited from suspension but it is less distinctive as a structure on its own. It is generally mixed with grain flow lamination (at the base of dune slip faces) or with ripple-associated tractional deposits. Grainfall lamination may be very hard to distinguish from subcritically climbing translantent stratification, which also forms low-angle, almost horizontal laminae. As in river dunes, grain fall bottomsets of eolian dunes interfinger with grain flow foreset deposits. However, the regular sequence of co-flow backflow units, as found in bottomsets of river dunes, is not present. Other characteristic features of the eolian environment are the various types of adhesion structures. *Adhesion ripples*, *adhesion warts* and *adhesion plane beds* have been recognized (Figure 7.13). All have in common that they form on damp surfaces where the grains become trapped by surface tension. Adhesion ripples have small wave

lengths (< 1 cm) and are typically not higher than a few mm. They grow slowly upwind by accretion of saltating sand as long as the capillary rise of moisture keeps pace with the rising surface (see also Plate 18). It can thus be an effective way of trapping eolian sediment, leading to rapid vertical accretion. Vegetation of course, can also help in this respect. When the surface dries out, ‘normal’ processes of traction, saltation and ripple formation take over again.







		TRANSLATENT STRATA	RIPPLEFORM LAMINAE
ANGLE OF RIPPLE CLIMB (α) RELATIVE TO INCLINATION OF RIPPLE STOSS SLOPE (β)	SUBCRITICAL ($\alpha < \beta$)	 SUBCRITICALLY CLIMBING TRANSLATENT STRATA	 TRUNCATED RIPPLE-FORESET CROSSLAMINAE
	CRITICAL ($\alpha = \beta$)	 CRITICALLY CLIMBING TRANSLATENT STRATA	 COMPLETE RIPPLE-FORESET CROSSLAMINAE
	SUPER- CRITICAL ($\alpha > \beta$)	 SUPERCRITICALLY CLIMBING TRANSLATENT STRATA	 COMPLETE RIPPLEFORM LAMINAE

Figure 7.11. Types of structures produced by eolian climbing ripples at various angles of climbing (modified after Hunter, 1977).

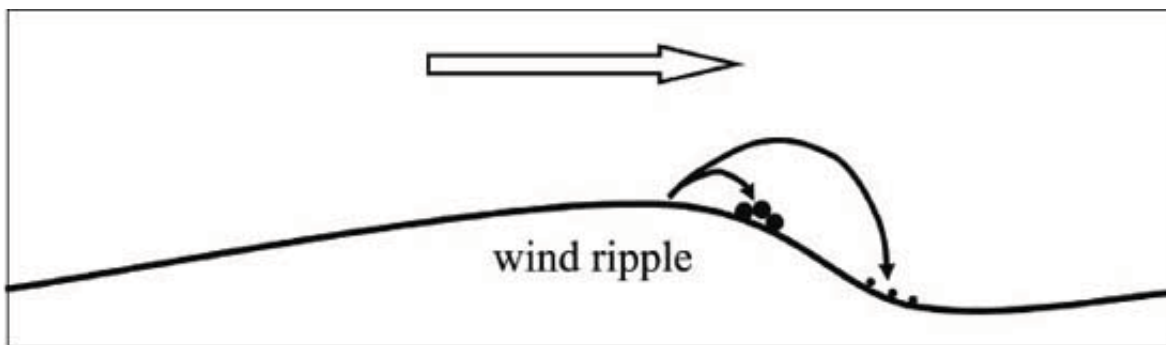


Figure 7.12. Inverse grading due to different saltation lengths of large and small grains (see also Plate 17).

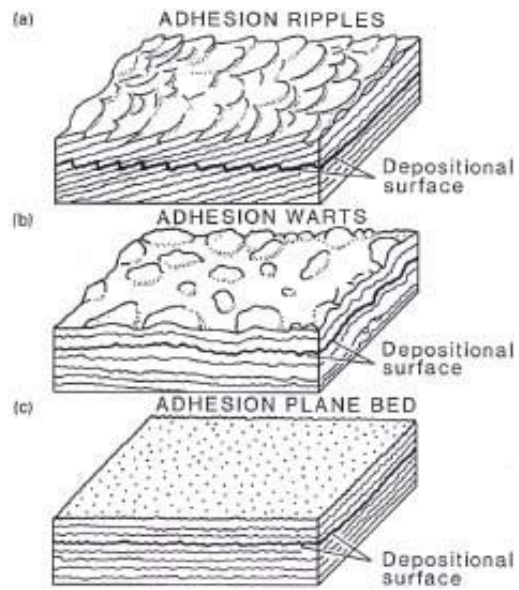


Figure 7.13. Block diagram illustrating the plan view shape and cross-sectional structure of the main types of adhesion structures (Kocurek and Fielder, 1982).

9 Plates

PLATE 1A (page 32 and 37)

FORESET AND BOTTOMSET DEPOSITS OF 2D FLUVIAL DUNES

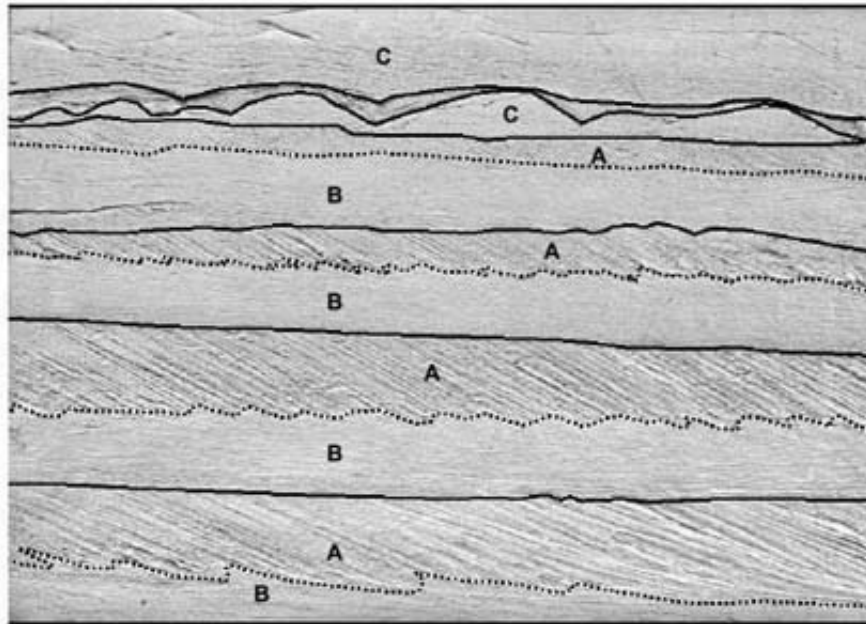
Unidirectional tabular crossbedding with well-developed bottomsets, lacquer peel image



PLATE 1B (page 32 and 37)

FORESET AND BOTTOMSET DEPOSITS OF 2D FLUVIAL DUNES

Uni-directional tabular cross-bedding with well-developed bottomsets, interpretation graph



Upper pointbar,
Holocene Rhine
deposits,
Wageningen,
Netherlands

After Boersma (1967)

<i>set content</i>	<i>interpretation of deposit</i>
A cross-stratification	accretion of dune lee (grainflows of coarse sand in foreset)
B cross-stratification	current ripples in dune vortex area (grainfall of fine sand in bottomset)
C cross-stratification	current ripples

PLATE 2A (page 36)
CROSS-LAMINATION BY 3D CURRENT RIPPLES
Small-scale trough cross-lamination in strike section, lacquer peel image



PLATE 2B (page 36)

CROSS-LAMINATION BY 3D CURRENT RIPPLES

Small-scale trough cross-lamination in strike section, interpretation graph



Glacial outwash plain deposits, Pleistocene-Eistertian, Den Helder, Netherlands

PLATE 3A (page 38)
CLIMBING RIPPLES
Ripple drift lamination, lacquer peel image

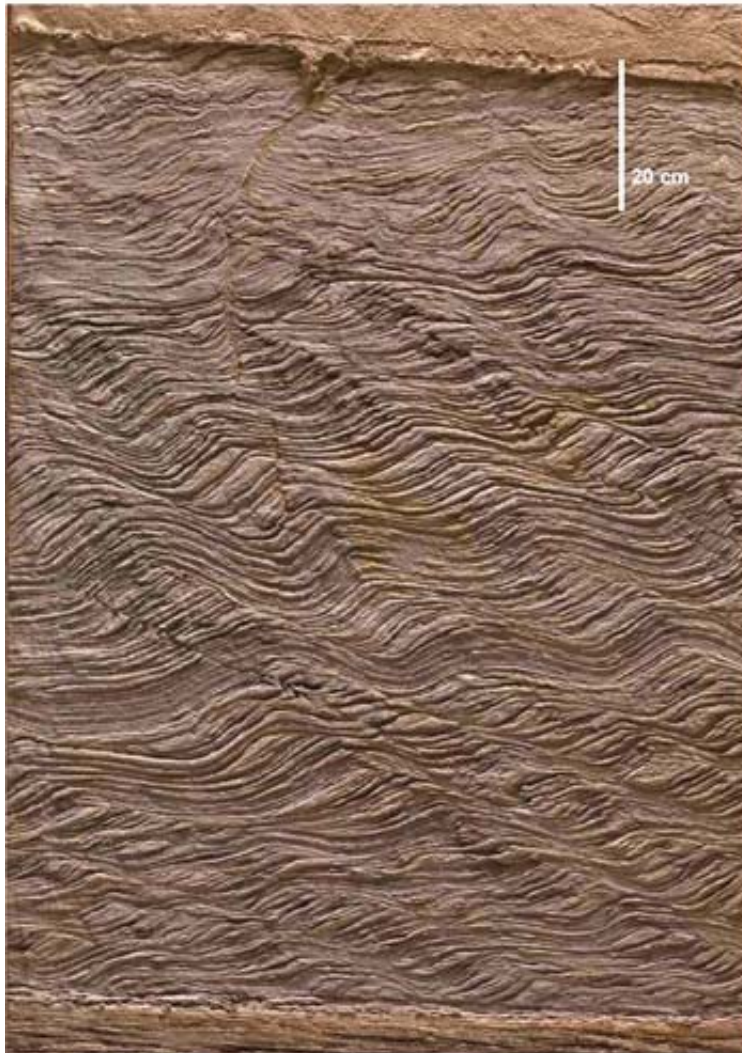
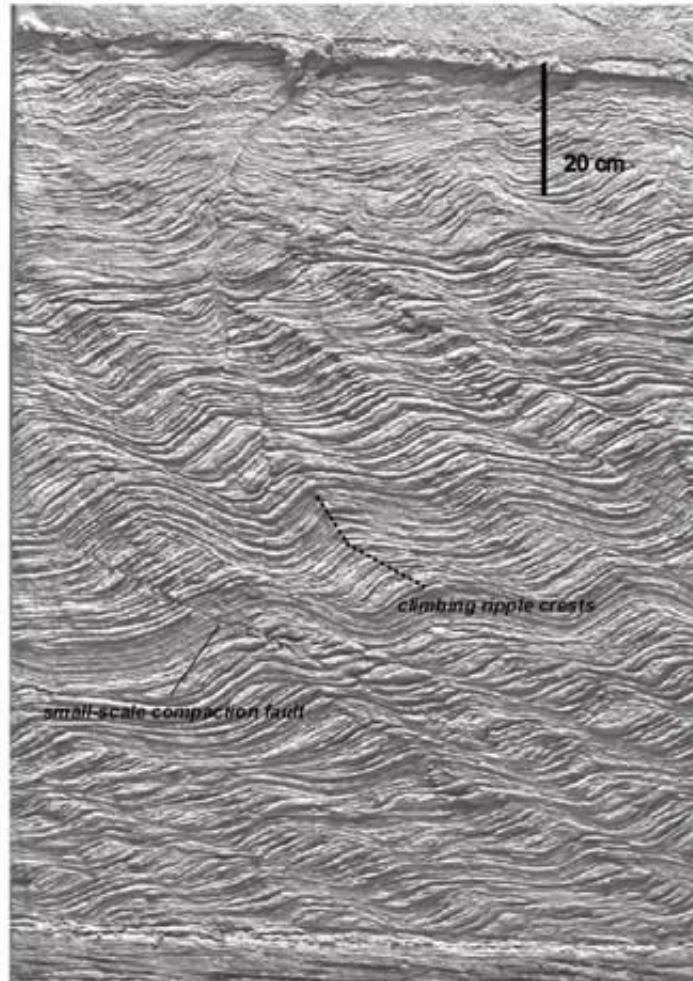


PLATE 3B (page 38)
CLIMBING RIPPLES
Ripple drift lamination, interpretation graph



Proglacial lake deposits, Pleistocene - Elsterian, Den Helder, Netherlands

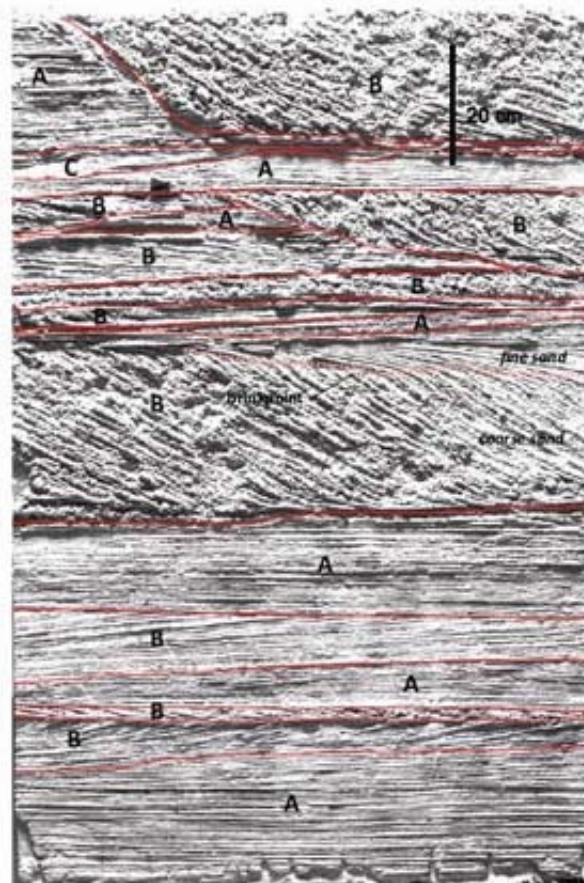
PLATE 4A (page 20, 37 and 40)

COMPOSITE SET OF EVEN LAMINATED AND CROSS-BEDDED SANDS
Alternation of upper plane bed fine-grained even laminated sands and coarser grained
cross-bedded lateral bar accretion units, lacquer peel image



PLATE 4B (page 20, 37 and 40)

COMPOSITE SET OF EVEN LAMINATED AND CROSS-BEDDED SANDS
 Alternation of upper plane bed fine-grained even laminated sands and coarser grained cross-bedded lateral bar accretion units, lacquer peel image



Glacio-fluvial outwash plain deposits, Saalenian, Werpeloh, Germany

	<i>set content</i>	<i>flow condition</i>	<i>interpretation of deposit</i>
A	even lamination	upper flow regime	deposition on a plane bed
B	large-scale x-stratification	flow expansion behind bar	lateral bar accretion
C	small-scale x-stratification	lower flow regime	deposition by current ripples

PLATE 5 (page 70)

DOUBLE MUD DRAPE OR MUD COUPLET

Diagnostic attribute for clastic tidal deposits - subtidal megaripple crossbedding



Oosterschelde construction pit (Netherlands)

Outcrop at approximate 15m below mean sea-level

ebb = dominant current, flood = subordinate current



Kristin Field, Garm Formation
well 6406/2-5, Norwegian Offshore



Smørbukk Field, Tilje Formation
well 6506/11-4st2, Norwegian Offshore

PLATE 6 (page 70)

SCHEMATIC DRAWING OF DUNE (MEGARIPPLE) BEHAVIOUR DURING A SINGLE FLOOD-EBB CYCLE WITH WEAK SUB-ORDINATE CURRENTS

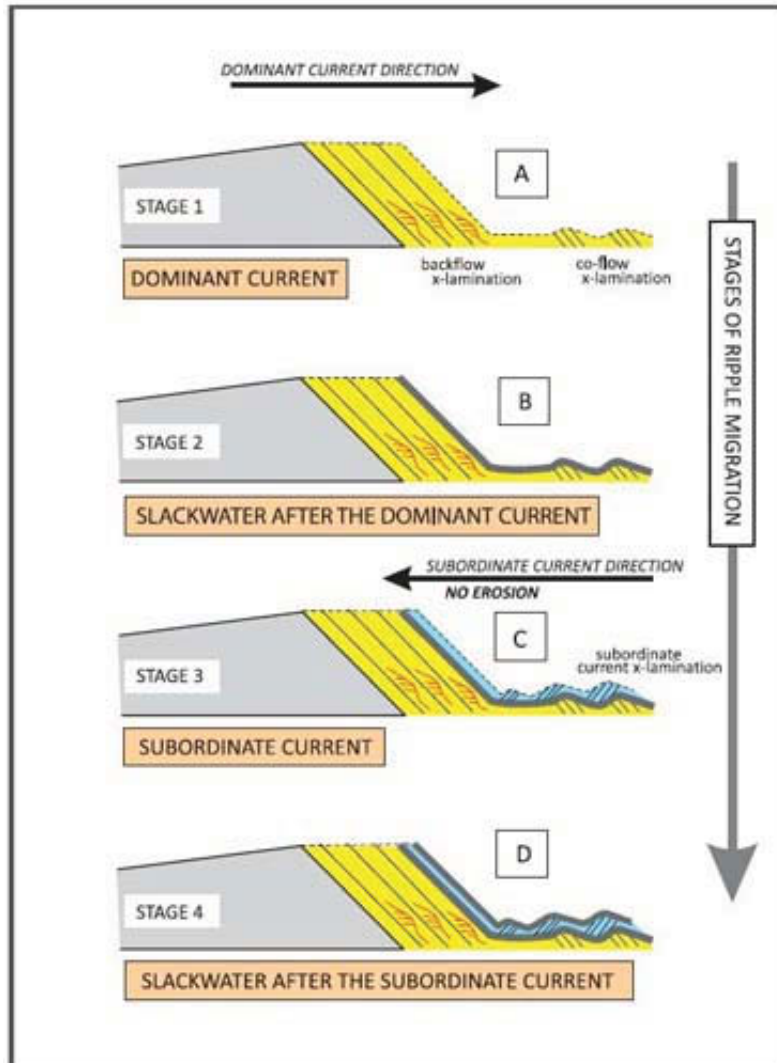
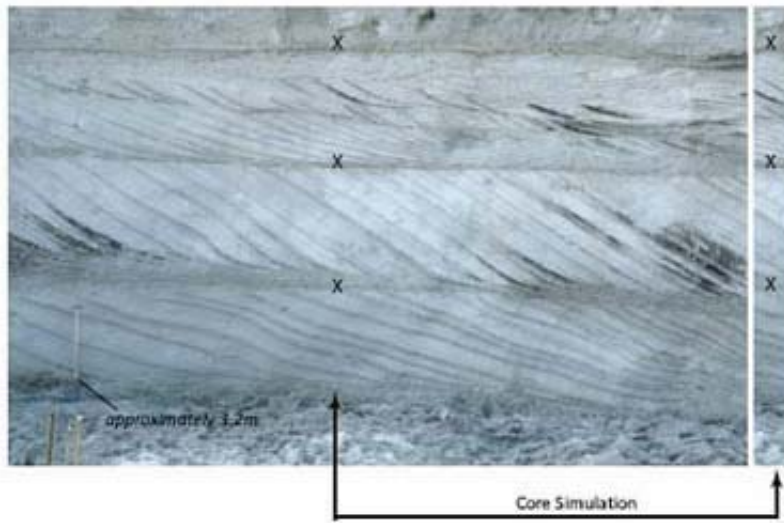


PLATE 7 (page 9 and 71)

EBB-ORIENTED CO-SETS WITH WELL DEVELOPED BUNDLE SEQUENCE

Subtidal co-sets of dune (megaripple) crossbedding, inshore tidal channel deposits, outcrop image

Oosterschelde construction pit,
outcrop approximately
15m below Mean Sea Level



dm = double mud drape
md = mud

Mud couplets and bundle sequence in
the Glauconitic Sandstone,
Lower Cretaceous
Alberta Canada

Courtesy Indranil Banerjee (1989)

PLATE 8A (page 31 and 37)

DETAILS OF TIDAL CROSS-BEDDING

Upper part of dune (megaripple) cross-bedding with preserved topset, lacquer peel

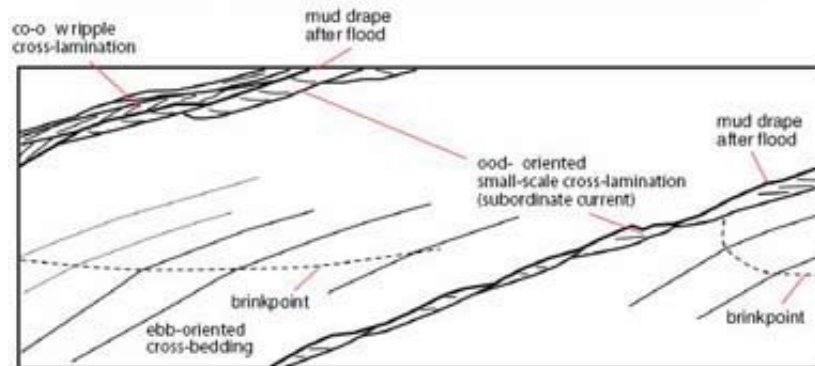


Tidal channel deposits, outcrop 11-13 m below mean sea level, age 18th century, Oosterschelde estuary mouth, Netherlands (Van den Berg, 1982)

PLATE 8B (page 31 and 37)

DETAILS OF TIDAL CROSS-BEDDING

Upper part of dune (megaripple) cross-bedding with preserved topset, interpretation graph



Tidal channel deposits, outcrop 11-13 m below mean sea level,
18th century, Oosterschelde estuary mouth, Netherlands
(Van den Berg, 1982)

PLATE 9A (page 31)

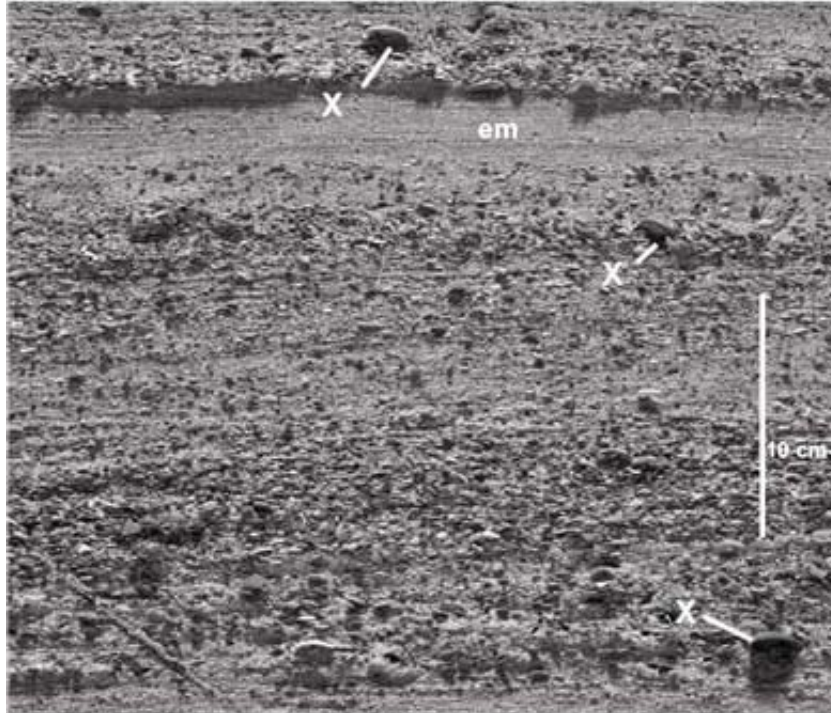
DETAILS OF SWASH LAMINATION
Upper plane bed on a beach, lacquer peel image



Lower foreshore exposure, Schoorl, Netherlands

PLATE 9B (page 31)

DETAILS OF SWASH LAMINATION
Upper plane bed on a beach, interpretation graph



X : Shells oriented predominantly with convex side upwards
em : Upper plane bed even lamination

Lower foreshore exposure, Schoorl, Netherlands

PLATE 10 (page 40)

DETAILS OF SWASH LAMINATION IN CORES
(Upper plane bed, upper shoreface)



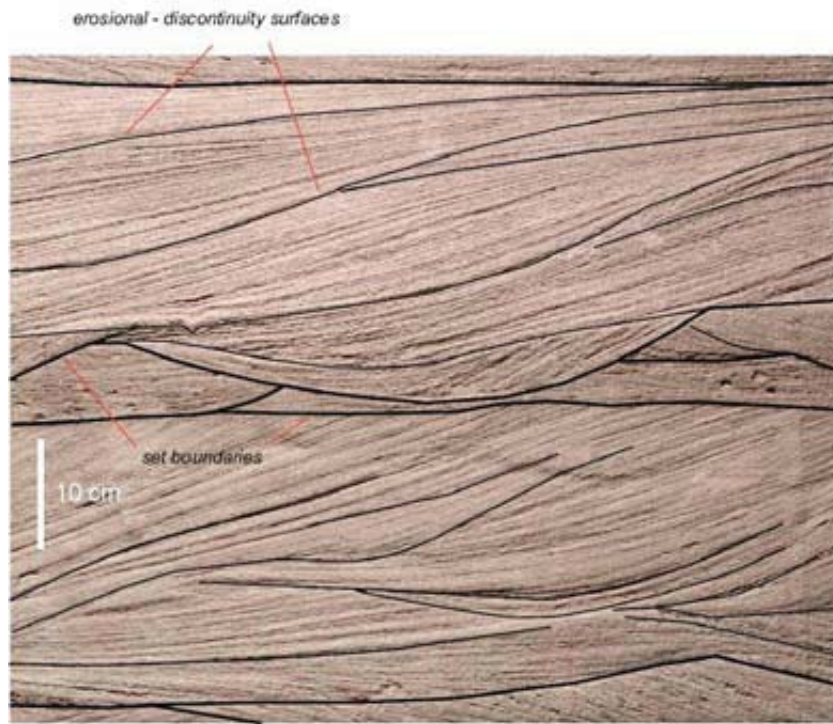
Tordis Field, Middle Jurassic, Brent Group, Offshore Norway
Well 34/07-14

PLATE 11A (page 58)
HUMMOCKY CROSS-STRATIFICATION
Upper shoreface, lacquer peel



Miocene outcrop, Garsdorf lignite mine, Germany

PLATE 11B (page 58)
HUMMOCKY CROSS-STRATIFICATION
Upper shoreface, lacquer peel



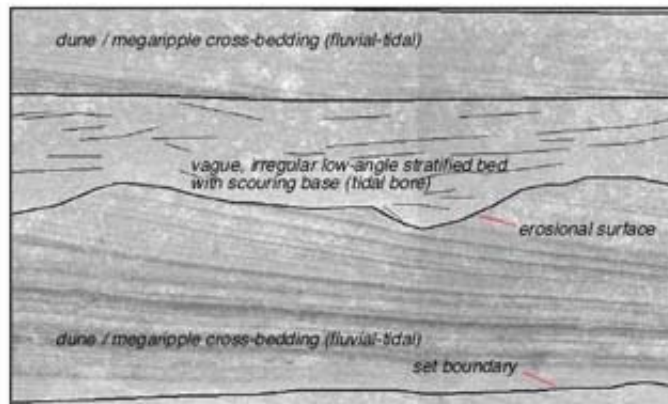
Miocene outcrop, Garsdorf lignite mine, Germany

PLATE 12 (page 58)
STORM WAVE STRATIFICATIONS AND CROSS-LAMINATIONS
Offshore to lowermost shoreface, core images



Tordis Field, Middle Jurassic, Brent Group, Offshore Norway
Well 34/07-14

PLATE 13 (page 72)
INTERPRETED TIDAL BORE DEPOSITS
(Fluvial-tidal transition zone, outcrop and interpretation graph)



Lorinha Formation, Late Jurassic, Praia de Areia Branca, Portugal
Personal comm. Allard Martinus, Statoil, Norway

PLATE 14A (page 77)
MUD CRACK STRUCTURES IN SHALLOW EPHEMERAL DEPOSITS
Distal glacial outwash plain, Saalian, Lunteren, Netherlands



PLATE 14B (page 77)
RAINDROP IMPRINTS AND CONVOLUTE LAMINATIONS FORMED
BY LIQUEFACTION IN WATER SOAKED AEOLIAN RIPPLE BEDS



Proximal aeolian sand sheet, SW Greenland

PLATE 15A (page 87)
SHEAR PLANES IN AEOLIAN GRAINFLOW DEPOSITS
Fine-grained sand, lacquer peel

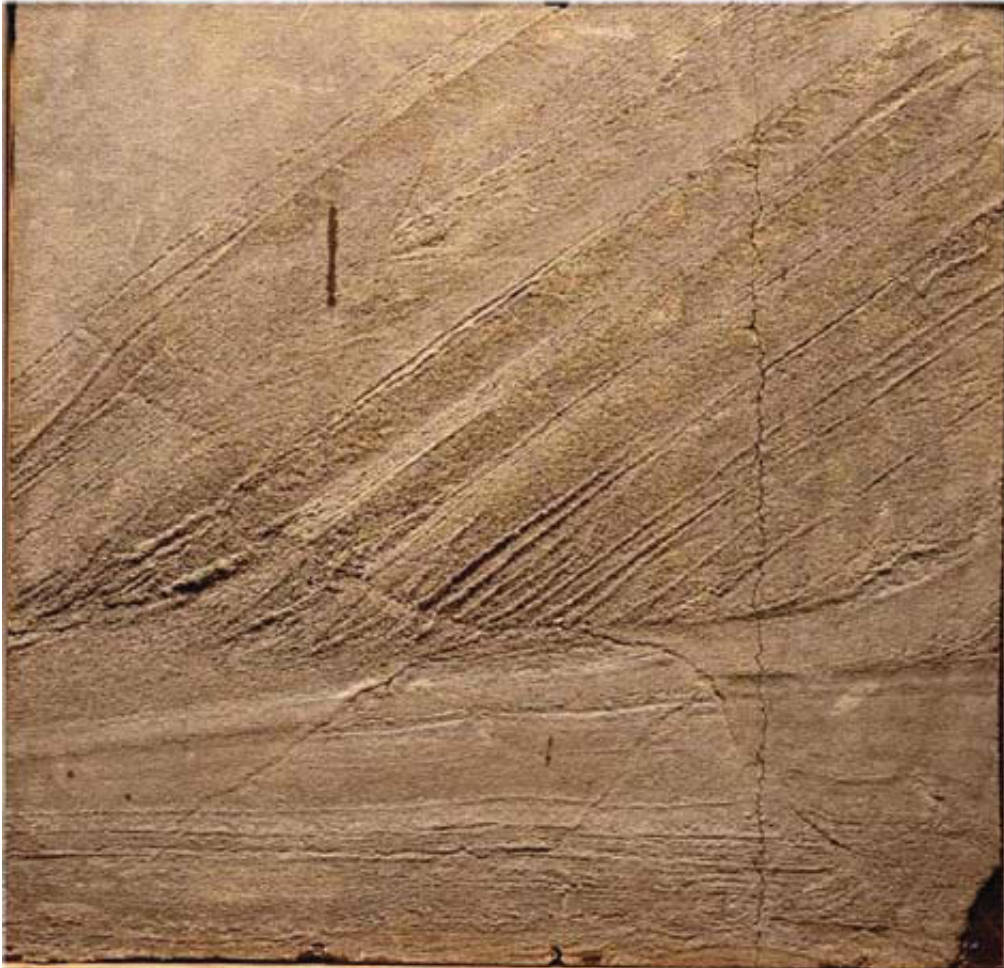
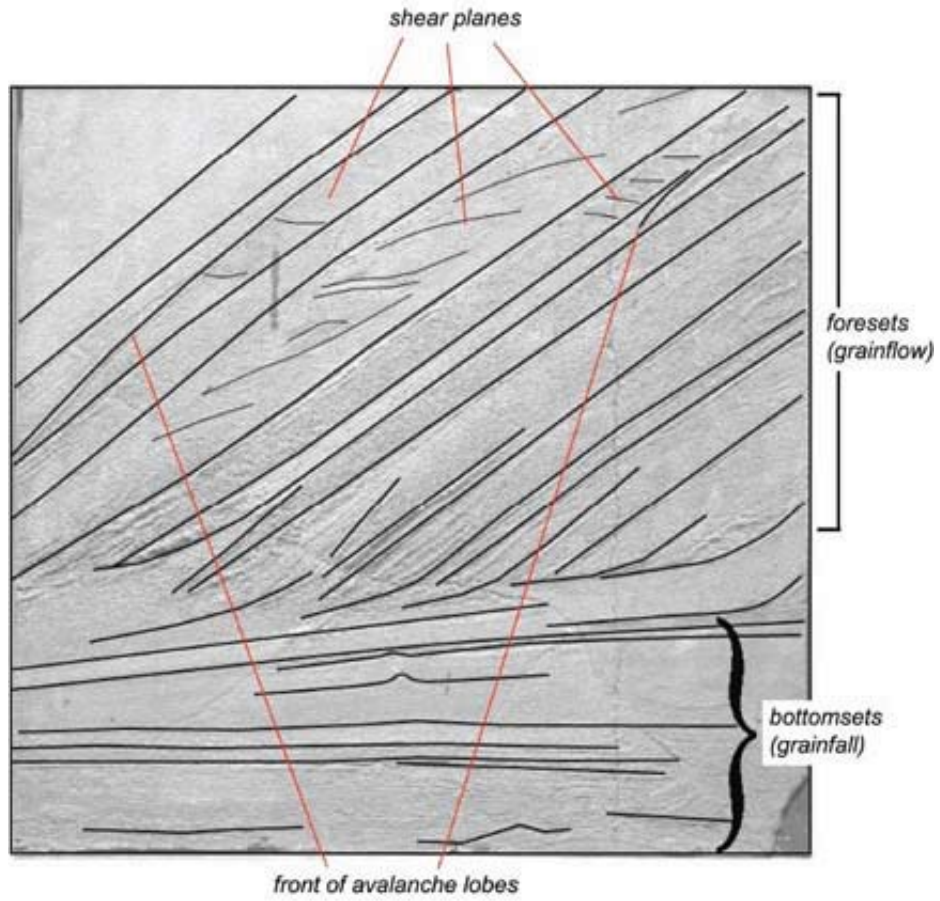


PLATE 15B (page 87)
SHEAR PLANES IN AEOLIAN GRAINFLOW DEPOSITS
Fine-grained sand, interpretation graph

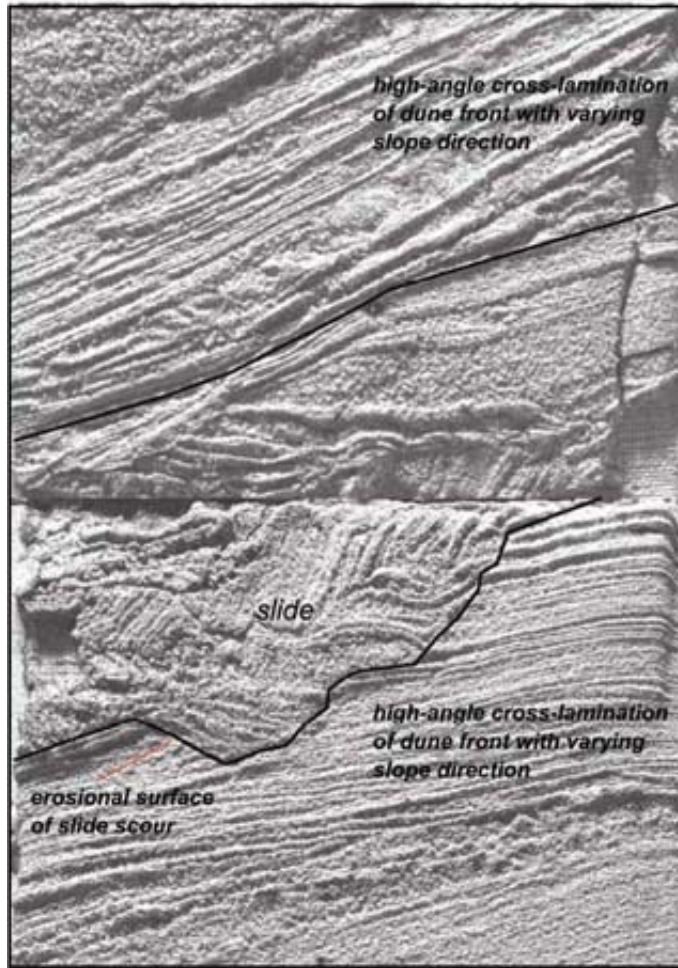


Coastal dune deposits, Schoorl, Netherlands

PLATE 16A (page 87)
SLIDE OF FRAGMENTED FROZEN UPPER LAYER
ALONG AEOLIAN DUNE FRONT
Fine-grained sand deposits, lacquer peel



PLATE 16B (page 87)
SLIDE OF FRAGMENTED FROZEN UPPER LAYER
ALONG AEOLIAN DUNE FRONT
Fine-grained sand deposits, lacquer peel

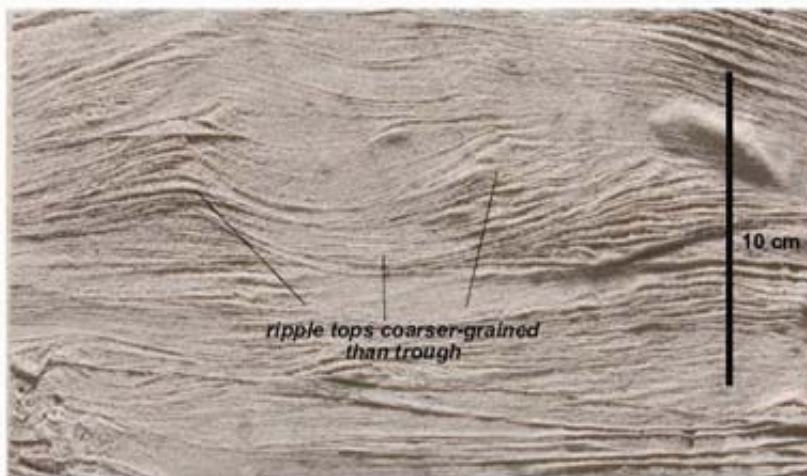


Aeolian dune deposits, SW Greenland

PLATE 17 (page 88)

AEOLIAN MULTI-DIRECTIONAL CROSS-LAMINATION

Moderately sorted medium-grained sand deposits, lacquer peel and interpretation graph



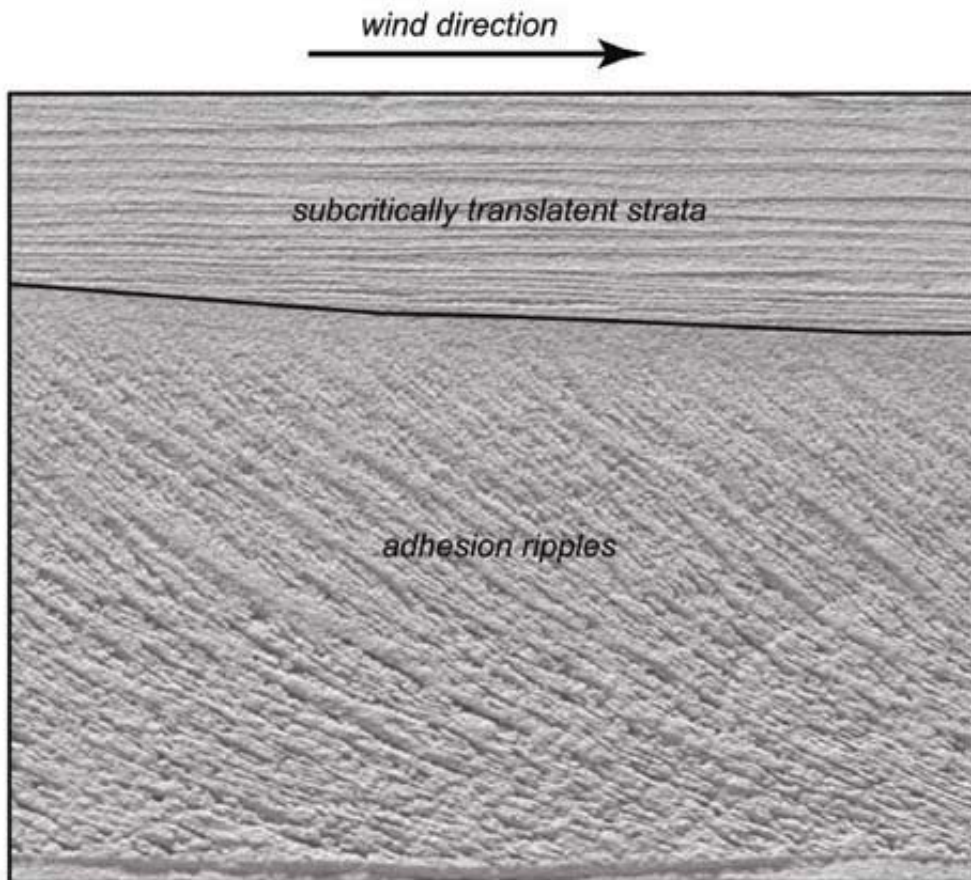
*ripple tops coarser-grained
than trough*

Aeolian proximal sand sheet, SW Greenland

PLATE 18A (page 88 and 89)
ADHESION RIPPLES AND SUBCRITICAL CLIMBING TRANSLATENT STRATA
Fine-grained sand deposits, lacquer peel



PLATE 18B (page 88 and 89)
ADHESION RIPPLES AND SUBCRITICAL CLIMBING TRANSLATENT STRATA
Fine-grained sand deposits, lacquer peel



Wind tunnel experiment (J. Schwan, unpublished)

8 References

- Alexander, J., Bridge, J.S., Cheel, R.J. and Leclair, S.F. (2001) Bedforms and associated sedimentary structures formed under supercritical water flows over aggrading beds. *Sedimentology*, **48**, 133-152.
- Allen, G.P., (1991) Sedimentary processes and facies in the Gironde estuary: a recent model for macrotidal estuarine systems. In: Smith, D.G., Reinson, G.E., Zaitlin, B.A. and Rahmani, R.A. (eds) *Clastic Tidal Sedimentology*. Canadian Society of Petroleum Geologists, Memoir 16, 29-40).
- Allen, J.R.L. (1979) A model for the interpretation of wave-ripple marks using their wavelength, textural composition and shape. *Journal of the Geological Society of London*, **136**, 673-682.
- Allen, J.R.L. (1984) Sedimentary structures, their character and physical basis. (two volumes) *Developments in Sedimentology*, **30**, Elsevier, Amsterdam, 593 p (v. 1) and 663 p. (v. 2).
- Allen, J.R.L (1985) *Principles of physical sedimentology*. Allen & Unwin, London, 272 pp.
- Allen, J.R.L. and Friend, P.F. (1968) *Bulletin of the Geological Society of America, Spec. Paper*, **106**, 21-74.
- Allen, J.R.L. and Leeder, M.R. (1980) Criteria for the instability of upper-stage plane beds. *Sedimentology*, **27**, 209-217.
- Allen, P.A. (1997) *Earth surface processes*. Blackwell, Oxford, 404 pp.
- Andersen, R.S. and Bunas, K.I. (1993) Grain size segregation and stratigraphy in aeolian ripples modeled with a cellular automation. *Nature*, **365**, 740-743.
- Arnott, R.W. and Southard, J.B. (1990). Exploratory flow-duct experiments on combined-flow bed configurations, and some implications for interpreting storm-event stratification. *Journal of Sedimentary Petrology*, **60**, 211-219.
- Baas, J.H. (2004) Conditions for formation of massive turbiditic sandstones by primary depositional processes. *Sedimentary Geology*, **166**, 293-310.
- Bartsch-Winkler, S. and Ovenshine, A.T. (1984) Macrotidal subarctic environment of Turnagain and Knik arms, Upper Cook inlet, Alaska: Sedimentology of the intertidal zone. *Journal of Sedimentary Petrology*, **54**, 1221-1238.
- Blatt, H., Middleton, G. and Murray, R. (1980) *Origin of sedimentary rocks*. Second edition, Prentice-

- Hall, Englewoods Cliffs, 782 pp.
- Boersma, J.R. (1967) Remarkable types of mega cross-stratification in the fluvial sequence of a subrecent distributary of the Rhine. Amerongen, The Netherlands. *Geologie & Mijnbouw*, **46**, 217-235.
- Boersma, J.R. and Terwindt, J.H.J. (1971) Neap-spring tide sequences of intertidal shoal deposits in a mesotidal estuary. *Sedimentology*, **28**, 151-170.
- Boersma, J.R. and Terwindt, J.H.J. (1981) Berms on an intertidal shoal: shape and internal structure. In: Nio, S.-D., Schüttenhelm, R.T.E. and Van Weering, T.C.E. (eds), *Holocene Marine Sedimentation in the North Sea Basin*. Spec. Publ. Int. Ass. Sedimentologists, **5**, 39-49.
- Bouma, A.H. (1962) *Sedimentology of some flysch deposits: a graphic approach to facies interpretation*. Elsevier, Amsterdam, 168 pp.
- Brand, K.J.J. (1985) Zeeuws-Vlaanderen, een gebied met een lange en rijke bedijkingsgeschiedenis. *Waterschapsbelangen*, **70**, 382-393.
- Bridge, J.S. (1996) *Fluvial sedimentology, a short course*. Department of Geological Sciences, Binghamton University, New York, 198 pp.
- Bridge, J.R. and Best, J.L. (1988) Flow, sediment transport and bedform dynamics over the transition from dunes to upper-stage plane beds: implications for the formation of planar laminae. *Sedimentology*, **35**, 753-763.
- Bridge, J.R. and Demicco, R.V. (2008) *Earth surface processes and sediment deposits*. Cambridge University Press, Cambridge, 815 pp.
- Brosche, P. and Wünsch, J. (1990) The solar torque: a leak for the angular momentum of the Earth-Moon system. In: Brosche, P. and Sündermann, J. (eds) *Earth's rotation from eons to days*. Springer Verlag, New York, 141-145.
- Brown, M.A., Archer, A.W. and Kvale, E.P. (1990) Neap-spring tidal cyclicity in laminated carbonate channel-fill deposits and its implications: Salem limestone (Mississippian), South-Central Indiana, U.S.A. *Journal of Sedimentary Petrology*, **60**, 152-159.
- Campbell, C.V. (1967) Laminae, set, bed and bedset. *Sedimentology*, **8**, 7-26
- Carling, P.A., Richardson, K. and Ikeda, H. (2005) A flume experiment on the development of subaqueous fine-gravel dunes from a lower-stage plane bed. *Journal of Geophysical Research*, **110**, art. no. F04S05, 15 p.
- Carter, R.G.W. (1988) *Coastal Environments, an introduction to the physics, ecological and cultural systems of coastlines*. Academic Press, London, 617 pp.
- Cartigny, M., Van den Berg, J.H., Mastbergen, Mulder, J. and Postma, G. (2009) On the relationship of bedforms of the upper flow regime. 2009 IAHR Congress Proceedings, Vancouver BC, Canada, August 9-14, 2009.

- Cartigny, M., Van den Berg, J.H., Mastbergen, D.R. and Postma, G. (2010) Cyclic steps formed by high-density turbidity currents in the Monterey submarine canyon. *Marine Geology*, in press.
- Catuneanu, O., Abreu V., Bhattacharya, J.P., Blum, M.D., Dalrymple, R.W., Eriksson P.G., Fielding C.R., Fisher, W.L., Galloway, W.E., Gibling, M.R., Giles K.A., Holbrook, J.M., Jordan, R., Kendall, C.G.St.C., Macurda, B., Martinsen, O.J., Miall, A.D., Neal, J.E. Nummedal, D., Pomar, L., Posamentier, H.W. Pratt, B.R. Sarg, J.F., Shanley, K.W. Steel, R.J., Strasser, A., Tucker, M.E. and Winker C. (2009) Towards the standardization of sequence stratigraphy. *Earth-Science Reviews*, **92**,1-33.
- Chanson, H. (2009) Current knowledge in hydraulic jumps and related phenomena. A survey of experimental results. *European Journal of Mechanics B/Fluids*, **28**, 191-210.
- Cheel, R.J. (1984) Heavy mineral shadows, a new sedimentary structure formed under upper flow regime conditions: its directional and hydraulic significance. *Journal of Sedimentary Petrology*, **54**, 1173-1180.
- Chepil, W.S. (1951) Properties of soil which influence wind erosion: IV. State of dry aggregate structure. *Soil Science*, **72**, 387-401.
- Church, M. and Jones, D. (1982) Channel bars in gravel-bed rivers. In: Hey, R.D., Bathurst, J.C. and Thorne, C.R. (eds.) *Gravel-bed rivers*, Wiley, Chichester, 291-338.
- Clemmensen, L.B. and Abrahamsen, K. (1983) Aeolian stratification in desert sediments. *Sedimentology*, **30**, 311-339.
- Collinson, J.D. (1970) Bedforms of the Tana River, Norway. *Geografiska Annaler*, **52A**, 31-56.
- Collinson, J.D. and Thompson, D.B. (1989) *Sedimentary structures (2nd edition)*. Chapman & Hall, London, 207 pp.
- Cooke, R.J. and Warren, A. (1973) *Geomorphology in deserts*. Batsford, London.
- Crisp, D.J. (1989) Tidally deposited bands in shells of barnacles and mollusks. In: Crick, R.E. (eds) *Origin, evolution and modern aspects of biomineralisation in plants and animals*. Plenum, New York, 103-124.
- Dalrymple, R.W., Knight, R.J., Zaitlin, B.A. and Middleton, G.V. (1990). Dynamics and facies model of a macrotidal sand bar complex, Cobequid Bay-Salmon River Estuary (Bay of Fundy). *Sedimentology*, **37**, 577-612.
- Dalrymple, R.W., Zaitlin, B.A. and Boyd, R. (1992). Estuarine facies models: Conceptual basis and stratigraphic implications. *Journal of Sedimentary Petrology*, **62**, 1130-1146.
- Davies, J.L. (1964) A morphogenic approach to world shorelines. *Zeitschrift für Geomorphologie*, **8** (Spec. No.), 127-142.
- De Boer, P.L., Oost, A.P. and Visser, M.J. (1989) The diurnal inequality of the tide as a parameter for recognizing tidal influences. *Journal of Sedimentary Petrology*, **49**, 912-921.

- De Mowbray, T. and Visser, M.J. (1984) Reactivation surfaces in subtidal channel deposits, Oosterschelde, Southwest Netherlands. *Journal of Sedimentary Petrology*, **54**, 811-824.
- De Raaf, J.F.M., Boersma, J.R. and Van Gelder, A. (1977) Wave-generated structures and sequences from a shallow marine succession, Lower Carboniferous, County Cork, Ireland. *Sedimentology*, **24**, 451-483.
- De Ronde, J.C. (1983) Changes of mean sea level and of mean tidal amplitude along the Dutch coast. In: Ritsema A.R. and Gürpınar, A. (eds) *Seismicity and seismic risk in the offshore North-Sea area*, 131-142.
- De Vries Klein, G. (1971) A sedimentary model for determining paleotidal range. *Bulletin of the Geological Society of America*, **82**, 2585-2592.
- Dott, R.H. and Bourgeois, J. (1982) Hummocky stratification: Significance of its variable bedding sequences. *Bulletin of the Geological Society of America*, **93**, 663-680.
- Dronkers, J. (1986) Tidal asymmetry and estuarine morphology. *Netherlands Journal of Sea Research*, **20**, 117-131.
- Dronkers, J. (2005) *Dynamics of coastal systems*. World Scientific, New Jersey, 519 pp.
- Fairbridge, R. W. and Sanders, J. E. (1987) The Sun's Orbit, A.D. 750-2050: basis for new perspectives on planetary dynamics and Earth-Moon linkage. In: Rampino, M.R., Sanders, J.E. Newman, W.S. and Königsson, L.K. *Climate: History, Periodicity, and Predictability*. Van Nostrand Reinhold, USA, 446-471.
- Fielding, C.R. (2006) Upper flow regime sheets, lenses and scour fills: Extending the range of architectural elements for fluvial sediment bodies. *Sedimentary Geology*, **190**, 227-240.
- Fredsøe, J. (1981) Unsteady flow in straight alluvial streams. Part 2. Transition from dunes to plane bed. *Journal of Fluid Mechanics*, **102**, 431-453.
- Friedrichs, C.T., Aubrey, D.G. and Speer, P.E. (1990) Impacts of relative sea-level rise on evolution of shallow estuaries. In: Cheng, R.T. (ed.) *Coastal and Estuarine Studies*, **38**. Springer, New York, 105-122.
- Fryberger, S.G. and Schenk, C. (1981) Wind sedimentation tunnel experiments on the origin of Aeolian strata. *Sedimentology*, **28**, 805-821.
- Harms, J.C., Southard, J.B. and Walker, R.G. (1982) *Structures and sequences in clastic rocks. Lecture Notes for Short Course No. 9*. Society of Economic Paleontologists and Mineralogists. Calgary.
- Houbolt, J.J.H.C. (1968) Recent sediments in the southern bight of the North Sea. *Geologie & Mijnbouw*, **47**, 245-273.
- Hunter, R.E. (1977) Basic types of stratification in small eolian dunes. *Sedimentology*, **24**, 361-387.
- Hsü, K.J. (1989) *Physical Principles of Sedimentology: a readable textbook for beginners and experts*.

- Springer-Verlag, New York, 233 p.
- Iversen, J.D. and White, B.R. (1982) Saltation threshold on Earth, Mars and Venus. *Journal of Atmospheric Science*, **33**, 2425-2429.
- Jopling, A.V. (1963) Hydraulic studies on the origin of bedding. *Sedimentology*, **2**, 115-121.
- Jopling, A.V. (1965) Hydraulic factors and the shape of laminae in laboratory deltas. *Journal of Sedimentary Petrology*, **35**, 777-791.
- Jopling, A.V. (1966) Some applications of theory and experiment to the study of bedding genesis. *Sedimentology*, **7**, 71-102.
- Julien, P.Y. and Klaassen, G.J. (1995) Sand-dune geometry of large rivers during floods. *Journal of Hydraulic Engineering*, **121**, 657-663.
- Julien, P.Y. and Raslan, Y. (1998) Upper-regime plane bed. *Journal of Hydraulic Engineering*, **124**, 1086-1096.
- Kennedy, J.F. (1963) The mechanics of dunes and antidunes in erodible-bed channels. *Journal of Fluid Mechanics*, **16**, 521-544.
- Keunen, P.H. (1965) Value of experiments in geology. *Geologie & Mijnbouw*, **44**, 22-36.
- Kleinbans, M.G. (2005a) Grain-size sorting in grainflows at the lee side of deltas. *Sedimentology*, **52**, 291-311.
- Kleinbans, M.G. (2005b) Phase diagrams of bed states in steady, unsteady, oscillatory and mixed flows. In: Van Rijn, L.C. *EU-Sandpit end-book*. Aqua Publications, The Netherlands, paper Q.
- Knighton, D. (1998) *Fluvial forms and processes*. Wiley, New York, 383 pp.
- Kocurek, G. and Fielder, G. (1982) Adhesion structures. *Journal of Sedimentary Petrology*, **52**, 1229-1241.
- Komar, P.D. (1976) The transport of cohesionless sediments on continental shelves. In: Stanley, D.J. and Swift, D.J.P. (eds.) *Marine sediment transport and environmental management*. Wiley, New York, 107-125.
- Komar, P.D. (1976) The transport of cohesionless sediments on continental shelves. In: Stanley, D.J. and Swift, D.J.P. (eds.) *Marine sediment transport and environmental management*. Wiley & Sons, New York, 107-125.
- Komar, P.D. and Miller, M.C. (1973) The threshold of sediment movement under oscillatory water waves. *Journal of Sedimentary Petrology*, **43**, 1101-1110.
- Komar, P.D. and Miller, M.C. (1975) The initiation of oscillatory ripple marks and the development of plane-bed at high shear stresses under waves. *Journal of Sedimentary Petrology*, **45**, 697-703.
- Kvale, E.P., Archer, A.W. and Johnson, H.R. (1989) Daily, monthly, and yearly tidal cycles within

- laminated siltstones of the Mansfield Formation (Pennsylvanian) of Indiana. *Geology*, **17**, 365-368.
- Kvale, E.P., Johnson, H.W., Sonett, C.P., Archer, A.W. and Zawistoski, A. (1999) Calculating the lunar retreat using tidal rhythmites. *Journal of Sedimentary Research*, **69**, 1154-1168.
- Kvale, E.P. (2006) The origin of neap-spring tidal cycles. *Marine Geology*, **235**, 5-18.
- Lacombe, P. and Jago, C.F. (1996) The morphological dynamics of intertidal megaripples in the Mawddach Estuary, North Wales, and the implications for palaeoflow reconstructions. *Sedimentology*, **43**, 541-559.
- Lambeck, K. (1980) *The earth's variable rotation: geophysical causes and consequences*. Cambridge Univ. Press, New York, 449 pp.
- Leckie, D.A. and Walker, R.G. (1982) Storm- and tide-dominated shorelines in Late Cretaceous Moosebar-Lower Gates interval - outcrop equivalents of deep basin gas traps in western Canada. *Bulletin of the American Association of Petroleum Geologists*, **66**, 138-157.
- Leeder, M.R. 1999 *Sedimentology and sedimentary basins, from turbulence to tectonics*. Blackwell, Oxford, UK, 592 p.
- LeFloch, 1961. *Propagation de la marée dans l'estuaire de la Seine et en Seine-maritime*. Thesis, Univ. Paris, 507 pp.
- Makse, H.A. (2000) Grain segregation mechanism in aeolian sand ripples. *The european physical journal*, E1, 127-135.
- Massari, F. (1996) Upper-flow-regime stratification types on steep-face, coarse-grained, Gilbert-type progradational wedges (Pleistocene, southern Italy). *Journal of Sedimentary Research*, **66**, 364-375.
- Mastbergen, D. R. and Van den Berg, J. H. (2003) Breaching in fine sands and the generation of sustained turbidity currents in submarine canyons. *Sedimentology*, **50**, 625-637.
- Mazumder, R. and Arima, M. (2005) Tidal rhythmites and their implications. *Earth-Science Reviews*, **69**, 79-95.
- McKee, E.D. and Bigarella, J.J. (1979) Sedimentary structures in dunes. In: McKee, E.D. (ed.) *A study of global sand seas*. *Geological Survey Professional Paper*, 1052.
- McKee, E.D. and Weir, G.W. (1953) Terminology for stratification and cross stratification in sedimentary rocks. *Bulletin of the Geological Society of America*, **64**, 381-390.
- Middleton, G.V. (1965a) Antidune cross-bedding in a large flume. *Journal of Sedimentary Petrology*, **35**, 922-927.
- Middleton, G.V. (1965b) *Primary sedimentary structures and their hydrodynamic interpretation*. S.E.P.M. Spec. Publ., 12, Tulsa.

- Middleton, G.V. and Southard, J.B. (1977) *Mechanics of sediment movement*. S.E.P.M. Short Course, 3. Binghamton, New York.
- Miller, M.C., McCave, I.N. and Komar, P.D. (1977) Threshold of sediment motion under unidirectional currents. *Sedimentology*, **24**, 507-527.
- Miller, M.C. and Komar, P.D. (1980) Oscillation sand ripples generated by laboratory apparatus. *Journal of Sedimentary Petrology*, **50**, 169-180.
- Mulder, T., Razin, P. and Faugeres, J.-C. (2009) Hummocky cross-stratification in deep-sea turbidites: Upper Cretaceous Basque basins (Western Pyrenees, France). *Sedimentology*, **56**, 997-1015.
- Nichols, M., Johnson, G.H. and Peebles, P.C. (1991) Modern sediments and facies model for a microtidal coastal plain estuary, the James Estuary, Virginia. *Journal of Sedimentary Petrology*, **61**, 883-899.
- Nielsen, L.S., Johannessen, P.N. and Surlyk, F. (1988) A late Pleistocene coarse-grained spit-platform sequence in northern Jylland, Denmark. *Sedimentology*, **35**, 915-937.
- Nio, S.D., Böhm, A.R., Brouwer, J.H., De Jong, M.G.G. and Smith, D.G. (2005) Climate stratigraphy, principles and applications in subsurface correlation. *EAGE Short Course Series*, **1**, 130 p.
- Nio, S.D., Siegenthaler, C. and Yang, C.S. (1983) Megaripple cross-bedding as a tool for reconstruction of the palaeo-hydraulics in a Holocene subtidal environment, S.W. Netherlands. *Geologie & Mijnbouw*, **62**, 499-510.
- Nio, S.D. and Yang, C.S. (1991) Sea-level fluctuations and geometric variability of tide-dominated sandbodies. *Sedimentary Geology*, **70**, 161-193.
- Oost, A.P., de Haas, H., Ijnsen, F., van den Boogert, J.M. and de Boer, P.L. (1993) The 18.6 yr nodal cycle and its impact on tidal sedimentation. *Sedimentary Geology*, **87**, 1-11.
- Postma, H. (1967) Sediment transport and sedimentation in the estuarine environment. In: (Lauff, G.H. (ed.) *Estuaries*. American Association for the advancement of science, Washington, 158-179.
- Postma, G., Nemeč, W. and Kleinspehn, K.L. (1988) Large floating clasts in turbidites: a mechanism for their emplacement. *Sedimentary Geology*, **58**, 47-61.
- Prave, A.R. and Duke, W.L. (1990) Small-scale hummocky cross-stratification in turbidites: a form of antidune stratification? *Sedimentology*, **37**, 531-539
- Pye, K. and Tsoar, H. (1990) *Aeolian sand and sand dunes*. Unwin Hyman, London, 396 pp.
- Reading, H.G. (1996) *Sedimentary environments, processes, facies and stratigraphy*. Third edition, Blackwell, Oxford, 688 pp.
- Reineck, H.-E. and Singh, I.B. (1973) *Depositional sedimentary environments*. Springer, Berlin, 439 pp.
- Ribberink, J.S. and Al-Salem, A. (1991) *Sediment transport, sediment concentration and bedforms in*

- simulated asymmetric wave conditions*. Report H840, part IV, Delft Hydraulics.
- Rosenberg, G.D. and Runcorn, S.K. (1975) (eds) *Growth rhythms and the history of the Earth's rotation*. Wiley, New York, 559 pp.
- Rousseaux, G. (2006) Physical distinction between rolling-grain ripples and vortex ripples: an experimental study. *Physical Review*, E **74**, 1-7
- Røe, S-L.(1987) Cross-strata and bedforms of probable transitional dune to upper-stage plane-bed origin from a Late Precambrian fluvial sandstone, northern Norway. *Sedimentology*, **34**, 89-101.
- Rust, B.R. (1971) Structure and process in a braided river. *Sedimentology*, **18**, 221-245.
- Salomon, J.C. and Allen, G.P. (1983) Rôle sedimentologique de la marée dans les estuaires a fort marnage. Compagnie Française des Petroles, *Notes et Memoires*, **18**, 35-44.
- Schwan, J. (1988) The structure and genesis of Weichselian to early Holocene aeolian sand sheets in western Europe. *Sedimentary Geology*, **55**, 197-232.
- Schwan, J. (1991) Palaeowetness indicators in a Weichselain Late Glacial to Holocene aeolian succession in the southwestern Netherlands. *Zeitschrift für Geomorphologie, Neue Folge*, supplement Band, **90**, 155-169.
- Scrutton, C.T. (1978) Periodic growth features in fossil organisms and the length of the day and month. In: Brosche, P. and Sündermann, J. (eds) *Earth's rotation from eons to days*. Springer Verlag, New York, 154-196.
- Shields, A. (1936) Anwendung der Aehnlichkeitsmechanik und der Turbulenzforschung auf die Geschiebebewegung. *Mitteilungen der Preussischen Versuchsanstalt für Wasserbau und Schiffbau*, **26**, Berlin, Germany, 26 p.
- Siegenthaler, C. (1982) Tidal cross-strata and the sediment transport rate problem: a geologists approach. *Marine Geology*, **45**, 227-240.
- Simons, D.B. and Richardson, E.V. (1963) Forms of bed roughness in alluvial channels. A.S.C.E. *Transactions*, **128-I**, 248-302.
- Smith, D.P., Kvitek, R., Iampietro, P.J. and Wong, K. (2007) Twenty months of geomorphic change in upper Monterey Canyon (2002-2005). *Marine Geology*, **236**, 79-94.
- Smith, D.P., Ruiz, G., Kvitek, R. and Iampietro, P.J. (2005) Semiannual patterns of erosion and deposition in upper Monterey Canyon from serial multibeam bathymetry. *Bulletin of the Geological Society of America*, **117**, 1123-1133.
- Sohn, Y.K. (1997) On traction-carpet sedimentation. *Journal of Sedimentary Research*, **67**, 502-509.
- Southard, J.B. and Boguchwal, L.A. (1990) Bed configurations in steady unidirectional water flows. Part 2. Synthesis of flume data. *Journal of Sedimentary Petrology*, **60**, 658-679.
- Speer, P.E. and Aubrey, D.G. (1985) A study of non-linear tidal propagation in shallow inlet/estuarine

- systems, part II, theory. *Estuarine Coastal and Shelf Science*, **21**, 207-224.
- Spinewine, B., Sequieros, O.E., Garcia, M.H., Beaubouef, R.T., Sun, T., Savoye, B., and Parker, G. (2009). Experiments on internal deltas created by density currents in submarine minibasins. Part II: morphodynamic evolution of the delta and associated bedforms. *Journal of Sedimentary Research*, **79**, 608-628.
- Swift, D.J.P., Figueiredo, A.G., Freeland, G.L. and Oertel, G.F. (1983) Hummocky cross-stratification and megaripples: a geological double standard? *Journal of Sedimentary Petrology*, **53**, 1295-1317.
- Tanner, W.F. (1956) Size and roundness in sediments: a discussion. *Bulletin of the Geological Society of America*, **67**, 535.
- Tsoar, H. and Pye, K. (1987) Dust transport and the question of desert loess formation. *Sedimentology*, **34**, 139-153.
- Van den Berg, J.H. (1986) *Aspects of Sediment- and Morphodynamics of Subtidal Deposits of the Oosterschelde (the Netherlands)*. Thesis, Utrecht, 126 pp.
- Van den Berg, J.H., Asselman, N.E.M. and Ruessink, B.G. (1995) Hydraulic Roughness of a Tidal Channel, Westerschelde Estuary, The Netherlands. In: Flemming, B.W. (ed.) *Special Publs. int. Ass. Sediment.*, **24**, 19-32.
- Van den Berg, J.H., Jeuken, M.C.J.L. and Van der Spek, A.J. (1996) Hydraulic processes affecting the morphology and evolution of the Westerschelde estuary. In: Nordstrom, K. and Roman, C.T. (eds.) *Estuarine Shores: Evolution, environments and human alterations*. Wiley, Chichester, 157-183.
- Van den Berg, J.H. and Van Gelder, A. (1993) A new bedform stability diagram, with emphasis on the transition of ripples to plane bed in flows over fine sand and silt. *Special Publs. int. Ass. Sediment.*, **17**, 11-21.
- Van den Berg, J.H. and Van Gelder, A. (1994) The Transition of Ripples to Upper Plane Bed in Flows over Very Fine Sand and Silt: an Analysis of Flume Experiments and Deposits of the Yellow River, China, *I.A.S., Spec. Publ.*, **17**, 11-21.
- Van den Berg, J.H. and Van Gelder, A. (1998) Discussion: Flow and sediment transport over large subaqueous dunes: Fraser River, Canada. *Sedimentology*, **45**, 217-221.
- Van den Berg, J.H., Van Gelder, A., and Mastbergen, D. R. (2002) The importance of breaching as a mechanism of subaqueous slope failure in fine sand. *Sedimentology*, **49**, 81-95.
- Van der Kreeke, J. and Haring, J. (1979) Equilibrium flow areas in the Rhine-Meuse delta. *Coastal Engineering*, **3**, 97-111.
- Van der Spek, A.J.F. (1994) *Large-scale evolution of Holocene tidal basins in the Netherlands*. Thesis, Utrecht, The Netherlands, 191 pp.
- Van Maren, D.S., Winterwerp J. C., Wang Z. Y. and Pu Q. (2008) Suspended sediment dynamics and morphodynamics in the Yellow River, China. *Sedimentology*, **56** (3), 785-806.

- Van Rijn, L.C. (1984) Sediment transport, Part III: Bed forms and alluvial roughness. *Journal of Hydraulic Engineering*, **110**, 1733-1754.
- Van Rijn, L.C. (1990) *Principles of fluid flow and surface waves in rivers, estuaries and oceans*. Aqua Publications, Amsterdam.
- Van Rijn, L.C. (1993) *Principles of sediment transport in rivers, estuaries and coastal seas*. Aqua Publications, Amsterdam.
- Van Straaten, L.M.J.U. and Keunen, P.H., (1957) Accumulation of fine-grained sediments in the Dutch Wadden Sea. *Geologie en Mijnbouw*, **19**, 419-432.
- Van Wagoner J.C., Mitchum, R.M., Campion, K.M. and Rahmanian, V.D. (1990) *Siliciclastic sequence stratigraphy in well logs, cores and outcrops*. AAPG Methods in exploration series, **7**, 55 pp.
- Walker, R.G. and James, N.P. (1992) Facies, facies models, and modern stratigraphic concepts. In: Walker, R.G. and James, N.P. (eds) *Facies models: response to sea-level changes*. Geol. Ass.Can., Waterloo, 1-14.
- Wang, Z.B., Jeuken, M.C.J.L., Gerritsen, H., De Vriend, H.J. and Kornman, B.A. (2002) Morphology and asymmetry of the vertical tide in the Westerschelde estuary. *Continental Shelf Research*, **22**, 2599-2609.
- Wells, J.W. (1963) Coral growth and geochronometry. *Nature*, **197**, 948-950.
- Williams, G.E. (1989) Tidal rhythmites: Geochronometers for the ancient Earth-Moon system. *Episodes*, **12**, 162-171.
- Williams, G.E. (2000) Geological constraints on the Precambrian history of Earth's rotation. *Reviews of Geophysics*, **38**, 37-59.
- Wilson, I.G. (1972) Universal discontinuities in bedforms produced by the wind. *Journal of Sedimentary Petrology*, **42**, 667-669.
- Yalin, M.S. (1964) *Journal of the Hydraulics Division, ASCE*, **90** (HY5), 105-119.
- Yang, B., Dalrymple, R.W. and Chun, S. (2006) The significance of hummocky cross-stratification (HCS) wavelengths: evidence from an open-coast tidal flat, South Korea. *Journal of Sedimentary Research*, **76**, 2-8.

INDEX

Terms given in *italics* are very often used and reference is made only to the page with their definition

<u>Index Terms</u>	<u>Links</u>			
A				
abrasion	79			
adhesion warts	89			
amphidromic point	62			
angle of repose				
dynamic	30			
static	30			
antidunes	26	27	28	29
	40	45	46	
aphelion	60			
apogee	60			
armouring	21			
B				
<i>bar</i>	32			
alternate	33	35		
braid	33	34	35	
chute	35			
diagonal	33	34		
lateral	33			
medial	33			
point	33	34	35	
side	33			
tail	33			
transverse	33			
unit	33	34	35	
basal laminar layer	42			
<i>bedforms</i>	6			
<i>bedding</i>	24			
<i>cross- (X-)</i>	35			
flaser	72	77		

Index Terms

Links

bedding (Cont.)

lenticular	72			
linsen	72			
low angle	57			
wavy	72			
bed-load transport	20	21		
<i>bed(s)</i>	7			
adhesion plane	89			
amalgamated	24	57		
heterolithic	23	24	61	72
	75			
lower plane	25	27		
upper plane	25	26	27	28
	29	37	39	40
	52	55	82	
bed shear stress	13	52		
bedset	7			
Bernoulli equation	14			
bioturbation	20	80		
bore				
breaking	65	66		
undular	65			
breakaparts	87			
brinkpoint	30	31	37	
buffer layer	17			
C				
cast				
flute	25			
load	74	75	76	77
channel water discharge	13			
chute-and-pools	29	39	40	45
climbing translantent strata	88			
closed work gravel	20			
cohesion	18	73	79	
conservation of mass	14			
conservation of energy	14			
contact load	80			

Index Terms

Links

convective acceleration	14			
cryoturbation	80			
current lineation	39			
current vector	13			
cyclic steps	29	39	40	45
D				
day				
lunar	60	61		
solar	60	61		
dish and pillar	77			
dispersive stress	44			
dissipative beach	49			
double mud drape	70			
<i>dune(s)</i> (2D, 3D)	25			
linguoid	25	26	32	35
	36			
lunate	25	26		
draa	81	84	85	
drag folds	87			
dynamic tidal theory	62			
E				
equal mobility	20	21		
equilibrium tidal theory	59			
equinoxes	60			
equivalent roughness length	18			
estuary				
tide-dominated	59	66	67	68
wave-dominated	67	68		
F				
facies				
depositional	6	7	11	
sedimentary	7	11		
facies associations	7			
fetch	47			

Index Terms

Links

flame structure	46	76	87	
flow				
back-	32	33	34	89
bidirectional	39	71		
co-	31			
combined	49	55	56	
debris	30	43	74	76
fluidized	73			
<i>grain</i>	30			
helical	17			
hyperconcentrated	43	44		
ideal	15			
laminar	14	42	43	
liquefied	73	74		
Newtonian	43			
opposed	48			
oscillatory (wave induced)	13	25	39	49
	50	54	55	56
	57			
overbank	77			
permanent	14	17	18	26
	28	29	85	
plastic	43	73	85	
reversing	41	72		
shooting	15			
steady	14	15	17	18
	24	25	26	27
subcritical	15	26	29	45
	88	89		
supercritical	15	26	29	39
	40	45	82	
threshold	28			
tidal	25	67	71	
tranquil	15			
<i>unidirectional</i>	13			
<i>uniform</i>	14			
unsteady	14	17	41	49
	71			

Index Terms**Links****flow regime**

lower	25	54		
tranquil	25			
upper	25	29	55	
rapid	25			

fluid

Bingham	73			
plastic	43	73	85	
ideal	15			

fluidization

73	74	77		
----	----	----	--	--

force

centrifugal	16	17	59	
chemical	18			
cohesive	80	81		
collisional	44			
Coriolis	62			
drag	79			
gravity	15	18		
hydrostatic	16	17		
lift	18	20	45	79
	80			
resistance	15			
tractive	59			

form-concordant

30				
----	--	--	--	--

form-discordant

30				
----	--	--	--	--

form roughness

13	18			
----	----	--	--	--

freezing

85	87			
----	----	--	--	--

friction

intergranular	73			
internal	73			
skin	13	18	27	

frosted appearance

79				
----	--	--	--	--

Froude Number

13	15	26	28	
29				

densiometric	45			
surge	48	65	66	

Index Terms

Links

G				
grading				
inverse	21	44	45	88
normal	21			
reverse	31	89	21	
(Grain) Reynolds Number	13	14	18	52
	74			
grain fall	31	85	89	
grain sorting	31	83		
gravel overpassing	20			
H				
heavy mineral shadows	39			
HCS = Hummocky Cross-Stratification				
hindered settling	44			
hiding	20			
hummocks	52	54	55	56
hydraulic jump	15	29	40	45
	46			
hydraulic rough	14	16	18	42
hydraulic smooth	14	27		
hypersynchronous	64			
hypochronous	64			
hysteresis effect	25			
I				
imbrication	39			
K				
kinetic sieving	20	31		
kinematic sorting	20			
L				
lag deposit	21	39	79	
lag effect	25			
laminasets	7			

Index Terms

Links

<i>laminae</i>	7			
<i>lamination</i>	24			
convolute	76	77		
<i>cross- (x-)</i>	37			
horizontal	39	40	57	89
parallel	33	39	56	57
ripple-drift	38	70		
wavy	43	56		
lamine	24			
liquefaction	73	74	77	
loess	79			
long term suspension	80			
lunar apse cycle	60			
lunar node cycle	60			
M				
megaripples	25			
mobile bed armour	21			
modified saltation	80			
month				
anomalistic	60			
sidereal	59	60	61	
synodic	60	61	63	
tropical	59	62	63	
Moss defects	80			
O				
open work gravel	20			
P				
parameter				
Bonnefille	26	43		
Mobility	20	26	27	54
particle	26	28		
Shields	18	19	27	51
	54			
wave grain mobility	54			

Index Terms

Links

parting lineation	39	40		
pavement	21	85		
perigee	60			
perihelion	60			
pitch and swell	76			
plane				
discontinuity	42	70		
pause	42			
principal bedding	37			
set-interruption	42			
preservation potential	25			
R				
reactivation surface	42			
reflective beach	49			
reptation	83			
resistance				
flow	13	18		
frictional	17			
hydraulic	16	28		
skin	13			
ripple steepness	50	83		
<i>ripples (2D, 3D)</i>	25			
adhesion	89	89		
anorbital	53			
asymmetrical wave	50			
ballistic	81	82	83	
granule	83	89		
linguoid	25	26		
lunate	25	26		
orbital	53	58		
post-vortex	50	56		
reversing crest	50			
rolling grain	49	55		
suborbital	53			
symmetrical	50	55		
vortex	49	50	55	56
<i>wave</i>	25			

Index Terms

Links

ripples (2D, 3D) (Cont.)

wind

50 81 82 83
88

rolling

20

S

saltation

20 79 80 81
82 83 88 89

section

dip

36 37

principal bedding-plane

37

strike

36 37 39

sedimentary dynamics

6 7 9 11

(sedimentary) sequence

23

Bouma

43

deltaic

7

turbidite

24 43 46

sedimentary structures

assemblages of

5 6

primary

5 6 7

secondary

5

selective transport

20

set

24

back-

39 40 45 46

bottom-

32 33 37 71
86 89

co-

37 70 71

fore-

30 31 32 37
39 42 45 66

77 86 89

form-

56

tabular

37 71

toe-

31 37 71

top-

37 86

trough-shaped

36 37

wedge-shaped

36 37 71 85

Shields diagram

18

Shields criterion

18 19 27 54

Index Terms

Links

Sliding	20			
stratal unit	7	8	10	11
surface traction	80			
syzygy	60			
tidal				
macro-	66			
meso-	66			
micro-	66			
tidal bundle	71			
tides				
neap	60	63	71	
spring	60	69	71	
SCS = Swaly Cross Stratification				
storm sands	57			
<i>stratification</i>	6			
<i>cross-</i>	24			
large-scale wavy	43			
hummocky cross-	45	57		
sinusoidal (cross-)	43			
swaly cross-	57			
stratigraphy				
climate	5	9	10	11
sequence	5	7	9	10
	11			
stratum	23	31	87	
stream power	13			
suspended bed-material transport	20			
swell	47	50	57	73
	76			
T				
tool marks	24	25		
traction carpet	43	44	45	
<i>turbulence</i>	13			
turbulent logarithmic layer	16			
turbidite	24	25	43	44
	45	46		

Index Terms**Links**

turbidity current	27	40	42	43
	45	46	74	76
	77			

V

varves	24			
velocity				
current	13	16	17	25
	42	61		
flow	13	14	15	16
	17	27	28	38
	40	48	66	67
fluid threshold	88			
shear	13	50	79	80
	81	82		
viscosity	13	14	19	27
	28	43	79	82
viscous sublayer	14	20	27	

W

wash load	20	80		
wave				
Kelvin	62			
plunging	49			
solitary	47			
spilling	47			
standing	62			
wave base	47			
wave-induced currents	49			
wet channel cross-section	13			

Z

zibar	84			
--------------	----	--	--	--